

Shear stress stimulated apical endocytosis in renal proximal tubule epithelia

by

Venkatesan Raghavan

Btech., Industrial Biotechnology, SASTRA University, India, 2011

Submitted to the Graduate Faculty of
The School of Medicine in partial fulfillment
of the requirements for the degree of
Doctor of Philosophy

University of Pittsburgh

2015

UNIVERSITY OF PITTSBURGH

School of Medicine

This dissertation was presented

by

Venkatesan Raghavan

It was defended on

September 18th, 2015

and approved by

Dr. Gerard Apodaca, PhD., Professor, Department of Medicine

Dr. Marcelo D Carattino, PhD., Associate Professor, Department of Medicine

Dr. Kirill Kiselyov, PhD., Associate Professor, Department of Biological Sciences

Dr. Panagiotis (Takis) Benos, PhD., Associate Professor, Department of Computational and

Systems Biology

Advisor: Dr. Ora A. Weisz, PhD., Professor, Department of Medicine

Copyright © by Venkatesan Raghavan

2015

Flow stimulated endocytosis in renal proximal tubule epithelia

Venkatesan Raghavan, B.Tech.

University of Pittsburgh, 2015

The proximal tubule (PT) plays a critical role in the reabsorption of ions, solutes and low molecular weight proteins from the glomerular filtrate. Although the PT has been known to acutely modulate ion reabsorption in response to changes in flow rates of the glomerular filtrate, whether apical endocytosis was regulated in response to changes in flow was unknown. I hypothesized that the fluid shear stress (FSS) caused by the flow of glomerular filtrate on the apical surface of the tubules would stimulate apical endocytosis in PT epithelia. I used a cell culture based parallel plate flow chamber system to test my hypothesis, and used PT cells from opossum, mice and humans in this study. I determined that FSS stimulated a rapidly reversible increase in apical endocytosis of both albumin (Megalin ligand) and dextran (fluid phase marker) in OK cells, which starts within 30 min of exposure to a FSS of 1 dyne/cm² and the response increases linearly for at least three hours so long as FSS is maintained. This FSS-stimulated increase in endocytosis is clathrin and dynamin mediated. Primary cilia act as the principal mechanosensor in this process, and cause an increase in [Ca²⁺]_i through the release of the ryanodine sensitive pool of calcium from the ER. In addition, purinergic signaling, triggered by the bending of cilia, is also important for both the FSS stimulated Ca²⁺ and endocytic responses.

Lowe syndrome is a rare X linked genetic disease that affects young boys. It is characterized by the loss of OCRL a lipid phosphatase, and causes proteinuria. The FSS stimulated increase in endocytosis is ablated in OCRL depleted human PT cells, and the length

of cilia in OCRL depleted cells is also higher. However, the lengthening of cilia is not responsible for the loss of FSS stimulated responses in these cells. This dissertation synthesizes our current understanding of mechanosensitive regulation of endocytic capacity in proximal tubule epithelia, suggests a mechanism that may define the reason for proteinuria in Lowe syndrome patients, and highlights areas of opportunity for future investigations.

TABLE OF CONTENTS

| | |
|---|-------------------------------------|
| ABSTRACT..... | IV |
| PREFACE..... | XIV |
| 1.0 INTRODUCTION..... | 1 |
| 1.1 ANATOMY OF THE MAMMALIAN KIDNEY | 1 |
| 1.2 PROXIMAL TUBULE FUNCTION | 3 |
| 1.2.1 MULTILIGAND RECEPTORS OF THE PROXIMAL TUBULE: | 4 |
| 1.2.2 ORGANIZATION OF THE APICAL ENDOCYTIC PATHWAY IN THE PROXIMAL TUBULE: | 12 |
| 1.2.3 MECHANOSENSATION IN THE PROXIMAL TUBULE: | 21 |
| 1.2.4 PT DYSFUNCTION AND LOW MOLECULAR WEIGHT PROTEINURIA | 25 |
| 1.3 LOWE SYNDROME..... | 26 |
| 1.3.1 PHENOTYPE, PREVALENCE AND CAUSES | 27 |
| 1.3.2 ROLE OF OCRL1 IN CILIOGENESIS | 33 |
| 1.3.3 ROLE OF OCRL1 IN MEMBRANE TRAFFIC | 34 |
| 1.4 SUMMARY | 38 |
| 2.0 FLOW STIMULATED ENDOCYTOSIS IN PT EPITHELIA..... | 42 |
| 2.1 ABSTRACT..... | ERROR! BOOKMARK NOT DEFINED. |

| | | |
|------------|---|-----------|
| 2.2 | INTRODUCTION | 43 |
| 2.2.1 | Significance..... | 44 |
| 2.3 | RESULTS..... | 46 |
| 2.3.1 | PROXIMAL TUBULE DERIVED CELL LINES HAVE ROBUST APICAL ENDOCYTIC UPTAKE OF MEMBRANE BOUND AND FLUID PHASE TRACERS | 46 |
| 2.3.2 | EXPOSURE TO FSS STIMULATES APICAL ENDOCYTOSIS IN PT CELLS..... | 48 |
| 2.3.3 | ONSET AND STRESS-DEPENDENCE OF FSS-STIMULATED ENDOCYTOSIS..... | 51 |
| 2.3.4 | REVERSIBILITY OF FSS DEPENDENT ENDOCYTOSIS | 54 |
| 2.3.5 | FSS-STIMULATED ENDOCYTOSIS OCCURS VIA A CLATHRIN- AND DYNAMIN-DEPENDENT PATHWAY | 56 |
| 2.3.6 | EXPOSURE OF PTS TO FSS CAUSES AN INCREASE IN BOTH SIZE AND NUMBER OF CLATHRIN COATED PITS | 58 |
| 2.3.7 | INCREASE IN CYTOSOLIC CA ²⁺ IS THE FIRST EFFECT IN PT CELLS IN RESPONSE TO EXPOSURE TO FSS..... | 60 |
| 2.3.8 | CA ²⁺ STIMULATED CA ²⁺ RELEASE FROM THE RYANODINE STORES OF CALCIUM IN THE ER IS REQUISITE FOR THE INCREASE IN THE CYTOSOLIC LEVELS OF CA ²⁺ | 62 |
| 2.3.9 | FSS STIMULATED INCREASE IN CYTOSOLIC CA ²⁺ IS REQUIRED AND SUFFICIENT FOR STIMULATED APICAL ENDOCYTOSIS | 64 |

| | | |
|--------|---|------------------------------|
| 2.3.10 | PRIMARY CILIA ARE REQUIRED FOR FSS DEPENDENT MODULATION OF ENDOCYTOSIS..... | 66 |
| 2.3.11 | PURINERGIC SIGNALING IS REQUIRED FOR FSS DEPENDENT MODULATION OF ENDOCYTOSIS..... | 68 |
| 2.4 | DISCUSSION..... | 69 |
| 2.5 | FUTURE DIRECTIONS..... | 74 |
| 3.0 | ROLE OF OCRL1 IN SHEAR STRESS STIMULATED APICAL ENDOCYTOSIS IN PROXIMAL TUBULE EPITHELIA | 78 |
| 3.1 | ABSTRACT..... | ERROR! BOOKMARK NOT DEFINED. |
| 3.2 | INTRODUCTION | 79 |
| 3.3 | RESULTS | 82 |
| 3.3.1 | FSS STIMULATED APICAL ENDOCYTOSIS IN OCRL1 DEPLETED PT CELLS IS DEFECTIVE | 82 |
| 3.3.2 | OCRL1 KNOCKDOWN CAUSES INCREASE IN CILIA LENGTH IN HUMAN PROXIMAL TUBULE CELLS | 84 |
| 3.3.3 | INCREASE IN CILIA LENGTH IS NOT RESPONSIBLE FOR DEFECTIVE FSS STIMULATED APICAL ENDOCYTOSIS | 86 |
| 3.3.4 | ATP AND RYANODINE STIMULATED ENDOCYTOSIS IS ABLATED IN OCRL1 DEPLETED CELLS | 88 |
| 3.3.5 | EGF STIMULATES ENDOCYTOSIS IN CONTROL AND OCRL1 DEPLETED CELLS | 90 |
| 3.4 | DISCUSSION:..... | 92 |
| 3.5 | FUTURE DIRECTIONS..... | 94 |

| | | |
|-------------------------|---|------------|
| 4.0 | MATERIALS AND METHODS | 97 |
| 4.1 | CELL CULTURE..... | 97 |
| 4.2 | SIRNA SEQUENCES..... | 98 |
| 4.3 | TRANSFECTION OF PROXIMAL TUBULE EPITHELIA | 98 |
| 4.4 | CALCULATION OF FSS..... | 99 |
| 4.5 | SET-UP OF FLOW-DEPENDENT ENDOCYTOSIS ASSAY | 101 |
| 4.6 | QUANTIFICATION OF FLOW-DEPENDENT ENDOCYTOSIS | 101 |
| 4.7 | MEASUREMENT OF $[Ca^{2+}]_i$ SIGNALING..... | 102 |
| 4.8 | INDIRECT IMMUNOFLUORESCENCE | 103 |
| 4.9 | MEASUREMENT OF CILIA LENGTH | 104 |
| 4.10 | TOTAL INTERNAL REFLECTION FLUORESCENCE IMAGING | 104 |
| 4.11 | WESTERN BLOTTING | 105 |
| APPENDIX A | | 106 |
| A.1 | INTRODUCTION | 106 |
| A.1.1 | Cellular functions of Calmodulin | 107 |
| A.1.2 | Cdc42..... | 108 |
| A.1.2 | N-WASP | 110 |
| A.1.3 | Cellular functions of ARP2/3 | 110 |
| A.1.4 | CDC42, N-WASP and ARP2/3 together orchestrate apical endocytosis in epithelial cells by modulating the cortical actin network..... | 111 |
| A.2 | ROLE OF CAM AND CAM ACTIVATED PROTEINS IN REGULATING FSS STIMULATED ENDOCYTOSIS | 114 |
| A.3 | ROLE OF CDC42 IN FSS STIMULATED ENDOCYTOSIS | 117 |

| | |
|---|------------|
| A.4 ROLE OF ACTIN DYNAMICS IN REGULATING FSS STIMULATED ENDOCYTOSIS..... | 120 |
| A.5 DISCUSSION..... | 122 |
| A.6 MATERIALS AND METHODS:..... | 124 |
| B.1 INTRODUCTION | 126 |
| B.2 PRIMARY CULTURES OF MOUSE PT ARE POLARIZED AND EXPRESS PT MARKERS: | 130 |
| B.3 RAB11A POSITIVE COMPARTMENTS IN PT CELLS RECEIVE FLUID PHASE CARGO..... | 133 |
| B.4 RAB11A POSITIVE COMPARTMENTS IN PTS RESEMBLE APICAL VACUOLES FOUND IN PROXIMAL TUBULES INVIVO. | 135 |
| B.5 APICAL VACUOLE LIKE COMPARTMENTS IN MOUSE PTS ARE HIGHLY DYNAMIC AND SORT MEMBRANE AND FLUID-PHASE CARGO:..... | 137 |
| B.6 DISCUSSION..... | 138 |
| B.7 APPENDIX B MATERIALS AND METHODS: | 141 |
| BIBLIOGRAPHY | 145 |

LIST OF TABLES

| | |
|--|----|
| Table 1. Ligands filtered through the glomerular barrier | 10 |
| Table 2 siRNA Sequences | 98 |

LIST OF FIGURES

| | |
|---|----|
| Figure 1. Schematic of the Multi-ligand receptors in the proximal tubule..... | 6 |
| Figure 2. Mechanosensors of the proximal tubule..... | 22 |
| Figure 3. OCRL1, structure, function and disease associated mutations..... | 28 |
| Figure 4. Apical endocytosis is robust in PT cell lines compared with cells from other segments of the kidney tubule. | 45 |
| Figure 5. Exposure to fluid shear stress increases apical albumin and dextran uptake in PT cell lines. | 47 |
| Figure 6. Time-course and FSS dependence of flow stimulated endocytosis | 50 |
| Figure 7. FSS stimulated endocytosis is rapidly reversible | 53 |
| Figure 8. Flow stimulated endocytosis is Clathrin and dynamin dependent | 55 |
| Figure 9. Exposure of pts to FSS causes an increase in both size and number of clathrin coated pits..... | 57 |
| Figure 10. FSS triggers an increase in cytosolic Ca ²⁺ | 59 |
| Figure 11 Calcium-stimulated calcium release from the ER causes the FSS stimulated increase in [Ca ²⁺] _i | 61 |
| Figure 12. FSS stimulated changes in intracellular calcium is requisite for the stimulation of apical endocytosis | 63 |

| | |
|---|-----|
| Figure 13. Primary cilia are requisite for the FSS stimulated responses | 65 |
| Figure 14. Purinergic signaling is requisite for the FSS stimulated responses | 67 |
| Figure 15. Model for acute modulation of apical endocytosis in the Proximal tubule..... | 73 |
| Figure 16. FSS stimulated apical endocytosis in OCRL1 depleted PT cells is defective..... | 81 |
| Figure 17. OCRL1 depletion leads to increased cilia length in human proximal tubule cells | 82 |
| Figure 18. Increase in cilia length does not cause defective FSS stimulated apical endocytosis . | 85 |
| Figure 19. ATP and ryanodine stimulated endocytosis is ablated in OCRL1 depleted cells | 87 |
| Figure 20. EGF stimulates endocytosis in control and OCRL depleted cells..... | 89 |
| Figure 21. Proposed model | 91 |
| Figure 22. Set-up of Flow-dependent endocytosis assay | 100 |
| Figure 23. Role of calmodulin and immediate downstream effectors in FSS stimulated endocytosis..... | 113 |
| Figure 24. Role of Cdc42 in FSS stimulated endocytosis | 116 |
| Figure 25. Critical role of actin dynamics in the FSS stimulated endocytic response | 119 |
| Figure 26. Proposed model for the downstream signaling cascade | 121 |
| Figure 27. Characterization of primary proximal tubule cell (PTC) cultures..... | 128 |
| Figure 28. Fluid-phase markers are not enriched in Rab11a-positive compartments in MDCK cells. | 132 |
| Figure 29. Rab11a-positive compartments in PTCs are highly dynamic | 134 |
| Figure 30. Segregation of megalin and albumin in PTC Rab11a-positive compartments..... | 136 |

PREFACE

I vividly remember the day I first stepped foot in the renal division at the University of Pittsburgh School of Medicine. I was here on a graduate school interview super-day, and that's when I first met Dr. Ora A. Weisz. She smiled while I rambled about the work I was doing as an intern in Boston, and said, "Keep an open mind, neuroscience isn't everything." About six months later, I joined her lab, and I knew she was right. I am extremely grateful to Dr. Weisz, my mentor, for being patient, and guiding me through the troughs and peaks of my graduate career. She has done more for me than I could have ever asked, and I have grown more under her tutelage than I ever did in my formative years. Her open-minded approach to problem solving, and constant push to innovate and expand the paradigms of our research have certainly rubbed off on me. She gave me several opportunities to mentor trainees across the experience spectrum, and these experiences truly enriched my graduate career. I am eternally grateful for all that she has done for me.

I would also like to thank my committee members Dr. Apodaca, Dr. Carattino, Dr. Kiselyov and Dr. Benos. I would like to thank Dr. Carattino for being a friend and a guide through my career at Pitt, and for training me to conduct live cell calcium monitoring experiments. I would also Dr. Apodaca for pushing me hard to structure better experiments, and rigorously test my hypotheses. I would also like to thank Dr. Benos, and Dr. Kiselyov for their

really great suggestions all through graduate school. Together my committee trained me to excel as a scientist overall!

I couldn't have done this thesis without the generous support of many people. First, I would like to thank my lab mates, for their continued support and for all the fun times over the past four years. I would like to thank Youssef Rbaibi for all his help in my primary project; I wouldn't have gotten this far if it wasn't for his help throughout my graduate career. I would also like to thank Dr. Baty for her insight into developing a FSS system to test my hypothesis. I would really like to thank my mentees Megan Eshbach, Francisco Carattino, and Simon Yohannes for being amazing students, and for their contributions to this work. I would really like to thank Dr. Mattila for sharing her experiences with me, and for being an amazing friend all through these years. Jennifer Bruns really helped me become a lot more organized when I started working in the Weisz lab, and I thank her for being a great friend! Over the past four years, I was fortunate to overlap with many former Weisz lab members. Dr. Alshogran was an awesome friend and teaching him helped me understand the premise of our experiments. I wish him the best on his new role as a professor at the Jordan University of Science and Technology. Dr. Youker taught me to use a confocal microscope, and I thank him for all the fun conversations we had in and outside the lab. Dr. Szalinski has been a tremendous source of support all through these years and I thank her for all the help. Dr. Mo has been an awesome friend all these years, and I wish her the best for her new baby! I would also like to thank Dr. Peter Friedman for stimulating conversations and Dr. McGarvey for help with FRET experiments.

I would also like to thank PIMB and my peers for all the fun times. I would really like to thank Susanna Godwin for being an awesome friend. I would also like to thank my classmates Branden and Stefan for being awesome buddies. I wish them both the best in their careers.

I would like to thank Dr. Anna Krichevsky, Dr. Sabrina Absalon and Dr. Galina Gabriely for teaching me all I know about molecular biology and for fostering my curiosity for life science research

I wouldn't be here if it wasn't for my friends outside the lab, who have watched out for me over the past four years, and have been strong pillars of support. I would first like to thank Venkat & Shuchi for being such awesome friends over the past four years. Right from introducing me to my fiancé, to cooking meals for me and dropping me back at the lab after every house party, you've just been awesome people! I would also like to thank Partha, Deepa, Sriram, Kavya, Vinay, Anusha, and all my other pals in Pittsburgh, for making this city livable. I would also like to thank Shivaram Shankar who has been an awesome friend for the past two decades. I would also like to thank my friends from high school who have supported me all through these years. I would also like to thank Vignesh, Sharath, Satheesh, and Prasanna for their support all though these years.

I would also like to thank my friend, philosopher, guide, and sister Bhooma Nalin for all her support all through these years. I wouldn't have chosen to study Biology if it wasn't for you. I would also like to thank Nalin for all the good times!

My parents made me the person I am, and I am eternally grateful for all their hard work, sacrifice and prayers, without which I wouldn't be here. I would especially like to thank my father for pushing me to go to graduate school, and for filling out my PIMB application 5 years back. You changed my life.

Finally, I would like to thank my fiancé Janani Jayaraman for being a pillar of support and for your patience all through these years. You made the past three years so much fun!! I would really like to dedicate this thesis to you.

1.0 INTRODUCTION

1.1 ANATOMY OF THE MAMMALIAN KIDNEY

The kidney in higher mammals filters blood plasma to remove toxins from our system. It is also the principal organ involved in regulating blood pressure, electrolyte balance, acid-base balance, and blood plasma composition. It receives the unfiltered blood through the renal artery and returns filtered blood through the renal vein to the inferior vena cava (1). The kidney contains two distinctive regions: the medulla, a discontinuous layer shaped like a pyramid, and the cortex, a continuous layer surrounding the medulla and extending to the outer portion of the kidney (2). In higher mammals, this complex three dimensional organ is made up of several fundamental functional building blocks called nephrons. Nephrons consist of five distinct segments: glomerulus, proximal tubule, loop of Henle, distal tubule and collecting duct, each of which is responsible for carrying out distinct functions.

In humans, the glomerulus is surrounded by Bowman's capsule and consists of endothelial cells, glomerular basement membrane and podocytes. The renal tubule comprises the proximal tubule, the loop of Henle, the distal tubule and the collecting duct. The glomerulus receives its blood supply from an afferent arteriole, which forms a network of capillaries through the fenestrated endothelium. The filtration takes place at the glomerular basement membrane and

slit-diaphragm. The blood pressure within the glomerulus serves as the driving force for filtration of water and solutes from the blood and into Bowman's capsule. This filtration is based on molecular weight, size, shape and electrical charge of the molecule such that large and negatively charged macromolecules are retained and those small and positively charged pass through into the filtrate.

The proximal tubules are the primary recipients of the glomerular filtrate and are critically important in retrieving 70% of water, ions and all the low molecular weight proteins from the filtrate. I will be discussing this segment in rigorous detail in section 1.2.

The Loop of Henle further recovers sodium, water and chloride from the glomerular filtrate. The descending limb is impermeable to urea and ions, and reabsorbs water, the loop is permeable to water and ions, the ascending limb and the thick ascending limb reabsorb sodium, potassium and chloride ions (2).

The distal convoluted tubule is the portion of the nephron that is immediately downstream of thick ascending limb that stems from the loop of Henle. The DCT is the shortest segment of the nephron, spanning only about 5 mm in length in humans, it plays a critical role in a variety of homeostatic processes, including sodium chloride reabsorption, potassium secretion, and calcium and magnesium handling. It is capable of responding to changes in hormonal changes such as aldosterone and in turn regulates the reabsorption of ions from the glomerular filtrate (2). The collecting duct determines the final amount of Na^+ K^+ and Cl^- that is eliminated in the urine.

The filtrate finally gets collected in the collecting duct that concentrates the urine received from different nephrons and regulates ion, and electrolyte reabsorption in response to changes in anti-diuretic hormone and aldosterone. The tubules are lined by principal cells and intercalated cells which perform the critical functions of the collecting duct. The filtrate from the collecting duct drains into the ureters and gets collected in the bladder as urine (2).

1.2 PROXIMAL TUBULE FUNCTION

The proximal tubule is the segment of the nephron that leads from the Bowman's capsule to the loop of Henle. As mentioned earlier, it plays a critically important role in retrieving important metabolites and low molecular weight proteins. The proximal tubule in turn is further segmented into three morphologically distinct parts. The S1 and the S2 segment together comprise the proximal convoluted tubule and S3 segment forms the proximal straight tubule that drains the glomerular filtrate into the descending limb of the loop of Henle (1). The epithelial cells that line the S1 and S2 segments of the proximal tubule are much taller than the cells that line the S3 segment and EM studies of rat proximal tubules have shown that all these cells present with elaborate brush border microvilli. The expression of some proximal tubule markers, such as γ -glutamyl transpeptidase, increases from the S1 to the S3 segment, whereas expression of the multiligand receptor megalin decreases (1, 3). The cells that line the proximal convoluted tubule have higher endocytic capacity and increased in comparison to the S3 segment.

In the next sections, I will be discussing in detail the characteristics of the proximal tubule that uniquely enable them to conduct the function of protein retrieval. I will also be

discussing the organization and regulation of the apical endocytic pathway in the proximal tubule epithelia. Further, I will discuss our current understanding of the mechanosensors of the proximal tubule and their function, and briefly describe diseases caused by proximal tubule dysfunction.

1.2.1 Multiligand receptors of the proximal tubule:

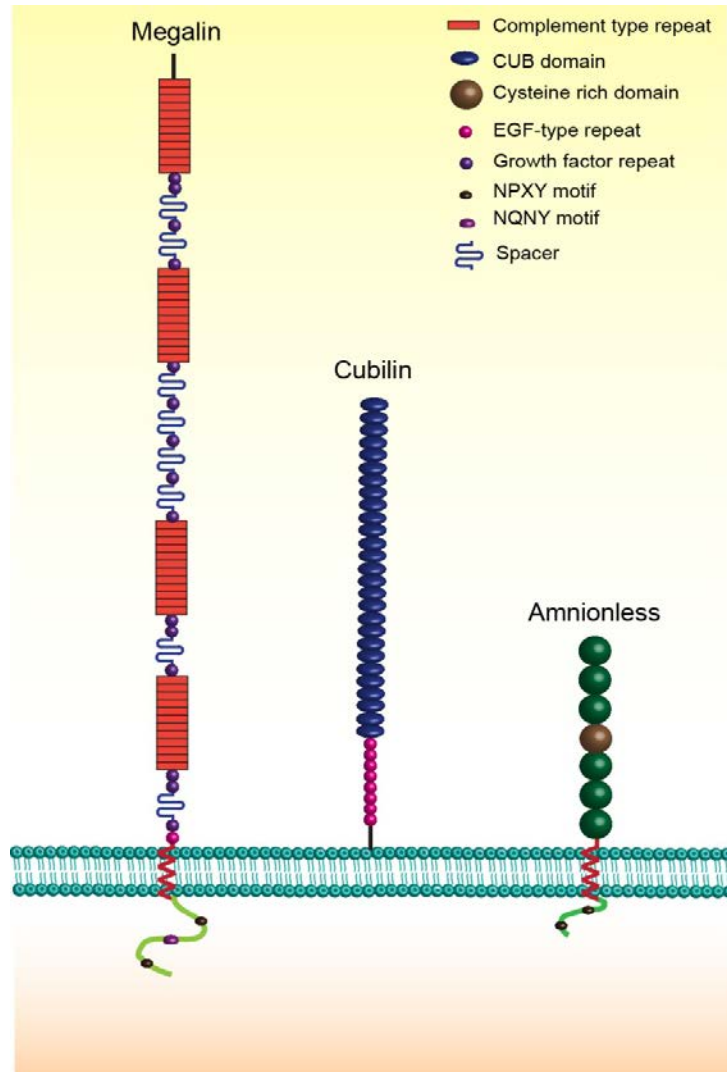
The multiligand receptors megalin and cubilin coordinate the uptake of most filtered proteins and many other small bioactive molecules from the ultrafiltrate. This section will provide a brief review of the structure, interactions, and trafficking of these proteins in the proximal tubule. Megalin and cubilin are also expressed both individually and together in other tissues and the reader is referred to an excellent review for a more detailed discussion of their possible functions at those sites (4).

Megalin (aka gp330, LRP2) is a member of the LDL receptor family of proteins that was originally identified by Farquhar and colleagues as a major pathogenic antigen in Heymann Nephritis in 1982 (5) and found to be equivalent to “brushin”, a ~600 kDa proximal tubule brush border protein previously described by the Muramatsu group (6). Within the kidney, megalin is expressed primarily at the apical surface and in apical endocytic compartments of epithelial cells that comprise the S1 segment of the proximal tubule, with decreasing expression in the S2 and S3 segments of the proximal tubule. Megalin is also expressed in podocytes, and it appears that antigenic responses to megalin in these cells (as opposed to the proximal tubule) is a primary cause of Heymann Nephritis (7).

The sequences of rat and human megalin were reported in 1994 and 1996, respectively (8, 9). Rat megalin contains 4660 amino acids and is a type I transmembrane protein with a large luminal domain that contains 36 LDL-R ligand binding complement type repeat motifs clustered into four domains. These domains are interspersed with EGF type repeats and beta propeller spacers characterized by YWTD motifs which mediate ligand dissociation in acidified compartments [for an excellent review on the structure and function of LDL receptor family member domains please see (10)]. The cytoplasmic tails of all LDL receptor family members are divergent other than the presence of two NPXY motifs that mediate endocytosis and an NPXY-like motif VENQNY (8) that may be important for apical delivery of the protein (11, 12). Like other members of LDLR family, megalin also contains an RXRR motif that can be cleaved by furin and related proteases. Cleavage at this site could explain the soluble form observed associated with cells and secreted into the urine (13). Megalin has also been demonstrated to undergo regulated intramembrane cleavage (14); however, the physiological significance of this is unclear (15, 16).

Folding and biosynthetic trafficking of megalin is facilitated by its interaction with a chaperone protein RAP (for receptor-associated protein) that is localized primarily to the endoplasmic reticulum but which can also accompany megalin to the plasma membrane (17, 18) and dissociates from the receptor in acidified compartments (19). RAP also interacts with the LDLR-related protein LRP. It has been proposed that binding to RAP prevents premature interaction of megalin with ligands along the biosynthetic pathway (18)

Figure 1. Schematic of the Multi-ligand receptors in the proximal tubule



The above schematic depicts the three multiligand receptors expressed in the proximal tubule. Megalin as described in the text and in table 1, regulates the uptake of most of the low molecular weight proteins from the glomerular filtrate and together with amnionless plays a critical role in the trafficking of cubilin and its ligands. Both megalin and amnionless have cytoplasmic tails that contain NPXY or NQNY consensus sequences that help them recruit clathrin adaptors to endocytic pits. The role of the different domains of these proteins is discussed in further detail in the text.

Megalin is the major calcium binding protein in the PT and was originally suggested to function as a calcium sensing receptor based on the observation that function-blocking antibodies that inhibited calcium regulation in parathyroid cells recognized megalin in proximal tubule cells (20, 21). Subsequent studies aimed at identifying the function of megalin demonstrated that it interacts with several proteins that also bind to LRP, including ApoE and lipoprotein lipase. Since then, interaction of megalin with an increasing number of filtered ligands has been reported (22). An essential role for megalin in the uptake of albumin and other filtered proteins was cemented in 1996 by the demonstration that mice lacking megalin exhibit low molecular weight proteinuria (23) and by the observation that RAP competes with albumin uptake in microperfused tubules (24) and together with animal studies, established the vital importance of this receptor in protein scavenging.

Cubilin is a 460 kDa receptor expressed abundantly in the proximal tubule that interacts with megalin and increases the multiligand binding capability of the complex. Cubilin was originally identified as the receptor for intrinsic factor-vitamin B₁₂ complex in the intestine (25) and subsequently shown to be identical to a previously described antigen that localized to coated pits in the rat proximal tubule (26, 27). The receptor was cloned from rat yolk sac in 1998 and named cubilin due to the presence of 27 tandem CUB domain repeats that encompass the majority of the protein sequence (28). Unlike megalin, cubilin has no transmembrane domain, and requires megalin for its association with the membrane. Cubilin binds to several of the proteins recognized by megalin, including albumin, hemoglobin RAP, and Ig light chains. In addition, cubilin has also been suggested to bind to other proteins that do not bind to megalin, including transferrin, intrinsic-factor vitamin B₁₂ complex, and apoA1. Cubilin-specific ligands

were originally identified in the urine of dogs with mutations in cubilin and in patients with Imerslund-Gräsbeck syndrome, who have vitamin B₁₂ malabsorption. However, there may be some species specific differences in cubilin binding selectivity, as unlike dogs lacking functional cubilin, cubilin knockout mice showed no increase in urinary excretion of transferrin (or apoA1) (29, 30).

Cubilin also interacts with amnionless, a 38-50 kDa transmembrane protein that like megalin, contains cytoplasmic NPXY motifs that direct internalization. Amnionless appears to be essential for cubilin transport to the apical surface, as cubilin is retained intracellularly in proximal tubule cells of amnionless knockout mice (31) and mutations in amnionless also cause Imerslund-Gräsbeck syndrome (32). Cubilin has been demonstrated to bind simultaneously to megalin and amnionless (33) but whether and how these three proteins interact functionally at the apical membrane of proximal tubule cells remains unclear.

Table 1 lists all the ligands known to be retrieved by the proximal tubule through their interactions with the multi ligand receptors megalin and cubilin. Megalin and cubilin together retrieve ~33 unique ligands from the glomerular filtrate. In my studies conducted in this thesis, I used fluorescently labeled albumin as a model ligand, as retrieval of albumin is orchestrated by both megalin and cubilin. I investigated both the regulation of albumin retrieval (studied in Chapter 2, Appendix A & B) and probed the reasons underlying the cause of low molecular weight proteinuria associated with a rare genetic disease called Lowe syndrome (Chapter 3).

More recently, the ubiquitously expressed MHC-related Fc receptor for IgG (FcRN) has also emerged as a potential receptor that participates in IgG and albumin recovery from the ultrafiltrate. This heterodimeric receptor, comprised of an MHC class I-like α chain and its obligatory β 2-microglobulin subunit, binds independently to IgG and to albumin at acidic pH but not at neutral pH. FcRN is known to play an important role in salvaging serum IgG and albumin in many non-renal tissues [reviewed in (34)]. The current model is that these proteins are taken up by pinocytosis and bind to FcRN in acidified compartments. Proteins that bind to FcRN escape the default route to the degradative pathway and are instead recycled to the cell surface where the increase in pH causes them to be released. Consistent with this model, FcRN knockout mice have half the levels of serum albumin as normal mice, apparently due to increased degradation kinetics (35).

Table 1. Ligands filtered through the glomerular barrier

| Megalin | Cubilin |
|--|--|
| <i>Vitamin binding proteins</i> | |
| Transcobalamin-vitamin B ₁₂ | Intrinsic factor-vitamin B ₁₂ |
| Vitamin D binding protein | Vitamin D binding protein |
| <i>Retinol binding protein</i> | |
| Apolipoproteins | |
| Apolipoprotein B | Apolipoprotein A-I |
| Apolipoprotein E | HDL |
| Apolipoprotein J/clusterin | |
| Apolipoprotein H | |
| <i>Low molecular weight peptides</i> | |
| PTH | |
| Insulin | |
| β_2 -microglobulin | |
| Epidermal growth factor | |
| Prolactin | |
| Lysozyme | |
| Cytochrome c | |
| α_1 -microglobulin | |
| PAP-1 | |
| Odorant-binding protein | |
| Transthyretin | |
| Other | |
| Albumin | Albumin |
| RAP | RAP |
| Ig light chains | Ig light chains |
| Hemoglobin | Hemoglobin |
| Plasminogen | Transferrin |
| Lactoferrin | Clara cell secretory protein |
| Thyroglobulin | |
| Ca ²⁺ | |
| Drugs and toxins | |
| Aminoglycosides | |
| Polymyxin B | |
| Aprotinin | |
| Trichosanthin | |
| Enzymes and enzyme-inhibitors | |
| PAI-1 | |
| PAI-1-urokinase | |
| PAI-1-tPA | |
| Prourokinase | |
| Lipoprotein lipase | |
| α -amylase | |

Table1. is adapted from Christensen et al. 2012

FcRN is expressed abundantly in the glomerulus and proximal tubule of the kidney. Within the glomerulus, FcRN expressed at the surface of podocytes may function to scavenge albumin and immunoglobulins from the basement membrane to limit clogging of the filtration barrier (36). In contrast, in the proximal tubule it has been suggested that FcRN binds to soluble albumin that dissociates from megalin/cubilin in acidified endocytic compartments and delivers it via transcytosis to the basolateral surface for reentry into the plasma (37). The extent to which this pathway in the proximal tubule contributes to serum albumin levels remains controversial. One key issue is the amount of albumin that actually reaches the proximal tubule. Micropuncture studies suggest that filtration is extremely efficient, with a glomerular sieving coefficient of ~ 0.0006 (38). More recent *in vivo* fluorescence-based and other measurements have varying reported results consistent with micropuncture studies or much higher values [nicely reviewed in (39)]. These measurements are complicated in part because low levels of fluorescently-tagged albumin entering the tubule must be quantified adjacent to the very high fluorescence levels of albumin injected into the circulation which enters the glomerulus, and the differences in results obtained are dependent in part on the settings used to establish fluorescence thresholds (40-42). Another key issue that remains to be addressed is the extent to which transcytosis of albumin occurs in the kidney, and how much of this is mediated by FcRN. *In vitro* studies using immortalized proximal tubule cells report apical to basolateral transcytosis of the megalin ligand retinol binding protein, which does not bind to FcRN, in immortalized rat proximal tubule cells (43). Similarly, *in vivo* studies have qualitatively documented transcytosis of ferritin across the rabbit proximal tubule, and folate and albumin across the rat proximal tubule (44-46). Tenten et al. attempted to address the role of FcRN mediated transcytosis of post-filtered albumin by observing the appearance in serum of tagged albumin expressed selectively in podocytes of

control and FcRN knockout mice (37). Moreover, this study made elegant use of two differentially charged versions of albumin to assess the potential contribution of backfiltration from podocytes through the negatively charged filtration barrier (37). Although tagged albumin could be detected in the serum, the capacity of this salvage pathway relative to the degradative pathway in proximal tubule cells could not be assessed in this study. Of note, however, earlier studies assessing the fate of radioiodinated albumin in HK-2 human proximal kidney cells, in perfused *ex vivo* rat kidneys, and in microperfused rabbit proximal tubules concluded that the majority of internalized albumin was degraded rather than transcytosed to the basolateral surface (47, 48).

1.2.2 Organization of the apical endocytic pathway in the proximal tubule:

As noted in the introduction, the apical endocytic pathway in proximal tubule cells is highly specialized for robust internalization, and is uniquely organized for this function (49). This preference for apically-driven endocytosis and the consequent organization of the endocytic pathway is recapitulated to differing extents in primary and immortalized cell culture models of the proximal tubule (3, 50, 51). To date, our most detailed information about the organization, cellular machinery, and regulation of the apical endocytic pathway in renal epithelial cells comes from studies conducted in Madin-Darby Canine Kidney (MDCK) cells, which maintain a limited apical endocytic capacity. As such, it is important to consider that findings in these cells may not necessarily translate into an accurate understanding of PT endocytic regulation. In the sections below, I describe briefly the current model for the PT endocytic pathway based on *in vivo* studies

and attempt to extend this model where possible based on results obtained using cell culture models.

Several key features of endocytosis are consistent in all cell types. These include the internalization of receptor-ligand complexes and other proteins in clathrin-coated or other vesicles, fusion of uncoated vesicles with each other and/or early endosomes, pH dependent dissociation of ligands from receptors in acidified compartments, recycling of membrane proteins to the surface in tubular structures that emanate from these endosomes, maturation of the globular portions of endocytic compartments into late endosomes, and transient fusion of invaginated late endosomes with lysosomes to deliver soluble ligands and membrane proteins (52, 53). Small GTP binding proteins termed Rabs are sequentially recruited onto these compartments and in turn activate downstream effectors that mediate changes in phosphoinositide composition, recruitment of motors and other cytosolic proteins, and ultimately Rab exchange to gradually alter the identity of these compartments along the endocytic cascade. While these steps likely also govern the progression of the PT apical endocytic cascade, we lack a detailed understanding of the identity of individual compartments that have been defined largely using morphological rather than molecular criteria.

In MDCK and several other polarized epithelial cell lines, proteins internalized from the apical plasma membrane via clathrin-dependent pathways enter Rab5 positive early endosomes that are slightly acidic (pH ~6.9)[reviewed in(54)]. Membrane proteins can recycle to the surface from this compartment via Rab4-positive tubules via a pathway termed fast recycling (55). A subset of membrane proteins escapes this step and traverses a supranuclear recycling

compartment of pH ~6.4 (Wand and Dunn) localized near the centrosome that has subdomains positive for Rab11a, Rab11b, and Rab25 (55, 56). A related recycling compartment marked by Rab8 also receives some apically recycling proteins in addition to cargo internalized from the basolateral surface (57-59). This compartment is called the central recycling endosome. The relationship between Rab8- and Rab11-positive compartments remains unclear, and discrepancies in the literature may reflect clonal drift between MDCK cell populations or other technical differences between studies from different laboratories (60, 61). Rab14 is another small GTPase which is known to play a critical role in delivering raft associated proteins to the apical surface in MDCK cells (62, 63). However, proximal tubule cells do not express Rab14 suggesting a redundant role for other Rabs or a significantly different arrangement of the apical endocytic pathway in PT cells. The proteins which transit the recycling endosomes either are recycled back to the surface, or enter other endosomal compartments deeper in the endocytic pathway. The retromer complex, is one such protein complex that sorts proteins and modulates the transit of proteins from the recycling compartments into the *trans*-Golgi network (TGN) (64). In most cases, recycling endosomes mature into later endosomal compartments, as they go through the Rab switch cascade, and the proteins localized in these compartments are ultimately targeted to lysosomal degradation.

Only some features of the apical pathway as described in MDCK cells appear to be recapitulated in PT cells *in vivo*. Indeed, electron microscopy studies investigating the internalization of filtered fluid-phase and membrane tracers in rodent proximal tubules have provided a very different morphological view of the apical endocytic pathway (49, 65). In these studies, rats, mice or rabbits were administered intravenous injections of the membrane and fluid

phase traces, and the kidneys were fixed by vascular perfusion at different time intervals to capture the maturation of the endocytic vesicles. Both fluid phase and membrane cargoes are internalized into clathrin coated structures that bud from the base of the brush border microvilli (49, 65-68). These clathrin coated invaginations are considerably more irregular in size and shape than those observed in other polarized cells such as MDCK cells or intestinal epithelial cells *in vivo*. This difference in endocytic pit structure may reflect the robust apical endocytic capacity of PT cells. The internalized invaginations are thought to release their clathrin coats and subsequently fuse with a dense subapical network of tubules (68, 69). Both membrane and soluble cargo in these compartments rapidly accesses large vacuolar compartments termed Apical Vacuoles (AVs) within 1-15 min after internalization. Recycling of membrane receptors and other proteins to the apical surface can occur from both the subapical tubules and from AVs (67). In contrast, ligands retrieved from the glomerular ultrafiltrate dissociate from megalin and cubilin within endocytic compartments as described below and are targeted to lysosomes for degradation and/or transcytosed and released in the basolateral milieu.

Apical endocytosis in PT epithelia is dependent on clathrin, actin, microtubules, and protein kinases. In addition to clathrin-dependent endocytic pathways, many polarized cells possess alternate internalization routes that do not require assembly of clathrin-coated structures. One major such pathway utilized in MDCK cells involves the internalization of M1-muscarinic receptor ligands via caveolae, which are small U-shaped structures whose formation is controlled by caveolins (70). Caveolar membranes are enriched in cholesterol, gangliosides, and saturated lipids that partition into semi-stable microdomains sometimes termed lipid rafts. However, although some PT immortalized cells express caveolin, this protein is apparently absent from PT

cells *in vivo* (71). Additional evidence corroborates the likelihood that apical endocytosis in PT cells *in vivo* occurs entirely via clathrin dependent pathways. Early EM studies of rodent PTs showed that the endocytic invaginations at the base of the microvilli are coated with electron dense clathrin cages that mediate membrane internalization (65). Subsequent clathrin coated pit and microvillar membrane fractionation studies conducted in rat PTs confirmed that apical multiligand receptors cluster in these coated pits upon ligand binding, before being internalized into tubular structures. Studies in immortalized OK cells, a well differentiated immortalized cell line that retains many characteristics of the PT, further support the requirement for clathrin in endocytosis of albumin (72, 73). Treatment of these cells with chlorpromazine, an inhibitor of clathrin-dependent endocytosis, or with inhibitors of the GTPase dynamin that regulates vesicle fission from the membrane, led to a dose-dependent inhibition of albumin uptake. In contrast, the cholesterol perturbing drugs filipin and nystatin, which perturb formation of caveolae, had no effect on albumin uptake (74, 75).

Uncoating of clathrin coated cages is ATP dependent and is an important step in the endocytic pathway. Therefore lowering cellular levels of ATP, for example by incubating cells with maleate disrupts apical endocytosis (65). Early studies suggested that megalin was always found in clathrin coated pits but not in endosomal compartments suggesting that these pits were retrieved selectively in PT cells (7). Later, immuno-gold labeling of rat PTs showed localization of anti-megalin antibodies within clathrin coated pits and in apical tubular compartments that were segregated from fluid phase cargo containing vesicles, suggesting that fast recycling may occur from these sites (76, 77). In MDCK cells, fast recycling is mediated via Rab4 positive compartments, which interface with the Rab5 positive early endosomal compartments to

coordinate rapid recycling of membrane proteins through a hybrid apical compartment (53). In one study conducted in zebrafish pronephros, megalin was found to transit through a Rab4 positive apical tubular compartment, suggesting the existence of a rapid recycling pathway in these PTs (78). The endocytic uptake of fluid phase markers through the Rab5 positive apical tubules is regulated by the Rab5 adaptor rabankyrin-5 (79).

In addition to Rabs 4, 5, and 11, a role for Rab38 in apical endocytosis in PT cells has recently emerged. Fawn-hooded hypertensive rats present with high low-molecular weight proteinuria, apparently due to knockout of this GTPase. Ectopic expression of Rab38 rescues the proteinuric phenotype in the rats, consistent with the idea that Rab 38 is a critically important component of the cascade in mediating and regulating apical endocytosis in proximal tubule epithelia (80).

Endocytosis of albumin is also highly dependent on the integrity of the actin and microtubule cytoskeletons. In OK cells, disruption of F-actin using cytochalasin-D or depolymerization of microtubules using nocodazole reduced endocytosis of albumin to <5% and <55% of that measured in untreated control cells respectively (72). Actin and microtubules may act as lines of transport to traffic endocytic vesicles. Cytoskeletal proteins, molecular motors and GTPases mediate the endocytic uptake of low-molecular-weight proteins. Myosin Heavy Chain 9 (MYH9), Myosin VI, actin and GIPC are requisite for driving microvilli localized megalin into clathrin coated pits. Deletion of MYH9, or Myosin VI in mouse models cause excessive low-molecular weight proteinuria, which underscores their importance in regulating apical

endocytosis (81, 82). Knockout of Myosin VI in mice causes lower association of Dab-2 with the clathrin coated pits, which in turn leads to defects in endocytosis and tubular proteinuria (82).

Acidification of endocytic vesicles and cargo sorting: Vacuolar H⁺ ATPase present on the PT apical surface and in endosomal compartments regulates a pH drop along the endocytic cascade. The pH of the glomerular ultrafiltrate in the lumen is ~7.4 and decreases to ~6.3 in apical vacuolar recycling compartments (83). This drop in pH triggers the dissociation of ligands bound to megalin and cubilin. Interestingly, albumin and IgG bind more tightly to the FcRN receptor at these lower pHs, and thus some released ligands may switch receptors within endocytic compartments to avoid default delivery to lysosomes (84).

Apical recycling of endocytic cargo in PT epithelia:

Internalized megalin and fluid phase markers such as HRP and also rapidly access AVs. AVs also act to segregate membrane bound and fluid-phase cargo (49, 67-69). EM studies document tubule like structures emanating from AVs that are thought to be enriched in membrane receptors and which may mediate their recycling to the apical surface via the “slow recycling” pathway. Based on two studies conducted in rabbits, the velocity of recycling from AVs has been estimated to be $\sim 6.2 \times 10^{-3} \mu\text{m}^2 \mu\text{m}^{-3} \text{s}^{-1}$. Electron microscopy studies of rabbit PTs perfused with inulin-gold have documented the existence of faster recycling pathways where cargo could be recycled by early dense-tubular structures which have very high surface to volume ratio (67).

Functionally, AVs may correspond to the Rab11-positive apical recycling endosome that mediates slow recycling in MDCKs. In Appendix B, I show that in PT cells isolated from mouse kidney cortex had numerous highly dynamic structures of varying sizes that morphologically resemble AVs (3). The identities of the other endocytic compartments in PT cells are still unknown, and the burden still remains on the field to investigate and determine the details of the apical endocytic pathway in PT cells.

The distinct organization of the endocytic pits observed in rat proximal tubules is not recapitulated by cells in culture (3). When we isolated primary proximal tubule cells from adult mouse kidneys, we observed that the cells in culture lost most of their brush-border microvilli, and instead had very rudimentary stubby microvilli (Appendix B). Also, the cells were not especially endocytically active, and the unusual tubule shaped clathrin coated invaginations were absent on the apical surface (Appendix B). Further, most of our understanding of the organization of the apical endocytic pathway in renal epithelial cells comes from studies conducted in Madin-Darby Canine Kidney (MDCK) cells where the organization of the apical recycling endosomes are extremely tubular and stable, as opposed to dynamic and vacuolar as we observe in primary mouse proximal tubule cells. Most PT derived cell lines, with the exception of OK cells, are not very well differentiated, and fail to retain their brush-border microvilli and tight junctions. Therefore, we should take these caveats into consideration while using cell lines as model systems to study the organization of the apical endocytic pathway.

Adaptors, CLASPS, and scaffolds that mediate apical endocytosis in PT cells

Clathrin adaptor proteins bind to multi-ligand receptors and regulate the endocytosis of their ligands. Apical endocytosis of megalin is regulated by clathrin adaptor Disabled 2 (Dab2) and CLASP Autosomal recessive hypercholesterolemia (ARH) which bind to the NPxY motifs of the cytosolic tail of megalin. Dab2 knockout mice present with mild low molecular weight proteinuria which underscores the role Dab2 plays in clearing Low molecular weight proteins (LMWP) from the glomerular filtrate (85). ARH colocalizes with megalin first at clathrin coated pits, then is found to associate with megalin in the pericentriolar recycling compartments and in the way back to the surface. In MDCK cells overexpressing mini-megalyn, ARH was shown to regulate the uptake of lactoferrin (76). There is evidence for ARH in regulating the proteolysis, mRNA level expression of megalin, and in targeting megalin to apical early endosomes (86). However, these functions of ARH in PT cells remain to be tested.

Other regulators of apical endocytosis in PT cells

Other transmembrane receptors like NHE3, CLC5, Angiotensin II type I receptor (AT1R), and Angiotensin II Type II Receptor (AT2R) also regulate apical endocytosis in PT epithelia. NHE3 (a Na⁺/ H⁺ exchanger) and CLC5 (a hydrogen-chloride antiporter) are known to directly associate with megalin and to traffic in the same compartments as megalin. AT1 and AT2 R have been widely implicated in regulating angiotensinogen uptake and in regulating associated signaling cascades (87).

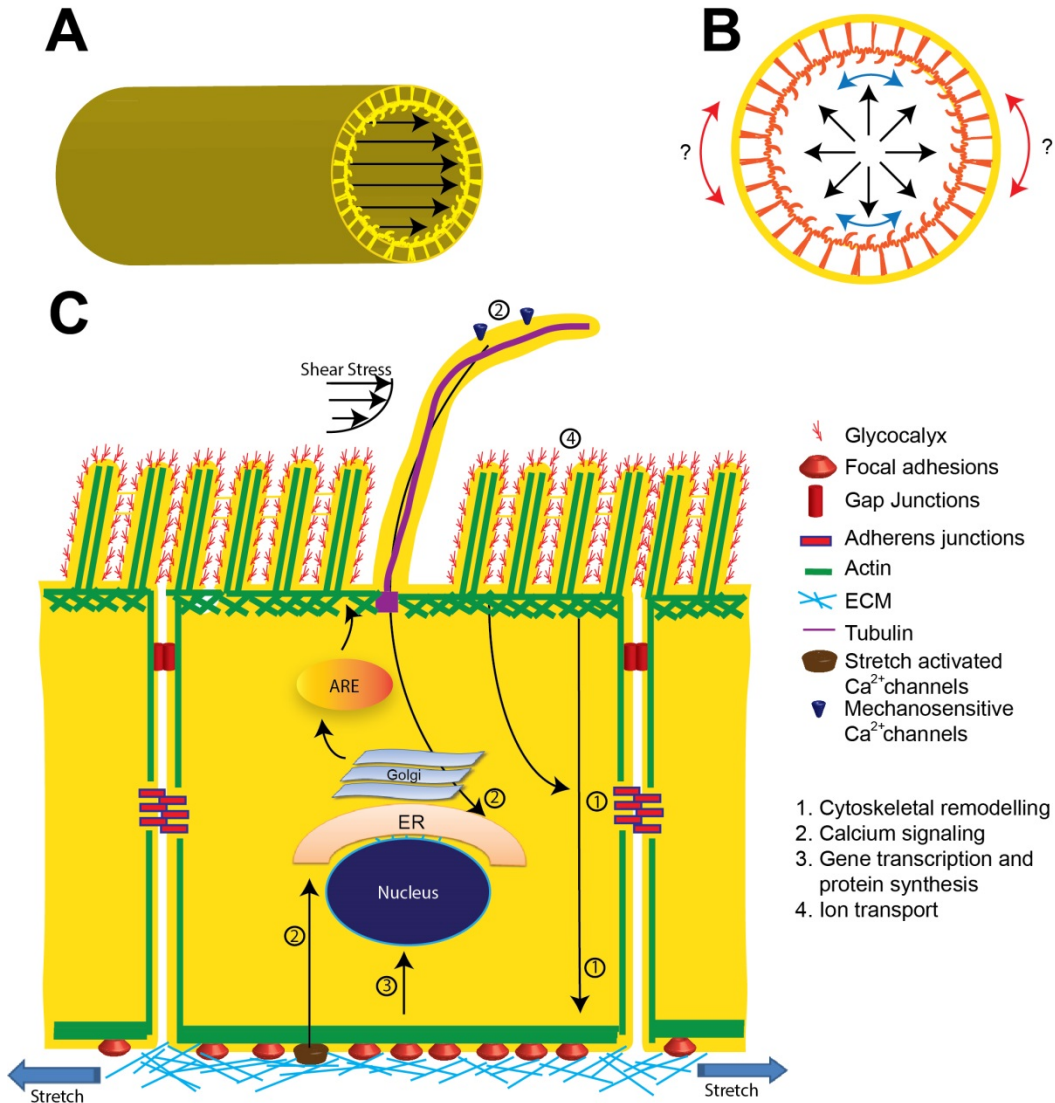
A unique feature of PT cells is that apical expression of megalin regulates the amount of apical endocytosis, and conversely the endocytic load regulates the apical expression of megalin. Megalin is specifically expressed in the zebrafish larval pronephros, and when knocked out,

results in the disappearance of Rab4-positive apical endosomes, and impairs the endocytic uptake of both membrane bound and fluid-phase cargo (88). Similarly, EM analysis of megalin KO mice revealed dramatic ultra-structural changes in the PT, including loss of clathrin-coated pits and vesicles. Conversely, the amount of albumin load controls the expression of megalin and its interaction with Protein Kinase B (PKB) in LLCPKI cells (89). Physiologic levels of albumin modulates the interaction of megalin with PKB, but when the cells were incubated with pathophysiologic levels of albumin overnight, the mRNA and protein levels of megalin decreased and so did its interaction with PKB (89).

1.2.3 Mechanosensation in the proximal tubule:

All cells in the body experience external mechanical forces such as shear stress and stretch. These forces are sensed by specialized structures in the cell known as mechanosensors. Cells lining the proximal tubule (PT) of the kidney are continuously exposed to variations in flow rates of the glomerular ultrafiltrate which manifest as changes in axial shear stress and radial stretch. Studies suggest that these cells respond acutely to variations in flow by modulating their ion transport and endocytic functions to maintain glomerulotubular balance. Conceptually, changes in the axial shear stress in the PT could be sensed by three known structures, namely, the microvilli, the glycocalyx, and primary cilia. The orthogonal component of the force produced by flow exhibits as radial stretch and can cause expansion of the tubule. Forces of stretch are transduced by integrins, by stretch-activated channels, and by cell-cell contacts all of which could act as mechanosensors, but their detailed discussion is outside the scope of this thesis.

Figure 2. Mechanosensors of the proximal tubule



(A) Schematic of the manifestation of flow as apical shear stress. (B) Increases in flow also manifest as radial stretch, a force exerted perpendicularly to the walls of the PT (blue arrows). Whether this stretch is also transduced to the basolateral surface (red arrows) in normal kidney tubules is unclear. (C) Mechanosensory cascades in the PT initiated by shear stress and stretch. Small changes in the bending of microvilli in response to shear stress are amplified by the apical cortical actin network to trigger downstream responses that include cytoskeletal re-organization (i.e. actin restructuring and formation of focal adhesions and tighter adherens junctions), redistribution and activation of ion transporters, and repositioning of apical endosomes. The glycocalyx may serve to increase the frictional coefficient of the apical surface and amplify the effects of microvillar bending. Basolateral and apical stretch causes integrin mediated cytoskeletal re-organization, Ca^{2+} signaling through stretch-activated calcium channels, and regulation of gene transcription and protein synthesis. See text for further details.

The role of flow in regulating ion reabsorption across the PT epithelium was initially studied using single tubule micropuncture and microperfusion of rat PTs in the early 1960s. These studies demonstrated that reabsorption of Na^+ , HCO_3^- , K^+ , and water were enhanced when perfused at higher flow rates in comparison to lower flow rates (90-94). Studies conducted since that time have shown that the apical surface of PT cells sense changes in shear stress through their microvilli and primary cilia, and that integrins and stretch sensitive channels on the basolateral surface can transduce changes in stretch into physiological responses (95-97). Our current understanding of the role of these cellular assemblies/structures in PT mechanosensation is summarized below.

PT mechanosensitive responses to shear stress. The most commonly used methods to study shear stress dependent effects are microperfusion of individually dissected tubules, tubular micropuncture, and exposure of cultured cells to fluid shear using parallel plate flow chambers. The microvilli, primary cilia, and the glycocalyx on the apical surface of PT cells have all been suggested to sense changes in the flow of glomerular filtrate entering the tubule lumen as described below.

Microvilli: The apical surface of rat PT cells contains ~6500 microvilli each approximately 2.8 μm in length. Each of these structures contains ~25-35 actin filaments arranged in bundles and cross-linked by fimbrin, villin, and espin (98). Beneath the apical surface, these filaments are integrated into a dense actin meshwork that can transduce and amplify even small changes in the bending of microvilli into signaling events that ultimately regulate ion-transport, cytoskeletal reorganization, biosynthetic traffic, and changes in endosome distribution. These changes are believed to be independent of the primary cilium because cells

were plated and studied prior to ciliogenesis (99). For a more detailed review on the role of microvilli in flow sensing the reader is referred to (96).

Glycocalyx: As in most cells, a layer of crosslinked mucins, glycoproteins, and glycolipids protects the apical microvilli of PT cells (100). While the glycocalyx is known to play a critical role in shear stress sensation in the vascular endothelium [reviewed in (101)], its role in mechanosensation in the renal PT has not been rigorously tested. In vascular endothelial cells, the glycocalyx is connected to the cytoskeletal network inside the cell, and when exposed to blood flow, transduces its bending moment to modulate endothelial cell function. The glycocalyx could magnify the physiologic effects of flow in the PT by increasing the frictional coefficient at the apical surface. However, treatment of immortalized PT cells with the glycocalyx-digesting enzyme heparinase III did not alter the cellular response to shear stress (99). In this study, only changes in flow-dependent changes in cytoskeleton remodeling were examined, and it remains possible that the glycocalyx mediates other flow-dependent responses.

Primary Cilia: Rat PT cells elaborate a single apical primary cilium typically 3-4 microns in length that extends somewhat beyond the microvillar surface (102). Over the past two decades, there has been an increasing appreciation of the function of these complex structures as mechanosensitive flow sensors in many tissue types including the distal tubule and collecting duct of the kidney. Although the kidney elaborates a primary cilium, its exact function in regulating a mechanosensory response in this system remains to be tested.

PT mechanosensitive responses to radial stretch. In addition to increased shear stress, a rise in intraluminal pressure dilates the tubular lumen and potentially triggers a stretch response. In isolated perfused proximal tubules and in unilateral ureteral obstruction disease models, stretch induced by increased flow is transduced into a change in the outer diameter of the tubule

as well as the lumen. It is unclear to what extent these changes in outer diameter also occur in proximal tubules within the intact normal kidney during normal variations in flow. Stretch is known to modulate Ca^{2+} signaling, cell volume, cytoskeletal reorganization, and gene transcription in kidney tubule cells (103-108). Integrins, gap junctions, and basolateral stretch-activated calcium channels have been documented to play a role in transducing these changes in stretch (105, 109, 110). In isolated PTs, and in cells cultured on stretchable membranes, mechanical stretch has been suggested to trigger formation of focal adhesions mediated by integrins, and to increase cytosolic levels of Ca^{2+} through stretch-activated calcium channels. More detailed discussions of how stretch regulates PT function can be found in these excellent reviews (96, 97).

Although FSS is known to modulate several key functions in PTs, the regulation of apical endocytic traffic by FSS still remains untested. I will be using OK cells to test the role of FSS in regulating apical endocytic traffic in renal proximal tubules.

1.2.4 PT dysfunction and low molecular weight proteinuria

One principal role of the proximal tubule is to retrieve low molecular weight proteins from the urine, PT dysfunction is often correlated with tubular or low molecular weight proteinuria. Tubular proteinuria is usually associated with rare-genetic diseases and other nephropathies. I have discussed Imerslund-Gräsbeck syndrome and Donnai Barrow Syndrome which are caused by mutations in amnionless and megalin respectively, in section 1.2.2. Cystinosis, heavy metal poisoning, and early diabetic nephropathy are other diseases that result in tubular proteinuria. Diabetic nephropathy is associated with the diabetic hyperfiltration

phenotype, which causes increased GFRs in patients, and this may result in the inability of PT cells to retrieve all the low molecular weight proteins from the glomerular filtrate. I will be discussing tubular proteinuria associated with the rare genetic diseases Lowe syndrome (caused by mutations in a lipid phosphatase) and Dent's disease (caused by mutations in CLC-5) in section 1.3.

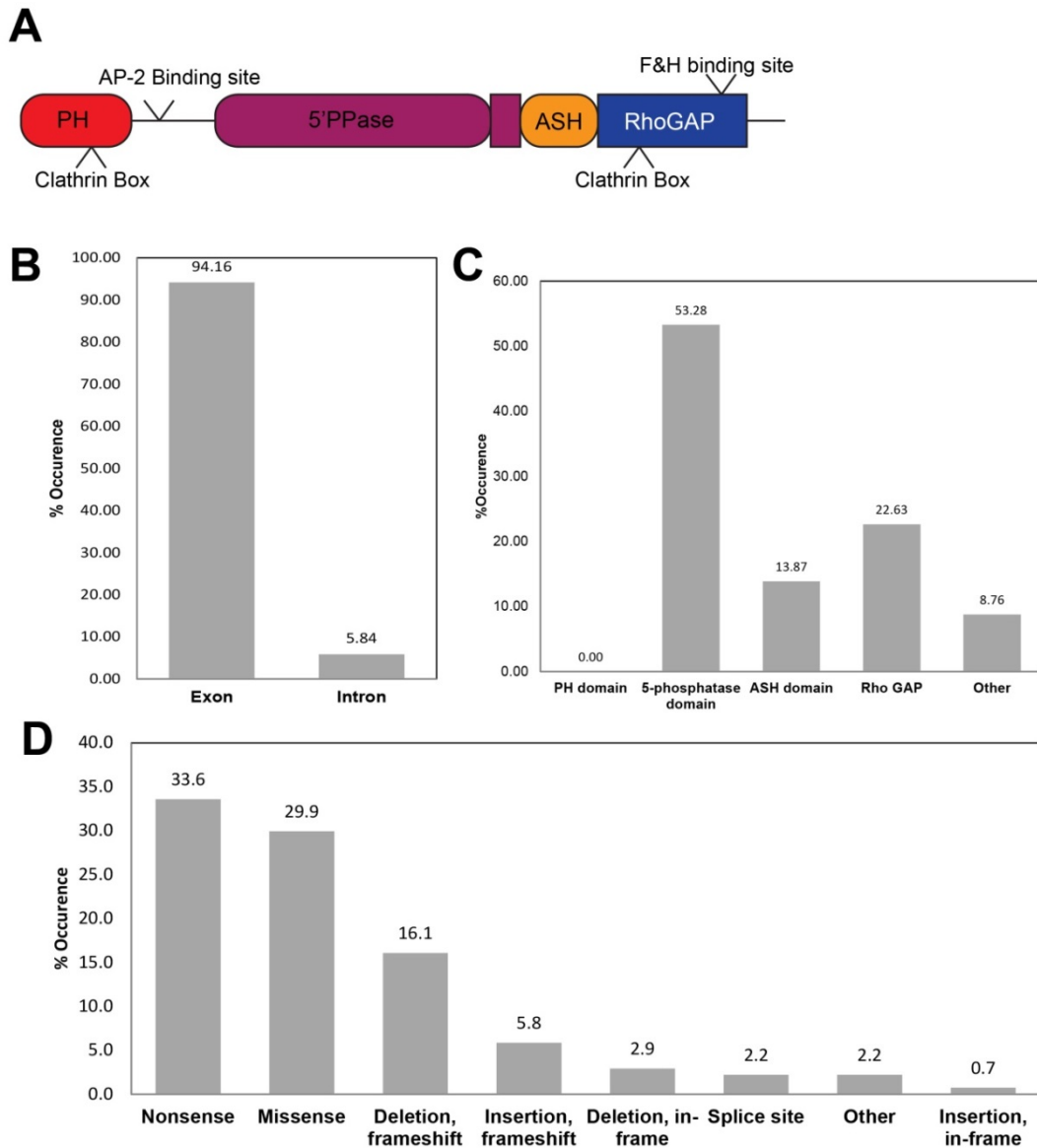
1.3 LOWE SYNDROME

Back in 1952 Charles Lowe came across a patient with a disease that caused organic-aciduria, decreased renal ammonia production, hydrophthalmos, and mental retardation (111). He and his colleagues were the first to document the existence of Oculocerebrorenal Dystrophy which was later renamed Lowe syndrome. As more patients with similar symptoms were reported, the field accepted three diagnostic identifiers to be associated with this disease, which were congenital cataracts, mental retardation and renal tubular dysfunction (112). As only young boys were diagnosed with the disease, an X-linked pattern of family inheritance was also documented. A few years later, the Lowe syndrome gene OCRL1 was found to be localized to the chromosomal location Xq 26.1 (113). From recent statistics, Lowe syndrome is a rare panethnic genetic disorder with an incidence of 1 in every 200,000 to 500,000 newborns worldwide.

1.3.1 Phenotype, prevalence and causes

The pathophysiology of Lowe syndrome is comprised of changes and defects in several organ systems. The severity of many symptoms varies broadly among different patients. As it is an X-linked recessive disease, Lowe syndrome almost always affects males (although chromosomal translocations affecting the OCRL1 gene locus have been reported to cause Lowe syndrome phenotypes in a very small number of female cases) (113). It is often diagnosed at very early stages (at birth or in the first years of life) based on physical abnormalities.

Figure 3. OCRL1, structure, function and disease associated mutations



(A) Schematic of Oculocerebrorenal of Lowe (OCRL) protein which is a Phosphatidylinositol-5' Phosphatase, and its subdomains. (B) Analysis of the database of OCRL patients surveyed till date hosted by Dr. Nussbaum. Graph shows % occurrence of mutations in introns versus exons in patients. Over 95% of mutations occur in exons. (C) Depicts the breakdown of percentage of mutations occurring in patient occurring in exons into domains specific rates of occurrence. In over 50% of the cases mutations arise in the 5' Phosphatase domain and cause loss of enzymatic function. (D) Over 60% of these mutations that occur in OCRL1 are caused by non-sense or missense mutations in the gene.

All known Lowe patients are born with bilateral cataracts, impaired vision, renal tubular dysfunction and moderate to severe mental retardation (112, 114). Facial characteristics in boys with the disease include small deep-set eyes, prominent foreheads, and abnormally lengthened faces (114). Glaucoma, keloids, strabismus and even blindness are common in patients as well (115, 116). It takes roughly 12 months to detect renal tubular dysfunction in children with Lowe syndrome, and their blood plasma creatinine levels typically stay in the reference range until they become teenagers (114). Chronic kidney dysfunction is associated with many Lowe patients in their late teens and 20s, and a high rate of infantile mortality has been noted for Lowe syndrome (117). About 30% of patients who survive infancy live until the third decade of their lives; however, the average lifespan of Lowe syndrome patients is rarely longer than 40 years(114). Death in these patients is usually caused because of chronic renal disease; however, other neurologic manifestations of this disease could prove to be fatal as well. The renal tubular dysfunction associated with Lowe syndrome is characterized by urinary loss of pathological levels of low-molecular-weight proteins, amino acids, calcium, bicarbonate, phosphate, L-carnitine and excessive water (114, 117). Massive loss of such important metabolites leads to bone problems like rickets and osteomalacia, and the chronic loss of water leads to dehydration in these boys. Older survivors of the disease have epithelial cell atrophy, tubular fibrosis, nephrocalcinosis and glomerular sclerosis (114, 117).

Most of the currently existing standard of care is palliative, and helps patients cope with the disease. This treatment strategy includes removal of cataracts through surgery, replacement therapy to compensate for metabolites lost through urination, and dialysis in older patients with chronic kidney failure (114, 116). Discovery of a novel target, or the mechanism underlying

proteinuria associated with this disease would be key to treating the proteinuric phenotype, which is the reason underlying high patient mortality in these patients.

OCRL1 structure and function

Fig. 3A depicts the modular domain structure of OCRL1. Red: N-terminal PH domain; Magenta: 5' phosphatase domain; Orange: ASH domain; dark-blue: RhoGAP domain. The clathrin binding boxes and the AP-2 binding sites are demarcated on the schematic. The bar graphs in Fig. 3 are syntheses of analysis conducted on the open source documentation of Lowe syndrome patients by Dr. Nussbaum's group. Fig. 3B shows that of all patient mutations of OCRL1, close to 95% of them occur in protein coding exons. Fig. 3C given that most mutations occur in the protein coding region, close to 55% of these mutations occur in the 5'-Phosphatase domain, resulting in a defective activity of the enzyme, which may be the underlying cause for Lowe syndrome. Close to 35% of other mutations that cause Lowe syndrome occur in the ASH or the RhoGAP domain. However, there is no data that correlates the severity of the disease to the mutation associated with the disease. Close to 60% of all mutations that cause the disease result in non-sense or missense mutations (Fig. 3D). Other types of mutations in OCRL1 that cause the disease are deletions, insertions and frame-shift mutations.

OCRL1 is a multidomain protein with an N-terminal PH domain, a central 5'-phosphatase domain, and C-terminal RhoGAP-like and ASH domains. The PH domain of OCRL1 was first discovered using 3D-NMR spectroscopy, and was found to lack the basic patch required for tethering to phosphoinositide-labeled liposomes (118). However, this domain has a loop with a clathrin-binding motif, which helps OCRL1 tether to endocytic clathrin coated pits

(119). This domain is connected to the 5'-phosphatase domain through an unstructured linker domain which has an FEDNF consensus motif, which binds directly to AP-2 (119).

Although the structure of the other domains of OCRL1 has been determined, the structure of the 5'-phosphatase domain of OCRL1 remains to be resolved. Most of our understanding of this domain in OCRL1 comes from sequence homology studies between it and a closely related homolog INPP5B, whose structure has been resolved. OCRL1 preferentially hydrolyzes PtdIns(4,5)P2 *in vitro*, in comparison to its other substrates such as PtdIns(3,4,5)P3 which is known to dephosphorylate extremely well *in vitro* (120). Although OCRL1 is an important PtdIns(4,5)P2 phosphatase, deletion of OCRL1 does not stimulate a large increase in PtdIns(4,5)P2 in cell lines or other models (121).

The ASH or the Hydin domain succeeds the 5'-phosphatase domain in OCRL1, and this domain is known to mediate interactions with the Rab family of small GTPases (122). Hence this domain is critically important for the proper sub-cellular localization of OCRL1. About 13% of disease associated mutations occur in this domain and this underscores the importance of the localization of OCRL1 for proper function (fig. 3C). As the ASH domain mediated interaction with Rabs are atypical, OCRL1 does not associate with a wide number of these GTPases.

The RhoGAP like domain is located right after the ASH domain, and this domain mediates interactions with both Rac1 and cdc42 small GTPases (123, 124). This domain is not catalytically active, and does not behave like a GAP, however, it tethers OCRL1 to sites of Cdc42 activity, which is associated with actin assembly. Another conserved region within the

RhoGAP-like domain binds to F&H motif of the APPL1 and IPIP27 isoforms which are endocytic adaptors that bind to clathrin coated pits. Like the PH domain, the RhoGAP domain has a clathrin binding loop that mediates its interactions with clathrin coated pits (125). Together, this domain along with the ASH and the PH domains suggest an important role for OCRL1 in endocytic traffic.

In mammalian cells, OCRL1 primarily localizes to the TGN and endosomal compartments. It can also be found in clathrin coated pits, at the base of primary cilia, at tight junctions in epithelial cell types, and at plasma membrane ruffles upon growth-factor stimulation depending on the observer (126-129). Although OCRL1 interacts with clathrin, and has been shown to localize to clathrin coated pits, we still don't understand the mechanism connecting the loss of catalytic function and defects in endocytosis. My goal in the third chapter is to establish a functional role for OCRL1 in modulating membrane traffic in PT epithelia.

OCRL1 knockout studies in mice have shown that deletion of the gene does not result in tubular proteinuria. This was because of the high expression of the comparable homolog INPP5B which compensates for the loss of OCRL1 (130). In humans, due to low expression of INPP5B, this compensatory mechanism may not exist. To use a more physiologically relevant system to study the effects of OCRL1, I will be depleting OCRL1 using siRNA in human proximal tubule cell lines in chapter 3 to test its role in regulating apical endocytosis.

Mutations in the OCRL1 gene have been found in a subgroup of patients originally diagnosed with Dent disease, another X-linked recessive disorder affecting only the kidneys. Dent disease, as previously mentioned in Section 1.2.5 is a rare genetic disease characterized by

mutations in the chloride transporter CLCN5 gene, known to interact with Megalin and cubilin (131). These patients with mutations in OCRL1 have been re-categorized as dent-2 patients, and these patients suffer from chronic tubular proteinuria(132). The reason underlying the occurrence of such mutations in the OCRL1 gene in dent disease patients still remains unknown. As the effects in Dent-2 are similar to Lowe syndrome, this disease has been an area of active focus for our lab.

In chapter 3 of this dissertation, I will be testing the role of OCRL1 in regulating apical endocytosis of the megalin & cubilin ligand albumin. As mentioned in section 1.2, the goal of my thesis is to focus on determining the role of FSS in modulating apical endocytosis in PT epithelia. I will be assessing the role of OCRL1 in the presence of FSS to determine its function in a more physiologically relevant system. My studies will improve our understanding of Lowe syndrome and thereby increase our ability to devise better therapeutic strategies to treat the proteinuric phenotype associated with the disease.

1.3.2 Role of ocr1 in ciliogenesis

Studies from labs around the world have implicated an important role for OCRL1 in the biogenesis of cilia. While two studies from patient fibroblasts and three knockdown studies of OCRL1 in multiple cell systems have shown a decrease in the number and length of cilia, our lab has consistently reported an increase in the length of cilia across 3 different cell lines, and in zebrafish models (129, 131, 133, 134). Localization studies have shown OCRL 1 to be in the primary cilium and at the basal body of retinal epithelial cells and trabecular meshwork cells of

the eye, respectively (129, 134). However, studies in renal epithelial cells have failed to localize OCRL1 to the primary cilium, but have seen it to be localized to the basal body. In all our experiments, we have seen OCRL1 to be predominantly localized to the TGN.

OCRL1 may be involved in the trafficking of important membrane components of the cilium, and therefore defects in protein causes defective ciliogenesis. As mentioned earlier in section 1.3, OCRL1 has well defined Rab binding and IPIP27 binding motifs in their ASH and RhoGAP-like domains respectively (125). Both Rab 8 and the endocytic adaptor IPIP27 are known to be important for ciliogenesis, therefore loss of OCRL1 may lead to dysfunctional ciliogenesis due to the defective or ablated interactions with these critical proteins (125).

As mentioned earlier, I want to test the role of OCRL1 in modulating the effects of FSS regulated apical endocytosis of megalin ligands. I predict an important role for the primary cilia in mediating the FSS stimulated effects in PT cells, therefore it would be interesting to see if the changes in mechanosensation are caused by defective ciliogenesis associated with OCRL1 depletion.

1.3.3 Role of ocr1 in membrane traffic

As mentioned in the earlier sections, there exists a breadth of literature implicating an important role for OCRL1 in membrane traffic. This role comes in four parts: (i) Association of OCRL1 with clathrin coated pits through its clathrin interaction domains, clathrin adaptor interactions, and AP-2 interaction loop (119); (ii) Association of OCRL1 with Rabs which are identifiers of endocytic vesicles, (iii) through the association of OCRL1 with cdc42 and Rho

GTPases which are involved in actin nucleation and remodeling (135), and finally (iv) through the fundamental function of OCRL1 as a PtdIns(4,5)P₂ phosphatase (120).

Since the identification of the interaction of OCRL1 with clathrin via the clathrin binding loops in the PH and the RhoGAP-like domains, OCRL1 has been implicated in modulating clathrin mediated endocytosis. OCRL1 recruitment to clathrin coated pits occurs at a late stage in the process of endocytosis, right before the vesicle is pinched off from the apical surface (136). The recruitment of OCRL1 to these pits seem to be important for hydrolyzing PtdIns(4,5)P₂ in these pits, and this event intersects with the release of actin, and actin associated proteins that are important for the formation of the clathrin coated pits. Therefore, one existing thought is that OCRL1 plays an important role in the formation of clathrin coated pits by modulating the actin dynamics. Another school of thought is that OCRL1 may be recruited during the later stages of pit formation to make to ensure its association with the vesicles and presence in the later stages of the endocytic pathway. A third train of thought is that, OCRL1 plays a redundant function in the clathrin coated pits, as similar phosphatases such as SHIP 2 and synaptojanin are also localized to the clathrin coated pits (137). However, as the apical endocytic load on proximal tubular cells is high, it is possible that the OCRL1 may play an important role in coordinating clathrin pit formation in PTs; therefore the defects in endocytosis are more pronounced in this cell type in patients with Lowe syndrome. Finally, a very recent study showed that OCRL1 interacts with SNX9 through a PXXP motif in its unstructured domain, and that this interaction might be critical to ensure uncoating of clathrin coated endocytic vesicles after pinching off. The study went on to conclude that OCRL1 regulates clathrin coated pit dynamics and therefore loss of OCRL1 causes defects in the efficiency of uncoating which may in turn be responsible for the

defects associated with Lowe syndrome (128). Although very minute amounts of OCRL1 are found to be localized to the apical surface of epithelial cells, the legitimacy of OCRL1s in playing a very critical function in the early stages of the endocytic cascade is still open to debate.

GST pull downs have shown OCRL1 is known to interact with Rab 6, Rab 8, Rab 14, Rab 31, and Rab35 through its ASH domain (138-141). These interactions recruit OCRL1 to the endosomal compartments where it hydrolyzes PtdIns(4,5)P2. Several studies have implicated OCRL1 in regulating the delivery of cargo from endosomal compartments to the TGN where OCRL1 is predominantly localized. OCRL1 has also been implicated in regulating recycling of the transferrin receptor to the surface in non-polarized MDCK cells, and in the delivery of mitogenic receptors to the lysosomes. In OCRL1 deficient cells receptors were held in large endosomal structures that had accumulated actin (135). The accumulation of polymerized actin networks around endosomal structures was visualized as actin comets when these OCRL1 deficient cells were subjected live cell microscopy (142). The polymerization of actin around the endosomal compartments is attributed to the increase in the local concentration of PtdIns(4,5)P2 on the endosomal membranes. PtdIns(4,5)P2 is known to both inactivate cofilin which is an F-actin severing protein, and to recruit N-WASP which is an actin nucleation promoting factor (143). The actin comets disappear in rescue experiments when cells are transfected with WT-OCRL1 and not the phosphatase deficient mutant, which again underscores the accumulation of PtdIns(4,5)P2 as the principal reason underlying actin comet formation (135).

As mentioned earlier, OCRL1 is abundant in the TGN and it has been detected in clathrin coated buds which emanate from the TGN. In one study, the surface delivery of TRPV6 was reduced in OCRL1 depleted cells; however, the precise mechanism underlying this defect was

not identified (144). In previous studies conducted in our lab, we did not observe any defects in the biosynthetic or the endocytic traffic of the multiligand receptor megalin in polarized MDCK cells (142). Therefore we initially thought that OCRL1 does not play a critical role in the initial stages of biosynthetic or endocytic traffic of these multiligand receptors.

In contrast to our previous experiments the presence of FSS could necessitate a critical role for OCRL1 in regulating apical endocytic traffic in PT epithelia. I test this hypothesis in chapter 3.

1.4 SUMMARY

SPECIFIC AIMS:

The kidney has an extraordinary ability to maintain stable fractional solute and fluid reabsorption over a wide range of glomerular filtration rates (GFRs) to preserve glomerulotubular balance. The majority of filtered water, sodium, proteins, and other solutes are reabsorbed in the PT, which plays a critical role in blood volume homeostasis and cardiovascular health. PTs selectively express the multiligand receptors megalin and cubilin which mediate retrieval of all the low molecular weight proteins from the glomerular filtrate. Defects in this process lead to low molecular weight proteinuria and chronic kidney disease. PT ion transport capacity responds acutely to changes in GFR, but it is unknown whether or how endocytosis in PT cells responds to changes in flow and the accompanying fluid shear stress (FSS). I discovered that apical endocytosis of albumin and fluid-phase markers is dramatically enhanced upon exposure of immortalized PT (but not other kidney segment) cell lines to FSS. Moreover, I found that this response requires the primary cilia on PT cells and is triggered by an increase in cytosolic Ca^{2+} concentration ($[\text{Ca}^{2+}]_i$) in response to FSS. My thesis project focused on understanding the effects of FSS on endocytosis and changes in $[\text{Ca}^{2+}]_i$ (Aim 1); and how defects in this process may contribute proteinuric disease (Aim 2). The appendices of this thesis describe studies to determine how changes in $[\text{Ca}^{2+}]_i$ are transduced to increase apical endocytic capacity in PT cells, and the organellar identity of apical endocytic compartments in these cells. (Appendices)

AIM 1. HOW DOES FSS AFFECT ENDOCYTOSIS AND CHANGES IN INTRACELLULAR CALCIUM IN PT CELLS?

As detailed in section 1.2.4 PT cells are capable of sensing changes in FSS and modulating ion-reabsorption. My primary goal was to determine whether PT epithelia also modulate their apical endocytic capacity. I determined the role of FSS in modulating apical endocytosis in PT epithelia using an opossum kidney cell model subjected to FSS. In chapter 2, I determined the threshold, time course, and reversibility of the endocytic response to changes in FSS. I also found that the FSS stimulated endocytosis is controlled by a clathrin and dynamin dependent pathway. I also determined the increases the average size of individual Clathrin Coated Pits (CCPs) on exposure to FSS using TIRFM. Further, I observed an immediate increase in $[Ca^{2+}]_i$ on exposure to FSS which is dependent on the presence of extracellular calcium, primary cilia, ryanodine sensitive ER stores of calcium, extracellular ATP and intact purinergic signaling. Finally, I determined that the FSS stimulated endocytic response also requires the cilia, extracellular ATP, release of ER calcium and intact purinergic signaling. Chapter 2 discusses these findings in detail and assesses future directions.

AIM 2. DOES DEFECTIVE MODULATION OF FSS-DEPENDENT ENDOCYTOSIS CONTRIBUTE TO TUBULAR PROTEINURIA?

Patients with Lowe syndrome, in which the phosphatidylinositol 5'-phosphatase OCRL1 is defective or absent, present uniformly with LMW proteinuria. Knockdown of OCRL1 has no effect on the basal (constitutive) level of endocytosis, and studies to date have failed to explain how loss of this enzyme results in proteinuria in Lowe syndrome patients. Recently, our lab

found that knockdown of OCRL1 causes cilia elongation in mammalian kidney cells and in zebrafish, and also disrupts zebrafish pronephric kidney function. I hypothesize that loss of OCRL impairs the ability of PT cells to respond to changes in GFR, and that this contributes to proteinuria in patients with Lowe syndrome. In Chapter 3, I described studies to determine the role of OCRL in the FSS stimulated endocytic cascade. I identified that the defect in FSS stimulated endocytosis is not due to the increased length of cilia in the proximal tubules.

APPENDICES: What is the downstream signaling cascade that leads to increased apical endocytosis in response to FSS, and what is the identity of these apical endocytic compartments in PT epithelia involved in this process?

I hypothesize that FSS-induced increases in $[Ca^{2+}]_i$ lead to a rapid increase in the average size and capacity of individual apical membrane (CCPs) via an actin-dependent pathway that involves activation of Calmodulin, Cdc42, and N-WASP. There is precedence for N-WASP-mediated modulation of CCP size in mammalian cells. I used different experimental approaches to systematically test the role of (a) calmodulin; (b) Cdc42 (an apically localized Rho GTPase), and (c) N-WASP in the mechanosensitive pathway by which increases in FSS lead to enhanced endocytosis.

My secondary goal was to determine the identity of the apical endocytic vacuolar compartments that I discussed in detail in section 1.2.2. I employed a mouse kidney derived primary PT epithelia and identified Rab 11a, a small GTPase as a marker of the apical vacuolar structures in PT epithelia.

Contributions:

I am thankful to Youssef Rbaibi for his contributions to this study. Youssef and I collaborated to conduct the experiments for Figures 6, 7, 12 and 13. I am also grateful to our collaborator Dr. Carattino

2.0 FLOW STIMULATED ENDOCYTOSIS IN PT EPITHELIA

2.1 OVERVIEW

Internalization of filtered low molecular weight proteins, vitamins, hormones, and other small molecules is mediated by the proximal tubule (PT) multiligand receptors megalin and cubilin. Changes in GFR and the accompanying fluid shear stress (FSS) modulate acute changes in PT ion transport thought to be mediated by microvillar bending. I found that FSS also affects apical endocytosis in PT cells. Exposure of immortalized PT cell lines to physiologically relevant levels of FSS led to dramatically increased internalization of the megalin/cubilin ligand albumin as well as the fluid phase marker dextran. FSS-stimulated apical endocytosis was initiated between 15 and 30 min post induction of FSS, occurred via a clathrin- and dynamin-dependent pathway, and was rapidly reversed upon removing the FSS. Exposure to FSS also caused a rapid elevation in intracellular Ca^{2+} [Ca^{2+}]_i, which was not observed in deciliated cells, upon treatment with BAPTA-AM, or upon inclusion of apyrase in the perfusion medium. Strikingly, deciliation, BAPTA-AM, and apyrase also blocked the flow-dependent increase in endocytosis. Moreover, addition of ATP bypassed the need for FSS in enhancing endocytic capacity. My studies suggest that increased [Ca^{2+}]_i and purinergic signaling in response to FSS-dependent ciliary bending triggers a rapid and reversible increase in apical endocytosis that contributes to the efficient retrieval of filtered proteins in the PT.

2.2 INTRODUCTION

Kidneys maintain stable efficient fluid and solute reabsorption over a wide range of GFRs, which is essential to preserve glomerulotubular balance (96, 145). The majority of filtered water, Na^+ , proteins, and other solutes are reabsorbed in the proximal tubule (PT), which plays a critical role in blood volume homeostasis. Internalization of filtered low molecular weight (LMW) proteins, vitamins, hormones, and other small molecules is mediated by the PT multiligand receptors megalin and cubilin (22). Defects in the uptake of these ligands leads to LMW proteinuria, which contributes to the pathogenesis of many renal diseases including acute and chronic kidney injury, metal toxicity, cystinosis, and the X-linked disorders Lowe syndrome and Dent disease (114, 146).

As discussed in the introduction, increases in GFR lead to acute changes in PT ion transport capacity. The sodium/hydrogen exchanger NHE3 rapidly accumulates at the apical surface in response to the increased fluid shear stress (FSS) on PT cells to enable increased Na^+ reabsorption (96, 147). Modeling studies have suggested that these flow-mediated changes in ion transport are regulated by a mechanosensitive mechanism induced by microvillar bending (148, 149). Increases in GFR also enhance the need for megalin/cubilin mediated uptake of filtered ligands. However, it is unknown whether or how endocytosis in PT cells responds to changes in FSS.

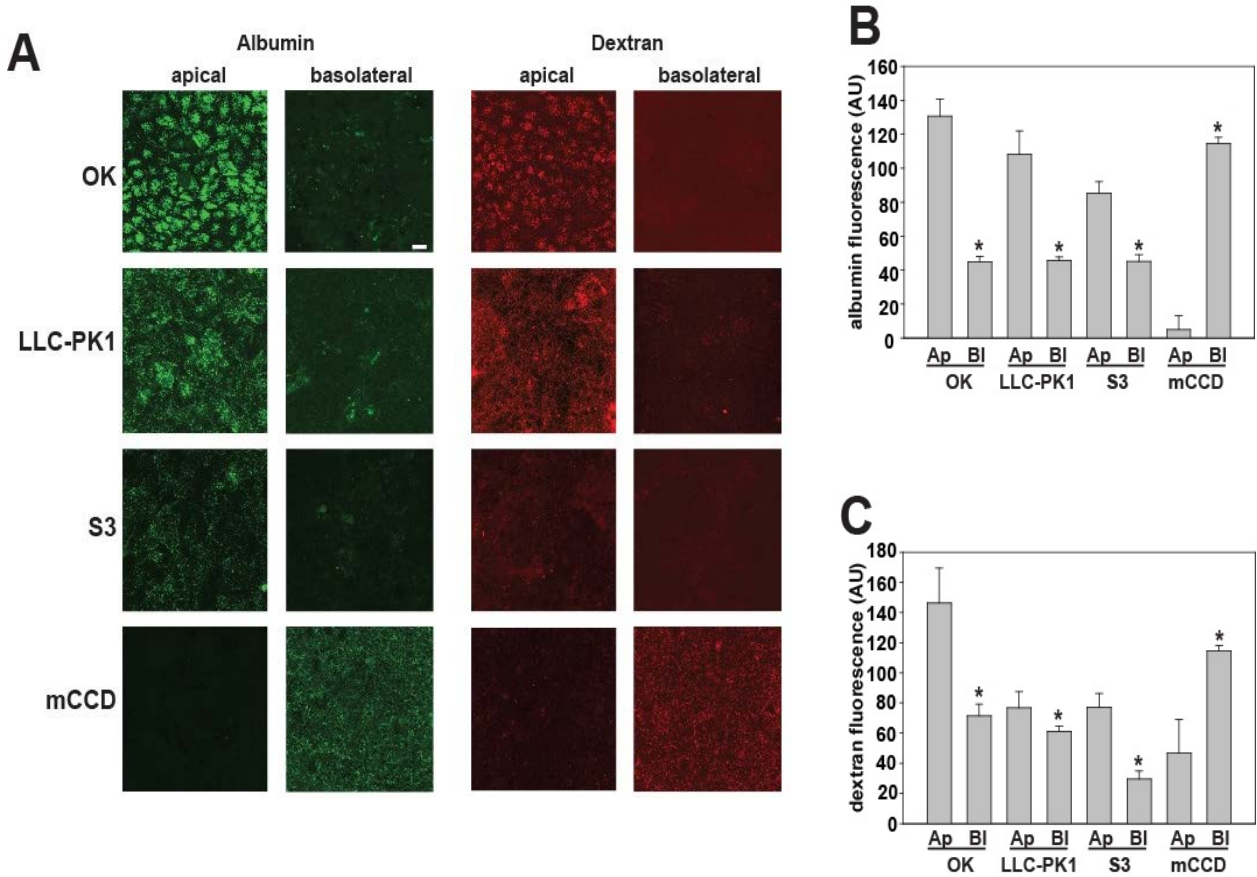
In this chapter, I discuss the effect of increased flow and the accompanying FSS on apical endocytosis in PT-derived epithelial cells. I find a rapid and sustained increase in endocytic uptake of both the megalin/cubilin ligand albumin and a fluid phase marker upon exposure to physiologically relevant levels of FSS. Both basal- and FSS-stimulated uptake were inhibited by perturbants of clathrin assembly and dynamin function. Exposure to flow also triggered an

increase in intracellular Ca^{2+} concentration ($[\text{Ca}^{2+}]_i$) that was dependent on TRP channel activity, release of extracellular ATP, and the presence of primary cilia. Importantly, deciliation of cells or inclusion of apyrase in the medium did not alter endocytosis under static conditions but completely abrogated the FSS-stimulated endocytic response. My data suggest that flow sensing by mechanosensitive channels in the primary cilia modulate acute apical endocytic responses in PT cells. I discuss the impact of these results on our understanding of normal and disease kidney physiology.

2.2.1 Significance

The proximal tubule (PT) of the kidney is the primary site for reabsorption of ions, solutes, and filtered low molecular weight proteins (LMWPs). PT cells rapidly modulate ion transport capacity in response to the fluid shear stress (FSS) that accompanies changes in glomerular filtration rate. I report here that PT cells also adjust their capacity for endocytosis in response to FSS. Apical endocytosis of the megalin/cubilin ligand albumin and of fluid phase markers is markedly increased upon exposure to FSS. Moreover, Ca^{2+} signaling mediated by the primary cilia on PT cells is required for this response. These studies define a novel pathway in PT cells that plays an essential role in maintaining kidney function.

Figure 4. Apical endocytosis is robust in PT cell lines compared with cells from other segments of the kidney tubule.



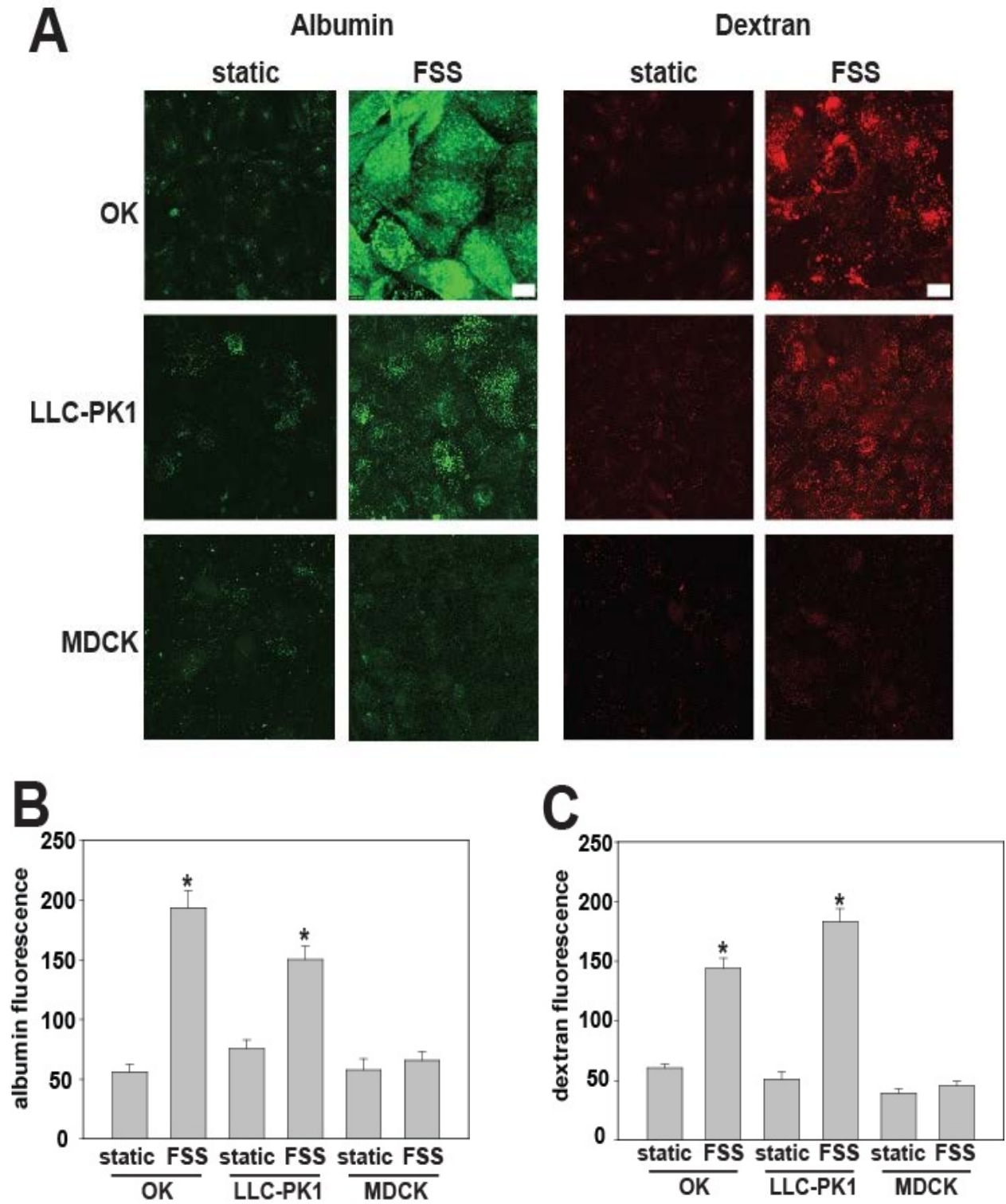
A) Confocal Micrographs of apical vs. basolateral endocytosis of albumin and dextran in OK, LLC-PK1, S3 mouse PT cells, and in mCCD cells. B) Images were quantified using confocal microscopy and graph represents albumin uptake in observations from 3 experiments * $p < 0.05$ using students t-test. C) Graph represents endocytosis of dextran from 3 experiments * $p < 0.05$ using students t-test. This shows that PT derived cell lines are more apically endocytically active than cells derived from distal portions of the nephron.

2.3 RESULTS

2.3.1 Proximal tubule derived cell lines have robust apical endocytic uptake of membrane bound and fluid phase tracers

As mentioned in chapter 1, EM studies of rodent proximal tubules have shown that epithelial cells that line the proximal tubule have robust apical endocytosis. To this end, cells lining the PT express high levels of the multiligand receptors megalin and cubilin, and are specialized to maintain robust apical endocytic capacity (3, 66, 67). To confirm that immortalized cell models of the PT retain a high capacity for apical endocytosis, OK cells and LLC-PK1 cells were exposed to apically- or basolaterally-added fluorescently tagged albumin (a megalin-cubilin ligand) and dextran (a marker for fluid phase endocytosis). As shown in Fig. 4, both of these cell lines internalized albumin and dextran preferentially from the apical surface. Similarly, murine S3 cells, derived from the S3 segment of the PT, also internalized albumin and dextran preferentially from the apical surface, although endocytosis was less robust than in the other PT cells (Fig. 4). As a control, I performed similar experiments in mouse cortical collecting duct (CCD) cells. These cells express little if any megalin, and not surprisingly, little albumin was internalized from either surface of these cells. However, consistent with previous studies demonstrating more efficient basolateral internalization rates compared with apical endocytosis (150, 151), I observed considerably greater levels of dextran internalized from the basolateral surface in these cells (Fig. 4).

Figure 5. Exposure to fluid shear stress increases apical albumin and dextran uptake in PT cell lines.



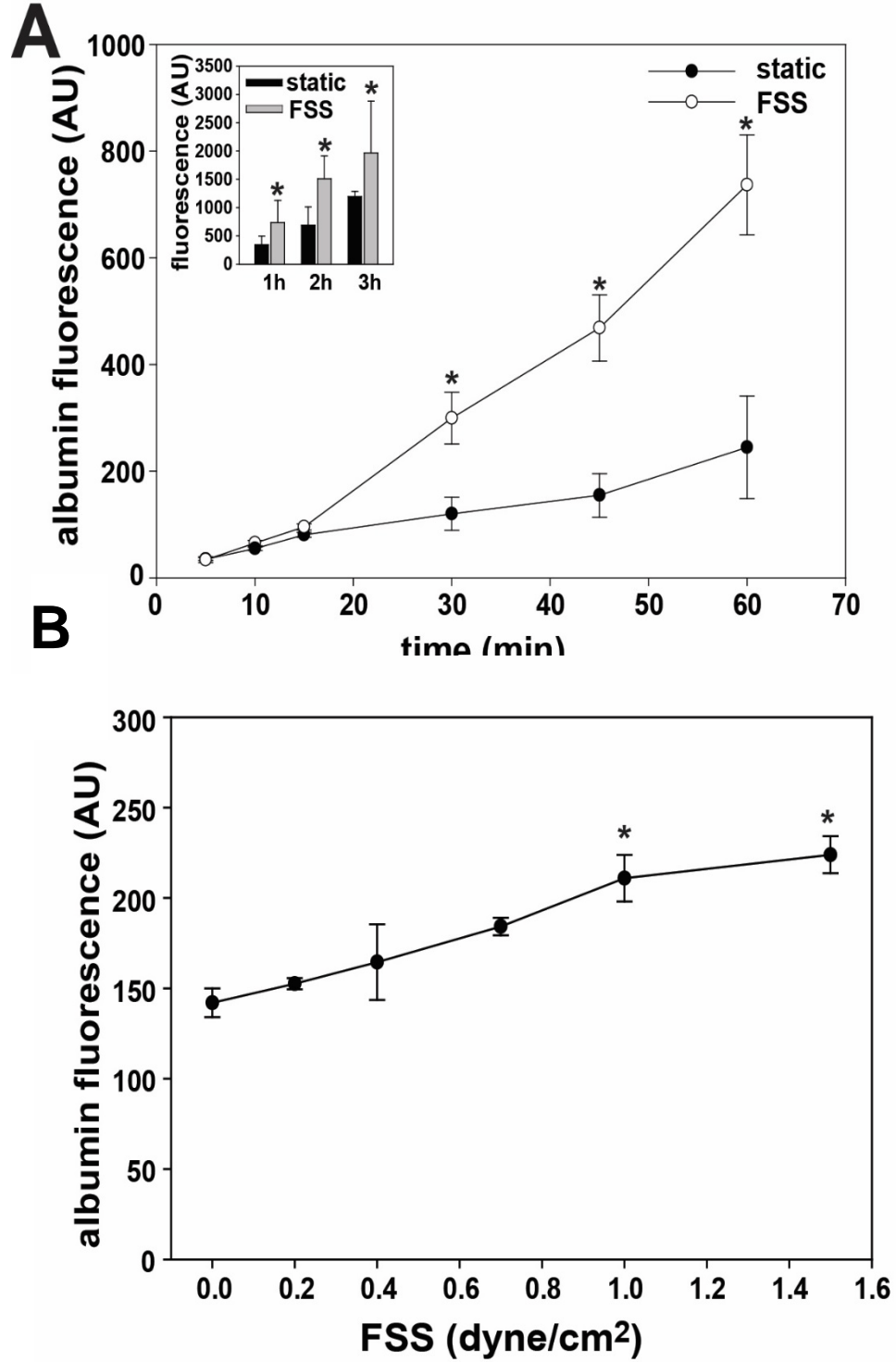
A) OK, LLC-PK1, or MDCK cells were incubated with 40 $\mu\text{g}/\text{mL}$ Alexa Fluor 647-albumin and 1 mg/mL rhodamine dextran for 3 h under static conditions or during exposure to 1 dyne/cm^2 fluid shear stress (FSS). Images of representative fields captured under identical conditions are shown. Scale bars: 10 μm . (B and C) The average albumin (B) and dextran (C) fluorescence intensity per field was quantitated in 30 fields taken from three independent experiments and the mean \pm SEM is plotted. * $p < 0.05$ vs. static control by Student's t-test.

2.3.2 Exposure to FSS stimulates apical endocytosis in PT cells

Healthy individuals efficiently clear low molecular weight proteins and other freely filtered megalin/cubilin ligands despite wide fluctuations in GFR. It is unknown whether endocytic capacity in PT cells varies with changes in fluid flow and the accompanying FSS. To test this, I asked whether changes in FSS result in increased apical endocytosis in immortalized PT cells. Polarized OK and LLC-PK1 kidney cells cultured in a parallel plate flow chamber were exposed for 3 h to physiologically relevant levels of FSS [1 dyne/cm^2 , corresponding to a GFR of 115 $\text{mL}/\text{min}/1.73\text{m}^2$ (99, 152, 153)] or maintained under static conditions. The megalin/cubilin ligand Alexa Fluor 647-albumin [40 $\mu\text{g}/\text{mL}$; the reported concentration of albumin in the PT is ~ 23 $\mu\text{g}/\text{mL}$ (154)] or the fluid phase marker Rhodamine-dextran were included in the perfusate, and the effects on receptor mediated and fluid phase endocytosis were quantified. I reproducibly observed a striking (typically \sim two-fold) and statistically significant increase in the uptake of both albumin and dextran in both cell lines exposed to FSS compared with controls maintained under static conditions (Fig. 5). Identical results were obtained when the cells were cultured in Ibidi 6-well slide chambers, which were used for most subsequent experiments. Because cells under FSS were exposed to a greater volume of medium than cells

incubated under static conditions, I confirmed that fluorescent albumin and dextran were not noticeably depleted from the medium under static incubation conditions; thus, this does not account for the difference in uptake that I observed (not shown; published in Raghavan et al.). My results are consistent with those of Ferrell et al., who recently reported similar effects of FSS on albumin uptake in OK cells (155). The increase in both receptor mediated and fluid phase uptake in PT cells upon exposure to FSS suggests a generic stimulation in endocytosis under these conditions, rather than a selective effect on megalin/cubilin trafficking. In contrast, apical endocytosis in MDCK Type II cells, which have hybrid characteristics of proximal and distal tubule cells, was unaffected by FSS (Fig. 5). Thus, the FSS-stimulated increase in endocytosis is apparently selective for cells of PT origin.

Figure 6. Time-course and FSS dependence of flow stimulated endocytosis



(A) Time course of onset of FSS-stimulated endocytosis. OK cells plated in Ibidi μ slide chambers were incubated under static conditions or exposed to 1 dyne/cm² FSS in the presence of 40 μ g/mL Alexa Fluor 647-albumin for the indicated time periods, then fixed, and average internalized fluorescence quantified from 15-20 fields per condition. * $p < 0.04$ vs paired static control by Student's t-test. Inset, albumin uptake over a 1-3 h time course. * $p < 0.02$ vs static control by t-test. (B) OK cells were incubated with 40 μ g/mL Alexa Fluor 647-albumin for 1 h under static conditions (0 dyne/cm²) or during exposure to the indicated FSS. Average internalized fluorescence was quantified from four wells for each time point. * $p < 0.05$ vs. all other conditions by ANOVA, except endocytosis measured at 1.0 vs 1.5 dyne/cm² are not significantly different from each other.

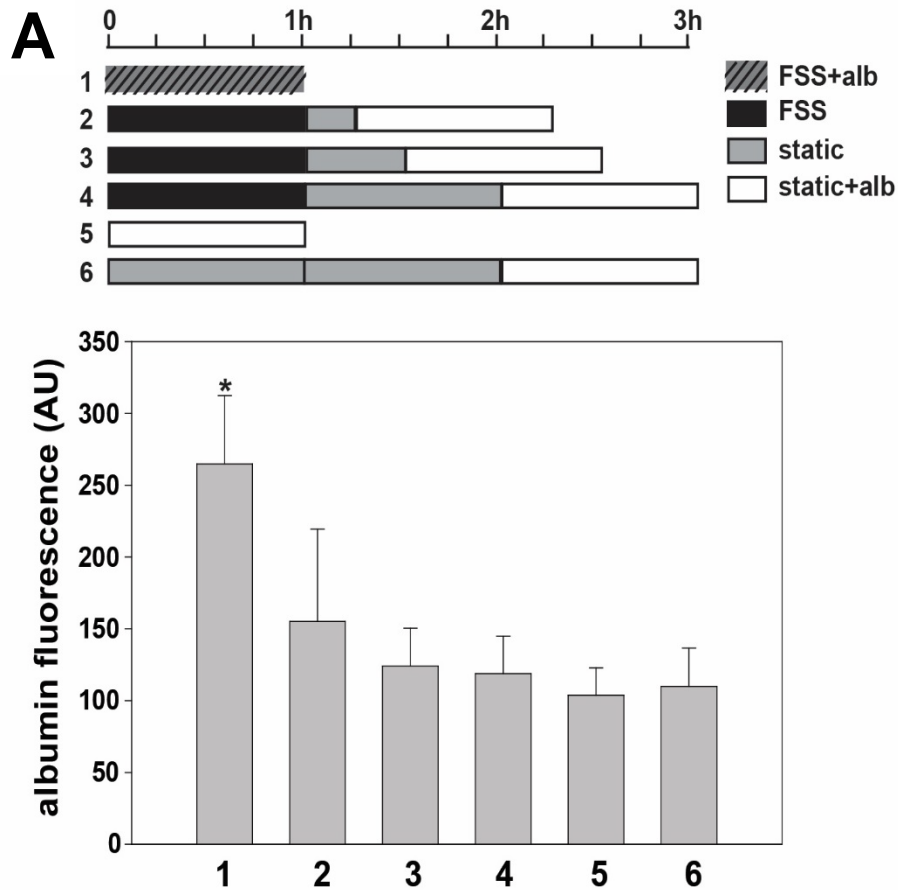
2.3.3 Onset and stress-dependence of FSS-stimulated endocytosis

To test the kinetics of FSS-stimulated endocytosis, I incubated OK cells under static conditions or exposed them to 1 dyne/cm² FSS in the presence of fluorescent albumin for various time points, then fixed and quantified uptake. As shown in Fig. 6A, uptake rates under FSS and static conditions were similar for the first 15 min, and then diverged. By 30 min of exposure to flow, there was a statistically significant increase in the overall amount of albumin internalized compared to cells treated under static conditions. This increased rate of uptake continued linearly for the remaining incubation period (Fig. 6A). In separate experiments, I monitored uptake over a 1-3 h incubation period (Fig. 6A, inset). Uptake of albumin in static and FSS-treated cells remained linear over this time period, with a roughly twofold increase in endocytosis in FSS treated cells compared with static at each time point.

In humans, normal GFR varies between 60-120 mL/min/1.73m² but can reach 160 mL/min/1.73m² in diseased individuals. To test whether PT cells adjust their endocytic capacity in response to changes in FSS induced within this range, I quantified the internalization of Alexa Fluor 647-albumin in OK cells exposed to FSS within a range of 0-1.5 dyne/cm² for 1 h. As

shown in Fig 6B, there was a general increasing trend in the amount of Alexa Fluor 647-albumin internalized by cells exposed to this range of FSS. Albumin internalization did not reach statistical significance relative to static controls (0 dyne/cm²) at 0.2, 0.4, and 0.7 dyne/cm², but was significantly different in cells exposed to FSS of 1.0 dyne/cm² and above. Importantly, there was a statistically significant increase in albumin uptake at cells exposed to 1.0 and 1.5 dyne/cm² compared with 0.7 dyne/cm² (equivalent to a GFR of ~60 mL/min/1.73m²). Exposure to higher FSS (1.5 dyne/cm², equivalent to a GFR of ~150 mL/min/1.73m²) did not increase endocytic capacity above the level observed at 1.0 dyne/cm² (Fig. 6B). This suggests that PT cells tune their internalization to maximum capacity in response to increased GFR within the normal physiologic range.

Figure 7. FSS stimulated endocytosis is rapidly reversible

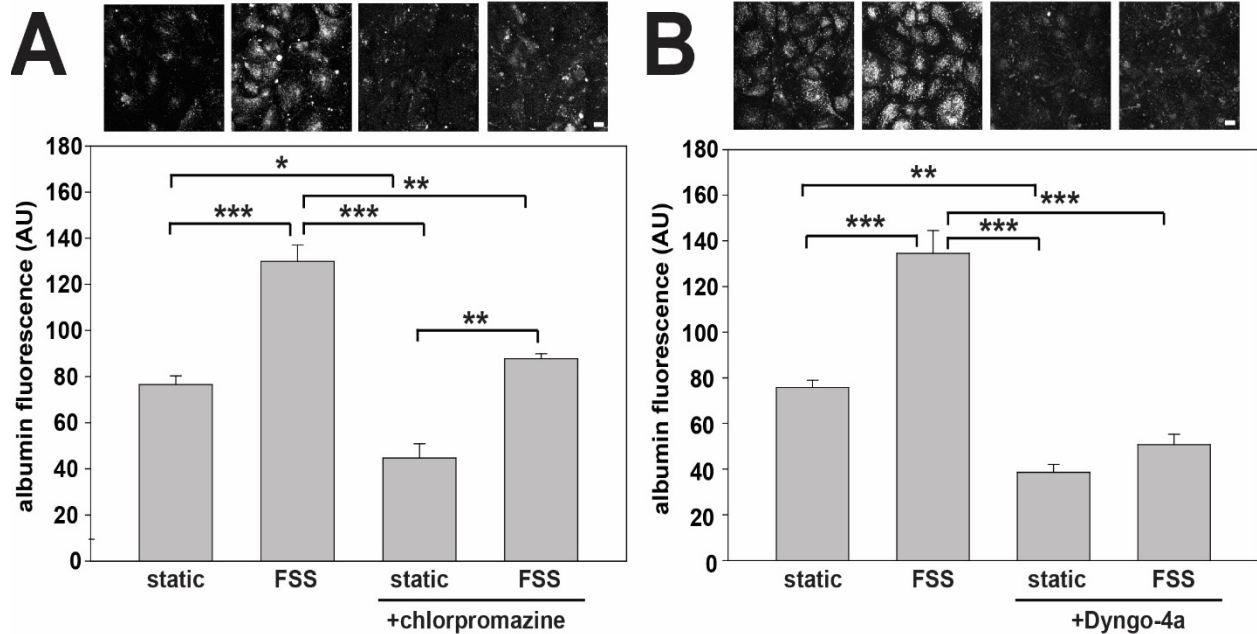


Reversibility of FSS-stimulated endocytosis. OK cells were exposed to 1 dyne/cm² FSS for 1 h in the presence (1) or absence (2-4) of 40 μ g/mL Alexa Fluor 647-albumin. Cells were then fixed immediately (1) or incubated under static conditions for 15 min (2), 30 min (3) or 60 min (4) prior to addition of 40 μ g/mL Alex Fluor 647-albumin for 1 h. As controls, Alexa Fluor 647-albumin was added to cells incubated under static conditions for 1 h at the start of the time course (5) or after 2 h (6) to coincide with the uptake period for sample 4. Internalized fluorescence was quantified for five fields per condition. The average fluorescence \pm range from two independent experiments is plotted. * $p < 0.05$ vs. static control (sample 6) by ANOVA with Bonferroni correction. All other pairwise comparisons are not significantly different

2.3.4 Reversibility of FSS dependent endocytosis

I measured the reversibility of the FSS-stimulated increase in endocytosis. To this end, I exposed cells to FSS for 1 h in the presence (Fig. 7, sample 1) or absence (Fig. 7, samples 2-4) of added albumin, then stopped the flow for various times (15-60 min; Fig. 7, samples 2-4) before adding fluorescent albumin to the cells for 1 h under static conditions. As controls, I incubated cells with fluorescent albumin for a 1 h period in the absence of flow either at the start of the experiment (at 0'; Fig. 7, sample 5) or coincident with the last uptake period (starting at 4; Fig. 7, sample 6). Albumin uptake in the presence of flow was robust compared with cells not exposed to FSS (Fig. 7, compare sample 1 to samples 5 and 6). Strikingly, reversal of the endocytic response to FSS was essentially complete by 15 min after the cessation of FSS (Fig. 7, sample 2).

Figure 8. Flow stimulated endocytosis is Clathrin and dynamin dependent

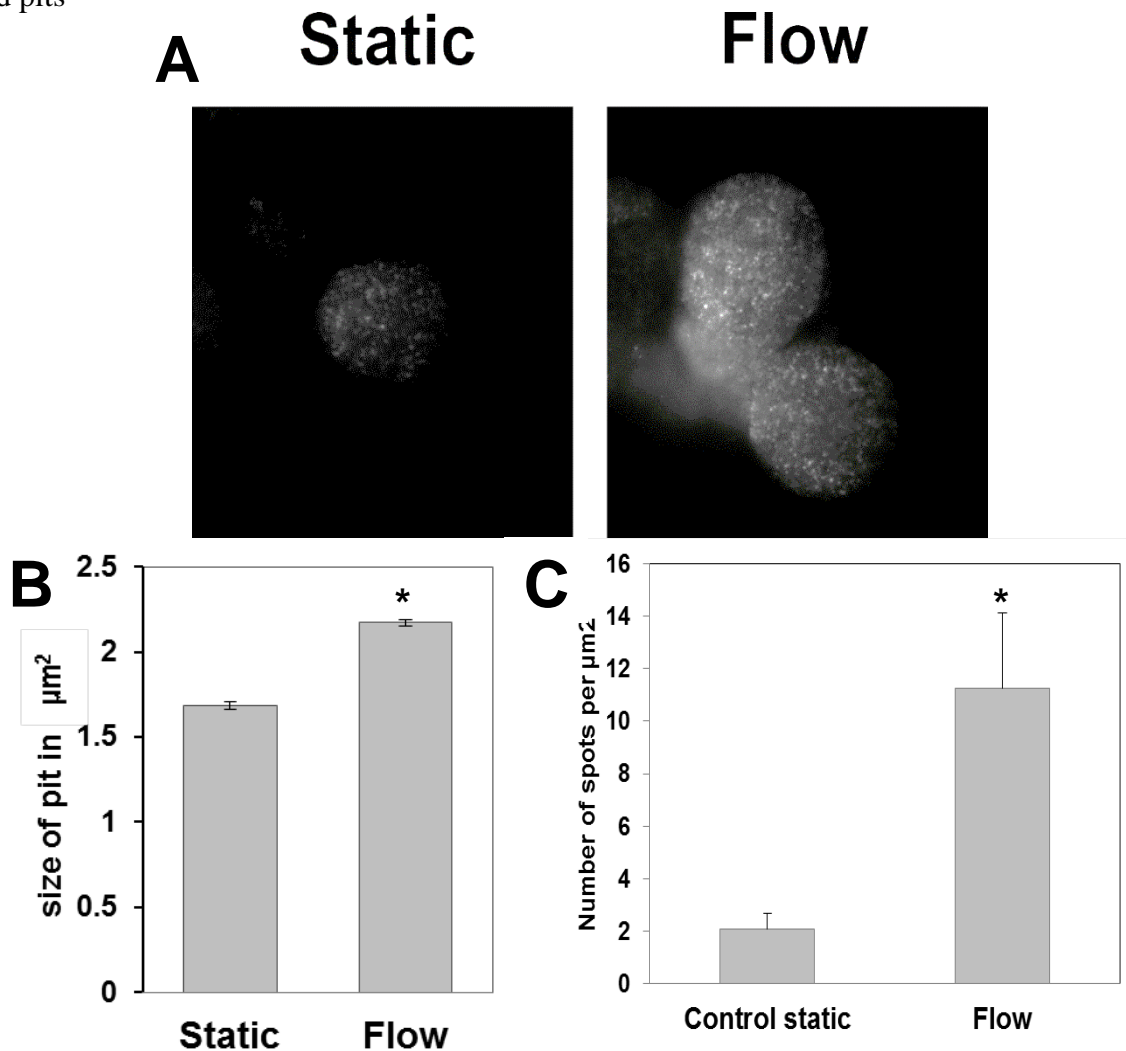


(A) OK cells cultured on Ibidi μ -slide chambers were pre-treated where indicated with 20 μ M chlorpromazine for 30 min. Cells were exposed to 40 μ g/mL Alexa Fluor 647-albumin for 1 h under static conditions or at 1 dyne/cm² (FSS). Albumin uptake was quantified as described in Methods, and the mean \pm SEM total albumin uptake in three independent experiments is plotted. (B) The effect of 30 μ M Dyngo-4a on basal and FSS-stimulated albumin uptake was quantified from four independent experiments. Mean \pm SEM is plotted. Maximum projections of representative fields of cells are shown above each bar in the graphs. Scale bar: 10 μ m. * p =0.014; ** p \leq 0.005; *** p <0.001 by ANOVA with Bonferroni correction. Other pairwise comparisons are not significantly different.

2.3.5 FSS-stimulated endocytosis occurs via a clathrin- and dynamin-dependent pathway

Megalin is internalized into clathrin coated pits that form at the base of microvilli of PT cells (65, 66). Although some immortalized PT cell lines express caveolin, caveolae are absent in PT cells in vivo (71), suggesting that clathrin-dependent endocytosis represents the primary mechanism for internalization of membrane and fluid from the apical surface of these cells. To test whether the FSS-stimulated component of albumin endocytosis occurs via a mechanism similar to that of basal uptake, I asked whether perturbants of clathrin-dependent endocytosis disrupted albumin uptake under static conditions and upon exposure to FSS. To this end, I preincubated cells for 30 min with chlorpromazine [a drug that inhibits assembly of clathrin coats] prior to addition of fluorescent albumin under static conditions or in the presence of 1 dyne/cm² FSS. I also observed that chlorpromazine did not completely ablate the FSS stimulated increase in endocytosis, and this could be due to the low dosage of the drug we used in this experiment. Treatment with chlorpromazine reproducibly and significantly inhibited both basal and FSS-stimulated endocytosis (by 42 and 33%, respectively; Fig. 8A). Treatment with the small-molecule dynamin inhibitor Dyngo-4a also reduced cell-associated albumin (by 49 and 62% in cells exposed to static and FSS conditions, respectively; Fig. 8B).

Figure 9. Exposure of pits to FSS causes an increase in both size and number of clathrin coated pits

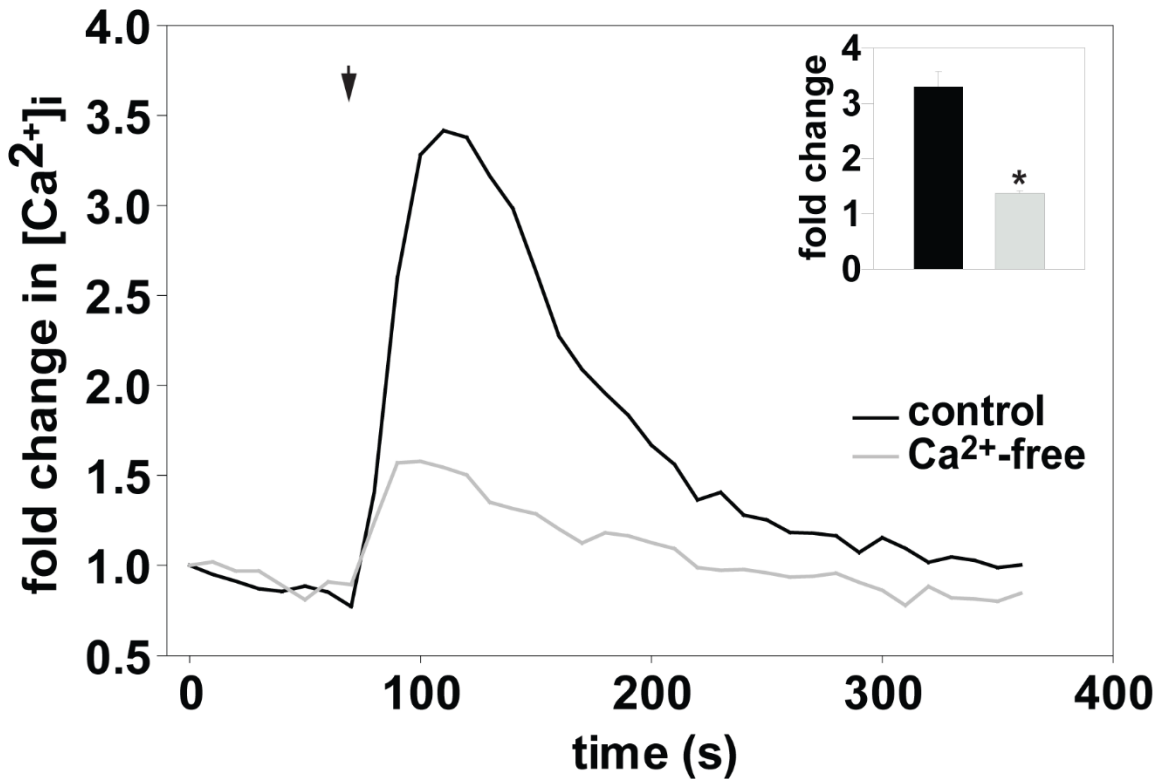


A) OK cells were transfected with ARH-tomato (to visualize CCPs) and were either subjected to FSS or kept under static conditions. Cells were fixed and subjected to TIRF microscopy. Images of representative fields are shown. (B) TIRF micrographs were analyzed using the growing spots function on IMARIS to quantitate the size of each clathrin coated pit in μm^2 , and (C) the number of spots per μm^2 was determined using Image J. The average size of ~6700 clathrin coated pits in 41 cells subjected to flow were 66% bigger than the ~7300 pits in the 53 cells incubated under static conditions across two experiments. * $p < 0.01$

2.3.6 Exposure of pts to FSS causes an increase in both size and number of clathrin coated pits

As shown in previous experiments, exposure of OK cells to FSS causes an increase in Clathrin mediated endocytosis. This increase could be caused because of the increase in endocytic capacity of each clathrin coated pit or by the increase in the total number of clathrin coated pits on the apical surface. As noted earlier in the introduction, the clathrin coated pits at the base of the microvilli in PT epithelia are distinctly different and tubular in comparison to other epithelial cells such as intestinal epithelial cells (65). To investigate the size and number of clathrin coated pits in PT cells, I transfected OK cells with ARH-tomato a Megalin CLASP that mediates clathrin recruitment to the base of microvilli. Cells were either kept under static conditions or exposed to FSS of 1 dyne/cm^2 for 1 hour, fixed and imaged using TIRF microscopy as explained in the Materials and Methods (Fig 9A). On examining ~7000 clathrin coated pits across two experiments I observed a 66% increase in the size of clathrin coated pits between the static and the FSS stimulated conditions (Fig 9B), and a 5 fold increase in the number of pits per square micron on the apical surface of OK cells (Fig 9C). This suggests that the FSS stimulated increase in endocytosis is caused by both an increase in the size of the clathrin coated pits and in sheer number of these pits on the apical surface. The individual pits obtained using this method are diffraction limited, therefore, this study has to be complemented with EM to understand the morphology and size of these CCPs.

Figure 10. FSS triggers an increase in cytosolic Ca²⁺

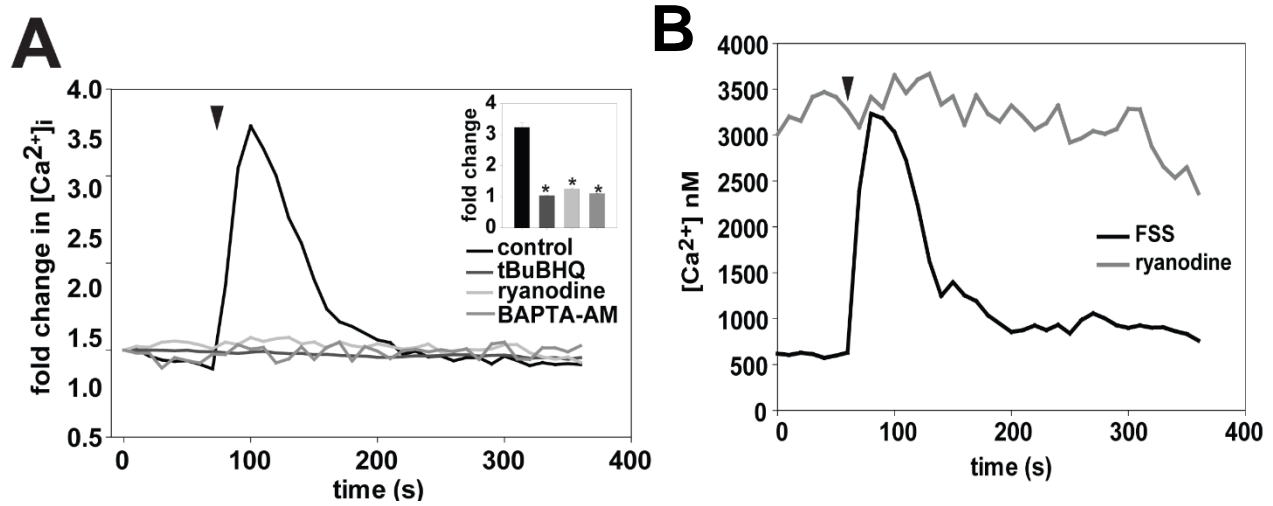


OK cells were loaded with Fura-2 AM and [Ca²⁺]_i measured upon exposure to 2 dyne/cm² FSS. FSS stimulates a rapid increase in [Ca²⁺]_i and this response requires extracellular Ca²⁺. Fura-2 AM loaded cells were perfused with Ca²⁺-containing (control, black traces in all subsequent panels) or Ca²⁺-free (light gray trace) buffer at 2 dyne/cm². The traces show fold change in [Ca²⁺]_i in a OK cell exposed to FSS. The inset shows the average peak fold change in [Ca²⁺]_i from 18 control cells (three experiments) and 28 cells perfused with Ca²⁺-free buffer (four experiments). P < by rank sum test.

2.3.7 Increase in cytosolic Ca^{2+} is the first effect in PT cells in response to exposure to FSS

Modeling studies have suggested that the flow-mediated changes in ion transport in the PT are regulated by a mechanosensitive mechanism induced by microvillar bending (148, 149). There is good evidence that primary cilia are not required for this pathway, as similar effects were observed in cells lacking mature cilia (99). In contrast, primary cilia are known to play an essential role in flow-mediated regulation of ion transport in the distal tubule (156). Genetic defects that affect cilia structure or function cause kidney disease, presumably as a consequence of aberrant FSS-dependent signaling (156, 157). Exposure to FSS is known to activate TRP channels localized on primary cilia to trigger an increase in $[\text{Ca}^{2+}]_i$ in many cell types, including kidney CCD cells (96, 156, 158). To test if exposure to FSS triggers a similar response in PT cells, polarized OK cells loaded with Fura-2 AM were perfused with Krebs buffer at a FSS of 2 dyne/cm² and fold change in $[\text{Ca}^{2+}]_i$, was determined as described in Materials and Methods. Exposure to FSS caused an immediate 3-4 fold increase in $[\text{Ca}^{2+}]_i$ that returned to baseline levels in 3-4 minutes (Fig. 10). The FSS-stimulated increase in $[\text{Ca}^{2+}]_i$ was not observed when Ca^{2+} was omitted from the perfusion buffer, demonstrating a requirement for extracellular Ca^{2+} in this response (Fig. 10).

Figure 11 Calcium-stimulated calcium release from the ER causes the FSS stimulated increase in $[Ca^{2+}]_i$

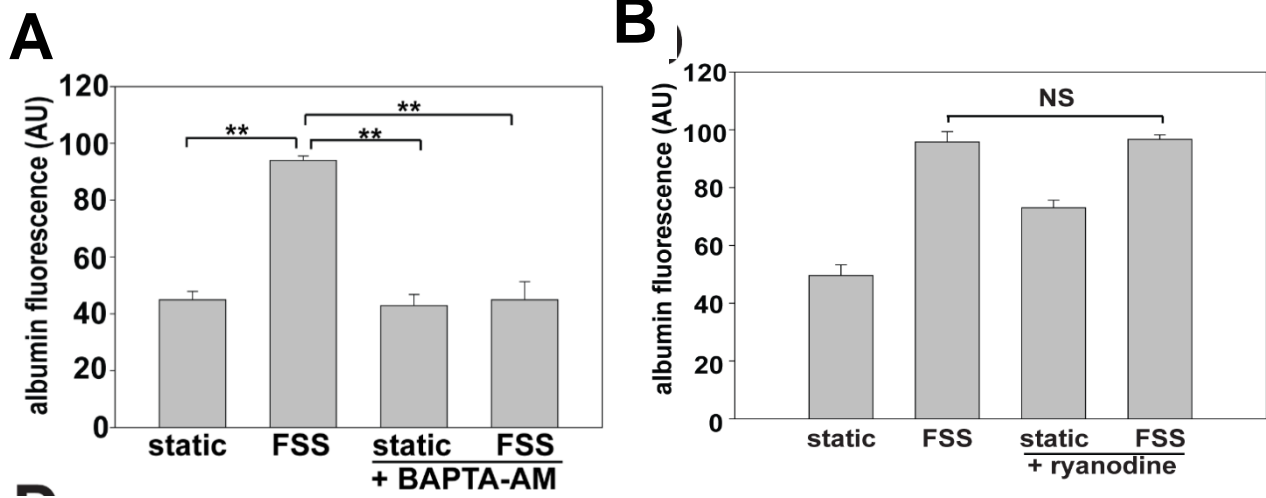


The Ca^{2+} response requires Ca^{2+} release from ryanodine sensitive ER stores. (A) Fura-2 AM loaded cells were treated with the SERCA inhibitor tBuBHQ (10 μ M; dark gray trace), BAPTA-AM (10 μ M; medium gray trace), or ryanodine (25 μ M, light gray trace). Inset shows the average peak fold change in $[Ca^{2+}]_i$ from 29 control (five experiments), 36 tBuBHQ-treated (four experiments), 47 BAPTA-AM-treated (three experiments), and 40 ryanodine treated cells (five experiments). (B) Representative Ca^{2+} traces showing changes in $[Ca^{2+}]_i$ upon exposure of control (black trace) or ryanodine-treated (medium gray trace) OK cells to FSS (marked by black arrowhead).

2.3.8 Ca^{2+} stimulated Ca^{2+} release from the ryanodine stores of calcium in the ER is requisite for the increase in the cytosolic levels of Ca^{2+}

Previous studies conducted in collecting duct cells have shown that the FSS-stimulated, cilium-dependent increase in $[\text{Ca}^{2+}]_i$ is mediated by Ca^{2+} -stimulated Ca^{2+} release from endoplasmic reticulum (ER) via ryanodine receptors (RyRs) (156). To assess the contribution of the Ca^{2+} -stimulated Ca^{2+} release to FSS-stimulated increase in $[\text{Ca}^{2+}]_i$, I treated OK cells with the SERCA inhibitor tBuBHQ to deplete ER reserves of Ca^{2+} and then subjected them to FSS. Resting $[\text{Ca}^{2+}]_i$ in tBuBHQ-treated cells was elevated relative to untreated cells as expected, and was unaffected upon exposure to FSS, confirming that ER stores of Ca^{2+} contribute to the FSS-stimulated rise in $[\text{Ca}^{2+}]_i$ (Fig. 11A). I then depleted the RyR sensitive pool of ER Ca^{2+} using ryanodine to test the role of RyRs in FSS-stimulated increase in $[\text{Ca}^{2+}]_i$. As shown in Fig. 11A, I observed that the flow stimulated increase in $[\text{Ca}^{2+}]_i$ was ablated post treatment with ryanodine, confirming that release of the RyR sensitive pool of ER Ca^{2+} is required for the flow stimulated increase in $[\text{Ca}^{2+}]_i$. I noticed that cells incubated with Ryanodine have a chronic increase in the cytosolic levels of Ca^{2+} confirming the release of RyR sensitive pool of ER Ca^{2+} (Fig. 11B). Additionally, buffering cytosolic Ca^{2+} by incubation with the cell permeable Ca^{2+} chelator BAPTA-AM inhibited the FSS-stimulated increase in $[\text{Ca}^{2+}]_i$ (Fig. 11A).

Figure 12. FSS stimulated changes in intracellular calcium is requisite for the stimulation of apical endocytosis

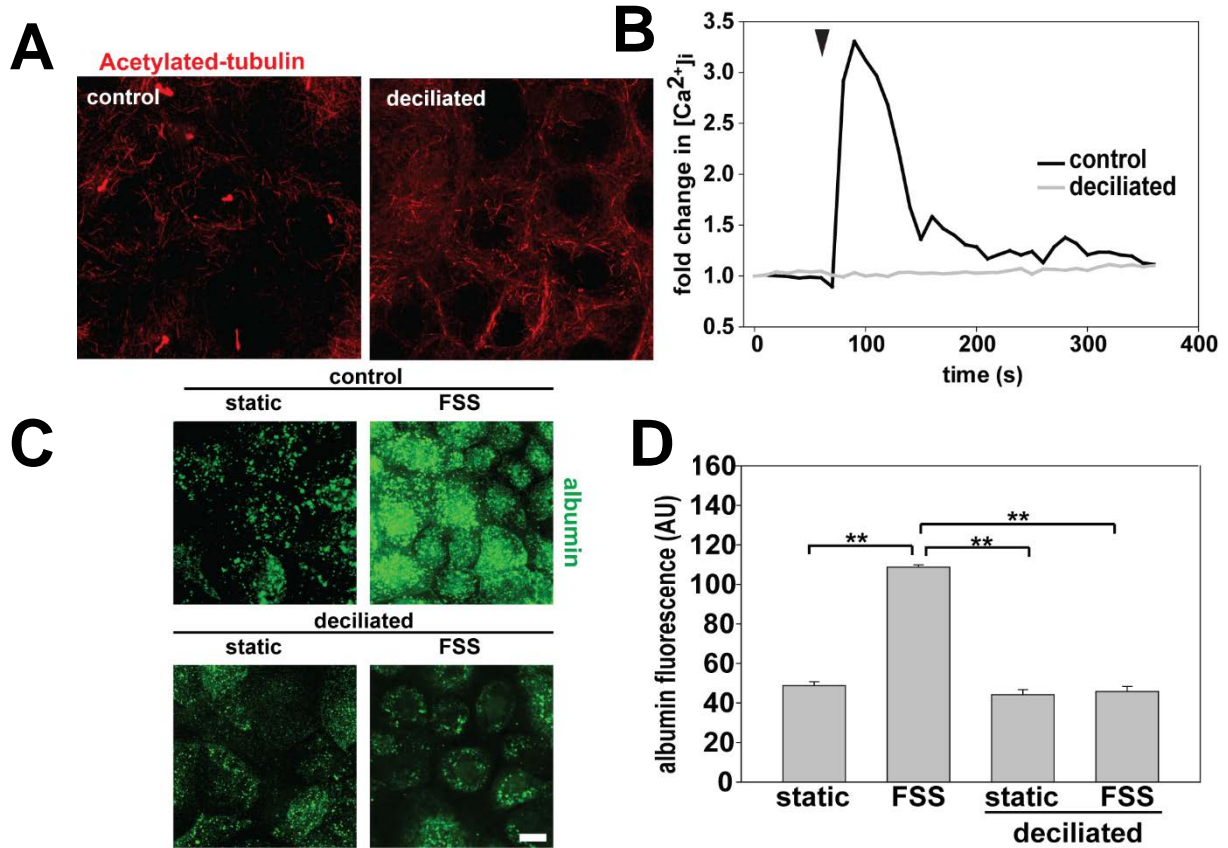


OK cells were loaded with Fura-2 AM and $[Ca^{2+}]_i$ measured upon exposure to 2 dyne/cm² FSS. (A) Quantitation of albumin uptake in control vs. cells treated with 10 μ M BAPTA-AM [mean \pm SEM of four experiments] incubated under static conditions or exposed to 1 dyne/cm² FSS for 1 h. ****P < 0.001** by ANOVA with Bonferroni correction. Other pairwise comparisons are not significantly different. (B) Endocytosis of Alexa Fluor 647-albumin was quantitated in OK cells incubated for 1 h under static or FSS conditions in the presence or absence of 10 μ M ryanodine as indicated. The mean \pm SEM of three independent experiments is plotted. Except where noted, all samples were significantly different from each other by ANOVA with Bonferroni correction; **P < 0.005**.

2.3.9 FSS stimulated increase in cytosolic Ca^{2+} is required and sufficient for stimulated apical endocytosis

I identified that Ca^{2+} -stimulated Ca^{2+} release from endoplasmic reticulum (ER) is critically important for the FSS stimulated increase in $[\text{Ca}^{2+}]_i$. I now wanted to know if the increase in $[\text{Ca}^{2+}]_i$ is requisite for the FSS stimulated increase in endocytosis. To do so, I buffered $[\text{Ca}^{2+}]_i$ in OK cells by including the Ca^{2+} chelator BAPTA-AM (Fig. 12A) in the perfusate. This selectively blocked FSS-stimulated but not basal uptake of albumin. Conversely, I wanted to ask if increase in $[\text{Ca}^{2+}]_i$ in the absence of flow would increase endocytosis. To do so, cells were either incubated under static conditions or subjected to FSS in the presence of $10\mu\text{M}$ ryanodine. Ryanodine stimulated endocytosis in the absence of FSS, and this effect was not further augmented by exposure of the cells to FSS (Fig. 12B).

Figure 13. Primary cilia are requisite for the FSS stimulated responses



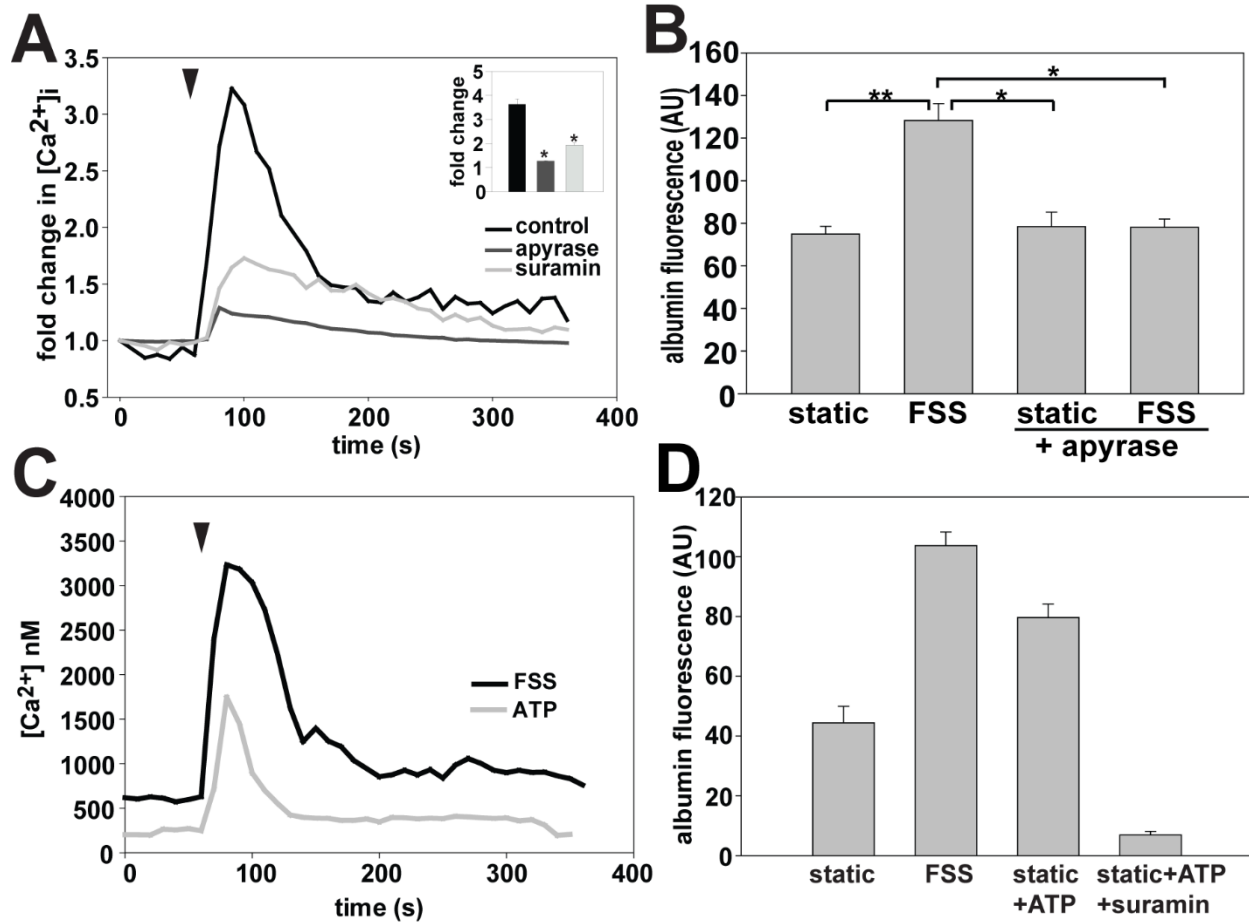
(A) Cells were fixed and processed to detect cilia (with anti-acetylated tubulin; red) and representative micrographs are shown above. (B) $[Ca^{2+}]_i$ does not increase in deciliated cells exposed to FSS. Cilia were removed from OK cells using 30 mM ammonium sulfate, then cells were loaded with Fura-2 AM and subjected to FSS (light gray trace). (C) OK cells were exposed to Alexa Fluor 647-albumin under static conditions or exposed to FSS (1 dyne/cm²) for 3h, internalized albumin (green); maximum projections of confocal stacks are shown. Scale bars: 10 μ m. (D) Quantitation of albumin uptake in control vs. deciliated cells [mean \pm SEM of three experiments] **p < 0.001 by ANOVA with Bonferroni correction. Other pairwise comparisons are not significantly different.

2.3.10 Primary cilia are required for FSS dependent modulation of endocytosis

As mentioned earlier in the introduction, primary cilia are critically important for mechanosensation and calcium signaling in the distal tubule and the collecting duct. However, their role in mediating mechanosensation in the proximal tubule is unclear. To test the role of the primary cilia in the FSS-stimulated increase in $[Ca^{2+}]_i$ I deciliated OK cells using 30 mM ammonium sulfate for 3 h. I previously showed that this treatment results in efficient and reversible removal of cilia [(133)and see Fig. 13A]. As shown in Fig. 13B, $[Ca^{2+}]_i$ in deciliated cells did not increase in response to FSS (Fig. 13B).

To test whether primary cilia dependent Ca^{2+} response are also required for the endocytic response to FSS in PT cells, I deciliated OK cells as above, and measured internalization of Alexa Fluor 647-albumin in cells incubated under static conditions or exposed to 1 dyne/cm² FSS. Strikingly, while basal albumin uptake under static conditions was unaffected in deciliated cells, the FSS-induced increase in endocytic uptake was almost entirely abrogated (Fig. 13 C,D). These results taken together strongly imply that the primary cilia play an important mechanosensory role in regulating the FSS stimulated responses.

Figure 14. Purinergic signaling is requisite for the FSS stimulated responses



OK cells were loaded with Fura-2 AM and $[Ca^{2+}]_i$ measured upon exposure to 2 dyne/cm² FSS. (A) The Ca^{2+} response requires extracellular ATP-mediated purinergic signaling. Fura-2 AM loaded cells were perfused with buffer containing 1 U/mL apyrase (dark gray trace) or were treated with suramin (200 μ M, light gray trace). Insets show observations from 24 control cells (four experiments), 48 cells perfused with apyrase (five experiments), and 24 suramin treated cells (four experiments). Error bars in insets show mean \pm SEM of the peak fold change in $[Ca^{2+}]_i$ responses for each condition and * p <0.001 by rank-sum test. (B) Quantitation of albumin uptake in control vs. cells treated with 1 Unit/mL Apyrase [mean \pm SEM of four experiments] incubated under static conditions or exposed to 1-dyne/cm² FSS for 1 h. * p <0.002, ** p < 0.001 by ANOVA with Bonferroni correction. Other pairwise comparisons are not significantly different. (C) Representative traces showing changes in $[Ca^{2+}]_i$ upon exposure of control (black trace) and The light gray trace shows the effect of acute addition of ATP in the absence of FSS on $[Ca^{2+}]_i$. Addition of ATP caused a statistically significant threefold increase in $[Ca^{2+}]_i$ (12 cells in 2 experiments; P < 0.001 vs. static control by rank-sum test.) (D) Endocytosis of Alexa Fluor 647-albumin was quantitated in OK cells incubated under static conditions \pm addition of 100 μ M ATP and 200 μ M suramin as indicated, or incubated at 1 dyne/cm² for 1 h.

The mean \pm SEM of five independent experiments is plotted. All samples were significantly different from each other by ANOVA with Bonferroni correction; $P \leq 0.006$.

2.3.11 Purinergic signaling is required for FSS dependent modulation of endocytosis

Bending of the cilium in kidney cells from the distal tubule is also known to cause extracellular release of ATP, which can trigger activation of purinergic receptors (P2YRs) causing a further increase in $[Ca^{2+}]_i$ (159). Therefore, I tested whether depletion of extracellular ATP alters the FSS-stimulated increase in $[Ca^{2+}]_i$ in PT cells. As shown in Fig. 14A, I found that inclusion of apyrase in the perfusion attenuated the FSS-stimulated increase in $[Ca^{2+}]_i$. The involvement of P2YRs in this signaling cascade was confirmed by addition of the pan P2YR inhibitor suramin, which also abrogated the FSS-stimulated Ca^{2+} response (Fig. 14A). Together, these data show that FSS triggers an increase in $[Ca^{2+}]_i$, which requires the primary cilium, extracellular Ca^{2+} influx, release of Ca^{2+} from ER stores through ryanodine receptors and ATP-dependent activation of P2Y receptors. Apyrase (Fig. 14B) in the medium also blocked FSS-stimulated but not basal uptake of albumin. I conclude that primary cilia and ATP-dependent P2YR signaling are both required for acute modulation of apical endocytosis in the PT in response to FSS.

Conversely, I asked whether increasing $[Ca^{2+}]_i$ in the absence of FSS is sufficient to trigger the downstream cascade that leads to enhanced endocytosis. As expected, addition of 100 μ M ATP in the absence of FSS caused an acute and transient 3-fold increase in $[Ca^{2+}]_i$ (Fig. 14C). Addition of ATP to cells incubated under static conditions also stimulated endocytosis by

roughly 50% (Fig. 14D). Both basal and ATP-stimulated endocytosis were profoundly inhibited by suramin (Fig.14D).

2.4 DISCUSSION

PT cells are specialized to internalize and recycle large amounts of apical membrane in order to effectively clear LMW proteins and other molecules from the glomerular ultrafiltrate. Defects in megalin or cubilin, which mediate the uptake of these filtered ligands (22), or saturation of this pathway as can occur in diabetic nephropathy (160), lead to tubular proteinuria and eventually to renal failure. However, surprisingly little is known about how apical endocytosis is regulated in PT cells, and whether this pathway can respond acutely to variations in glomerular filtration rate to maximize uptake efficiency of filtered ligands.

Studies conducted in the past decade have underscored the importance of FSS in affecting the organization of the cytoskeleton, activity of certain transcription factors, and the trafficking and retention of transporters that regulate vectorial ion transport in PTs (96, 147). My studies here demonstrate an additional role for FSS in the modulation of apical endocytosis in the PT. From My experiments I conclude that: (i) exposure to FSS increases apical endocytic uptake of fluid phase and membrane bound cargos in immortalized PT cells in culture; (ii) the FSS-stimulated endocytic response is rapid, reversible, and is mediated by a clathrin- and dynamin-dependent pathway; (iii) FSS also stimulates an immediate spike in intracellular Ca^{2+} mediated by Ca^{2+} -dependent Ca^{2+} release from ER stores; (iv) the primary cilium of PT cells is the principal mechanotransducer mediating the spike in FSS-stimulated intracellular Ca^{2+} and the subsequent endocytic response; and (v) release of extracellular ATP triggered by the bending of

primary cilia in the presence of flow is required for activation of P2YRs and for FSS-stimulated endocytic responses in PT cells. A working model for how this signaling cascade might modulate endocytic capacity is shown in Fig. 15.

I observed a dramatic increase in the rate and capacity of internalization of both membrane and fluid phase markers in several immortalized PT model cell lines, suggesting that exposure to FSS triggers a generic increase in membrane and fluid uptake capacity. In contrast, apical endocytosis in a cell line with characteristics of the distal tubule was not altered by exposure to FSS. A recent study also reported a similar effect on albumin uptake in OK cells cultured in a microfluidic chamber and exposed to FSS (155). Additionally, I observed that PT cells in mouse kidney slices exposed to FSS also internalized greater levels of fluorescent dextran compared with slices incubated under static conditions (data not shown). Both basal and flow-stimulated uptake in OK cells was inhibited by blockers of clathrin- and dynamin-mediated endocytosis, suggesting that exposure to FSS augments the capacity of the same clathrin-dependent apical internalization pathway that operates under static conditions. Stimulation of endocytic capacity was initiated rapidly upon exposure to FSS and ended within ~15 min of removal of the FSS stimulus. Moreover, I observed a statistically significant increase in the extent of endocytosis within the normal range of FSS encountered in the PT (0.7-1.0 dyne/cm², equivalent to GFR of 60-115 mL/min/1.73m²). Indeed, endocytic capacity reached maximal levels at FSS corresponding to the upper limit of normal GFR and was not further enhanced by higher FSS, suggesting that the inability to further increase endocytic capacity may contribute to tubular proteinuria. These characteristics of the endocytic response are consistent with a physiological role for FSS-stimulated endocytosis in the PT as a mechanism to accommodate normal variations in GFR throughout the day.

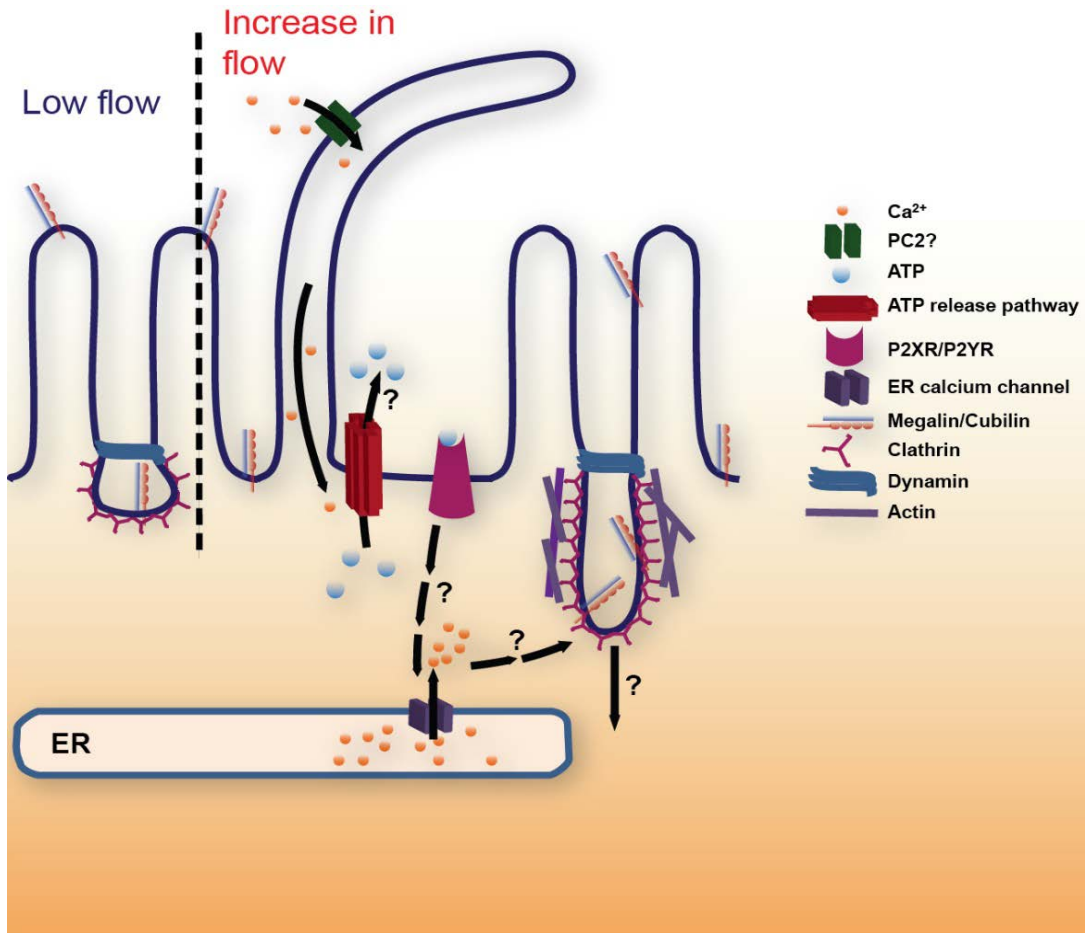
Exposure of PT cells to FSS triggered an immediate increase in $[Ca^{2+}]_i$ that was not observed in the absence of the primary cilium or of extracellular Ca^{2+} . I interpret this result to mean that Ca^{2+} influx mediated by a mechanosensitive channel in the cilium (likely polycystin-2) initiates the Ca^{2+} response to FSS. Similar to cascade that has been dissected in kidney cells in the distal tubule, I found that the FSS-stimulated increase in $[Ca^{2+}]_i$ also requires the activation of P2YRs by extracellular ATP and the release of ER Ca^{2+} stores via the ryanodine receptor. Although we predict that extracellular ATP plays an important role in the FSS stimulated signaling cascades, the role of other purines in this process cannot be completely discounted. Notably, deciliation or depletion of extracellular ATP also inhibited FSS-stimulated endocytosis in PT cells, suggesting that the increase in $[Ca^{2+}]_i$ triggered by FSS is a required step in the cascade that leads to the endocytic response. Moreover, transient or sustained elevation of $[Ca^{2+}]_i$ in the absence of FSS was sufficient to stimulate endocytic capacity. Other GPCRs in the PT cells, such as the AT1AR could also play a critically important role in transducing the FSS stimulated changes in PT cells as mentioned previously in Chapter 1.

How does initiation of the mechanotransduction cascade by FSS ultimately lead to an increase in endocytic capacity in PT cells? In principle, either an increase in the number of clathrin coated pits or an increase in the size of individual pits could account for the enhanced uptake I observed. Electron microscopy studies examining PT cells in vivo show strikingly irregular clathrin-coated invaginations at the base of apical microvilli (65, 67, 69). Fluid phase and membrane tracers are internalized in these unevenly shaped structures, which bud from the apical membrane and fuse with a subapical network of tubules (65). My data suggest that exposure to FSS increases both the average size and the number of these clathrin-coated structures to accommodate larger endocytic capacity. Consistent with this, there is precedence

for modulation of clathrin-coated pit size in nonpolarized cells to accommodate larger cargoes such as virus particles (161). Unlike “traditional” clathrin-mediated endocytosis, internalization of these large cargoes requires modulation of actin dynamics at the coated pit site. I further hypothesize that the increase in number of the CCPs we observed in fig. 9 is caused by the upregulation of the cascade that leads to increased number of coated pits. I hypothesize that a similar pathway could be triggered upon FSS-stimulated $[Ca^{2+}]_i$ increases in PT cells.

The involvement of primary cilia in the endocytic response to FSS is the first known function for cilia in PT cells and raises the possibility that defects in ciliogenesis could impair the regulation of apical endocytic uptake in these cells. Genetic defects that alter ciliary function or structure lead to renal disease. To date, all disorders that result in shortened primary cilia in the kidney cause cystic disease, presumably as a consequence of aberrant flow-dependent signaling (156, 157). In contrast, transient elongation of cilia has been observed during kidney development and during recovery from acute kidney injury (162, 163). It is unclear how changes in cilia length might impact the endocytic response to FSS in the PT. Strikingly, however, cilia length has been found to be altered in cells and zebrafish depleted of OCRL1, the phosphatidylinositol 5'-phosphatase defective or absent in patients with Lowe Syndrome, an X-linked disorder that results in tubular proteinuria (129, 133, 164). While the precise effects or mechanism are not yet clear, as both longer and shorter cilia were reported, these studies provide a tantalizing link that could explain how loss of OCRL1 function leads to tubular proteinuria in Lowe Syndrome patients. Future studies will be required to examine whether defects in the modulation of endocytosis by FSS contribute to kidney disease in these and other patients with tubular proteinuria.

Figure 15. Model for acute modulation of apical endocytosis in the Proximal tubule



My data support a model in which exposure to FSS increases apical endocytic capacity in PT cells via a pathway that requires ciliary bending, and entry of extracellular Ca^{2+} via a ciliary-localized cation channel [possibly polycystin-2 (PC2)] that lead to increases in $[\text{Ca}^{2+}]_i$, which are further amplified by Ca^{2+} release from endoplasmic reticulum (ER) stores. Bending of the primary cilium also causes release of ATP to the luminal surface which in turn activates P2YRs and further increases $[\text{Ca}^{2+}]_i$. Endocytosis from the apical surface of polarized cells is known to occur exclusively at the base of microvilli via a clathrin- and dynamin-dependent pathway that is dependent on actin. I hypothesize that increased $[\text{Ca}^{2+}]_i$ triggers a cascade that ultimately modulates actin dynamics to increase the size and volume of individual apical clathrin-coated pits.

2.5 FUTURE DIRECTIONS

The observations above suggest a model whereby ciliary bending activates cation channels (possibly polycystin-2) that lead to a small increase in $[Ca^{2+}]_i$ which triggers extracellular ATP release to activate P2Rs and stimulates further Ca^{2+} release from ER stores, ultimately leading to enhanced endocytosis (Fig. 15). Needless to say, many gaps in our understanding of the steps and implications of this model remain, and are discussed further below.

Although primary cilia are required for the endocytic response to FSS, the mechanosensitive channel that initiates the response remains to be identified. An obvious candidate is the transient receptor potential (TRP) channel polycystin-2 (PC-2), which is important for flow-dependent responses in the distal tubule (156). The related TRPV4 channel has also been implicated in mechanosensation in the distal tubule, possibly by forming a complex with PC-2 (165-168); however, TRPV4 is not expressed in the PT (169).

An unresolved general question of broader significance is the relationship between cilia length, Ca^{2+} signaling, and the endocytic response. Mutations in many proteins involved in ciliary biogenesis lead to cystic kidney disease, and both shorter and longer cilia can be observed under these conditions. However, the relationship between FSS, ciliary length, and Ca^{2+} release from ER stores is unknown: is Ca^{2+} release graduated or binary when the other variables are altered? Surprisingly, there have been no studies where the effect of different FSS on $[Ca^{2+}]_i$ in cells with varying cilia length has been systematically measured. Interestingly, the cilioplasm appears to be segregated from the cytosol, and can function as a discrete Ca^{2+} signaling domain (170, 171). A modeling study predicts that longer cilia are more sensitive to flow, and consistent with this idea, two reports suggest that FSS-stimulated Ca^{2+} signaling is blunted in cells with

shortened cilia (162, 172, 173). However, one of these groups also observed blunted Ca^{2+} responses in young mice, which have longer cilia than their older counterparts (162). Thus, there may be an optimal cilia length that enables maximal signaling.

Another essential question to address is what maintains the endocytic response to flow after the initial and transient spike in $[\text{Ca}^{2+}]_i$? Endocytosis rates increase in PT cells within 15-30 min after exposure to FSS, and this increased rate of uptake persists long after $[\text{Ca}^{2+}]_i$ has returned to baseline levels, so long as the FSS is maintained [at least up to 3 h (174)]. Moreover, once the flow is removed, endocytic rates return to normal very rapidly. This suggests that an as yet undetermined and sustained signal/secondary messenger is initiated by the increase in $[\text{Ca}^{2+}]_i$ that continues to sense the level of FSS and maintain enhanced endocytic capacity.

In other tissue types, such as mast cells and neurons, a rapid spike in $[\text{Ca}^{2+}]_i$ triggers rapid exocytic membrane trafficking events which are regulated by calcium-sensing membrane fusion promoting proteins like synaptotagmin. These exocytic events cause an increase in the membrane surface area, and in order to recoup the lost membrane, cells trigger endocytosis. This phenomenon is called compensatory endocytosis. In my study, I have focused on understanding the endocytic trafficking events that are triggered by the spike in $[\text{Ca}^{2+}]_i$ in PTs as endocytic trafficking is the most physiologically important function of the PTs. Monitoring the immediate changes in exocytosis in response to changes in FSS is another area open for further study.

My model hypothesizes that subsequent to ciliary bending, the release of ATP into the extracellular milieu is critically important for the FSS-stimulated response. Moving forward, it is important to define the mechanism(s) underlying flow-mediated ATP release from PT cells. Several pathways are known to enable ATP release in the kidney and other organs (175). First, ATP can be released by the connexin (Cx) family of gap-junction channels. Cx30 hemichannels

have been demonstrated to play a role in luminal ATP release in the distal tubule (176), and several members of the connexin family are reported to be expressed in the PT, including Cx26, Cx32, Cx37, Cx40, and Cx43 (177-181). Second, the channel-forming pannexin1 (Panx1) protein is widely expressed in the kidney, including the PT, and has been found to play a role in luminal ATP release (182). Several chloride channels, including maxi anion channels, voltage-regulated ion channels, and tweety anion channels have also been implicated in ATP release from cells (175). Finally, ATP may be delivered to the extracellular milieu through constitutive vesicular release or through Ca^{2+} -triggered exocytosis, as has been demonstrated in MDCK cells (183).

I consistently observed that the pan-purinergic receptor blocker suramin inhibits both the increase in $[\text{Ca}^{2+}]_i$ and endocytosis in response to FSS, consistent with a critical role for purinergic signaling in mediating these FSS dependent responses. Purinergic receptors that have been variously reported to be expressed in the PT include P2X1, P2X4, P2X5, P2X6, and P2X7, and P2Y1, P2Y2, P2Y4, P2Y6, and P2Y11 (184-189). Some discrepancies in expression of these receptors have been reported in different studies, and there may also be species-dependent differences. The purinergic receptor involved in this cascade can be identified by knocking down candidates and/or through pharmacological interventions.

P2X receptors typically trigger ER Ca^{2+} release via activation of ryanodine receptors, whereas P2YRs are commonly thought to signal via IP3 receptors. While I observed that ryanodine added at concentrations where it functions as an agonist of the ryanodine receptor can trigger endocytosis even in cells maintained under static conditions, I do not know whether it is required for the FSS-stimulated endocytic response. Identifying the ER Ca^{2+} release channel

involved in the endocytic response to FSS is challenging, but may also provide clues as to which purinergic signaling mechanism (P2X or P2Y) is relevant.

Finally, I lack an understanding of how increases in $[Ca^{2+}]_i$ are transduced into enhanced endocytic capacity. The increase in endocytosis could be due to an increase in the number of coated pits and/or an increase in their average size. There is precedence for actin-dependent modulation of coated vesicle size, as recent studies have shown that actin is required for clathrin-mediated uptake of larger cargoes such as virus particles, whereas endocytosis of most cargoes in nonpolarized cells is largely actin-independent (190). Coated pit morphology at the apical surface of PT cells is highly irregular compared with other polarized epithelial cells consistent with dynamic variation in endocytic pit capacity. My recent unpublished results suggest that Cdc42 a small GTPase involved in regulating actin dynamics may play a role in coupling the initial Ca^{2+} response to flow into enhanced apical endocytosis.

In addition to the cell-based studies mentioned above, utilizing two-photon microscopy to visualize endocytosis of albumin or fluid phase markers in the proximal tubules of rodents would give us greater insight into the regulation of apical endocytosis in response to variations in GFR. An alternate method that we will be using in the near future is to set up a single tubule perfusion system to study the regulation of apical endocytosis in response to variations in intra-tubular flow-rate.

changes in $[Ca^{2+}]_i$. Apical endocytosis in both OCRL1 knockdown and control cells could be stimulated by downstream activation of Cdc42, a small GTPase whose activity is modulated by $[Ca^{2+}]_i$ and which is essential for the endocytic response to FSS. Loss of OCRL1-dependent FSS sensing in PT cells may explain the underlying cause of tubular proteinuria in Lowe syndrome patients.

3.2 INTRODUCTION

Lowe syndrome is an X-linked disease caused by mutations in the phosphatidylinositol phosphatase OCRL1. A hallmark of Lowe syndrome is tubular proteinuria, which results from inefficient uptake of filtered proteins by cells lining the PT. However, defects in apical endocytosis have not been demonstrated in kidney cells depleted of OCRL1. In this chapter, I discuss the possible role of OCRL in regulating the FSS stimulated endocytic cascade in renal proximal tubule epithelia.

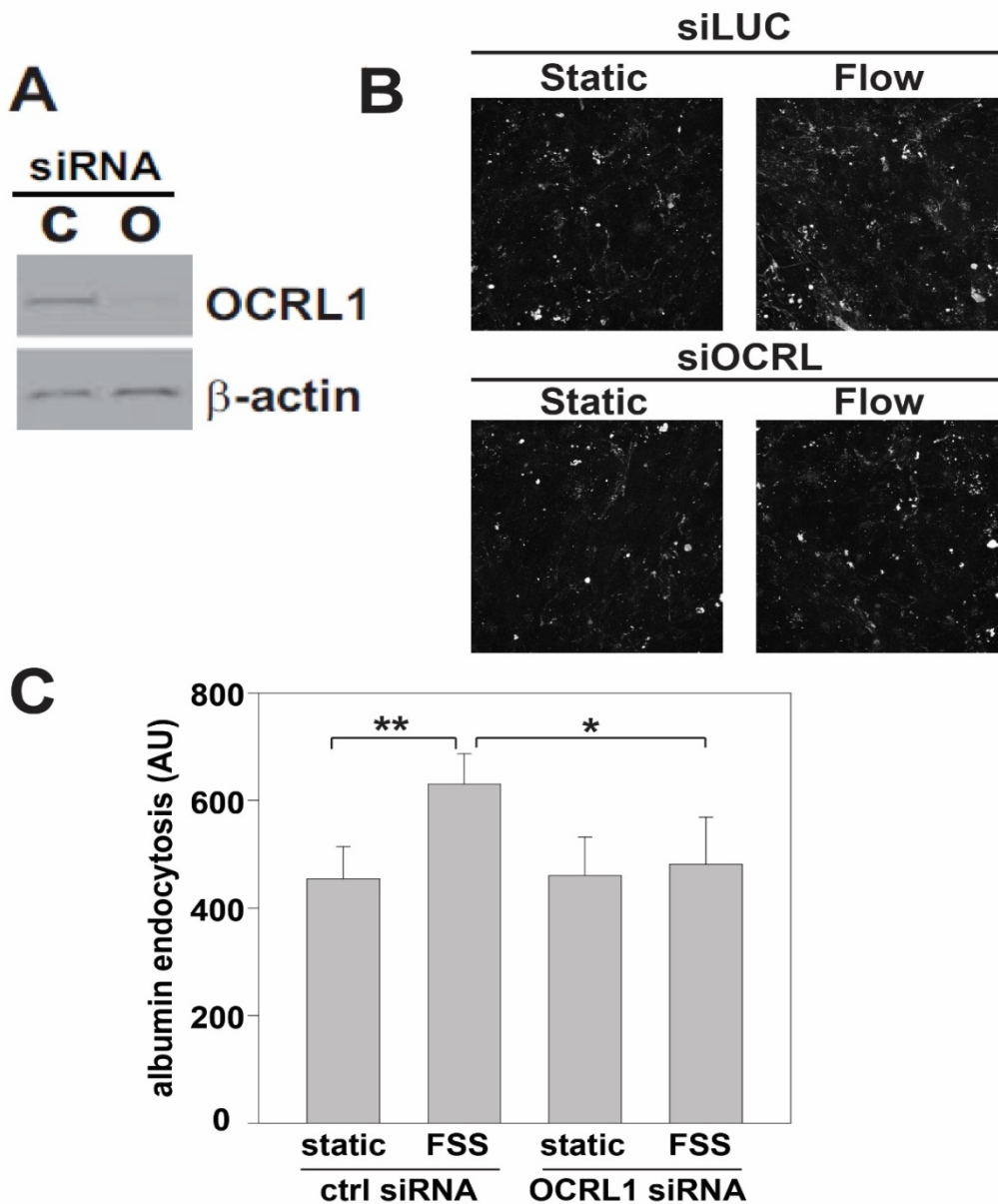
The mechanism by which loss of OCRL1 function causes proteinuria is unclear, but is unlikely to be due to a direct effect on megalin trafficking. OCRL1 is primarily localized to the *trans*-Golgi network, but a subpopulation of the protein is associated with clathrin-coated pits and endosomes, and is known to interact with clathrin, numerous Rab proteins, and APPL1 (119, 125, 135, 136, 191-195). No defects in megalin endocytosis in OCRL1-depleted cells have been reported. However, several laboratories, including ours, have identified defects in protein recycling and/or in lysosomal protein delivery in OCRL1-depleted cells (125, 135, 142, 191).

This finding is consistent with clinical observations that Lowe syndrome patients have elevated plasma levels of lysosomal hydrolases (196-198).

Recently, our lab and others found that depletion of OCRL1 in zebrafish and mammalian kidney cells alters ciliary biogenesis (129, 133, 164, 199). Zebrafish express a single copy of *ocrl* that is expressed early in development in the pronephric kidney, brain, and eye: the organs affected most in Lowe syndrome patients (133). Injection of zebrafish larvae with increasing amounts of a translation-blocking morpholino resulted in progressively impaired development, characterized by pericardial effusion, hydrocephaly, and tail curvature. These phenotypes, which are consistent with a defect in osmoregulation, were rescued by injection of wild type but not catalytically inactive OCRL1 mRNA [(133)]. Moreover, our lab previously measured a striking defect in renal clearance of freely filtered fluorescent dextran injected into the cardinal vein of zebrafish embryos [(133)]. In fish, PT endocytosis plays a major role in renal clearance (78, 200, 201), and we observed a dramatically reduced number of fluorescent endocytic vesicles in the PT of morphant fish. This defect may be due to alterations in ciliary function, as cilia in the pronephric kidney were markedly longer in the morphants [(133)].

In chapter 2, I showed that apical endocytosis in PT cells is modulated by fluid shear stress (FSS) via a pathway dependent on primary cilia, purinergic signaling, and release of $[Ca^{2+}]_i$ stores from the endoplasmic reticulum (ER). To test whether OCRL1 depletion impairs the endocytic response to FSS, I knocked down the protein in human proximal tubule HK-2 cells. I determined that OCRL acts downstream of the calcium signaling cascade upregulated in PT cells in the presence of FSS. However, the exact role of OCRL in the FSS stimulated endocytic cascade is still unclear, and further investigation is necessary.

Figure 16. FSS stimulated apical endocytosis in OCRL1 depleted PT cells is defective



(A) HK-2 cells transfected with control or OCRL1 siRNA were solubilized and blotted with anti-OCRL1 antibodies or β -actin antibody as a loading control. Control or OCRL1-depleted HK -2 cells were incubated under static conditions or at 1 dyne/cm² FSS for 1 h in the presence of AlexaFluor 647-albumin, then fixed, imaged, and albumin uptake quantified as described in Methods. Representative fields are shown in (B) and the mean \pm SE of three independent experiments in plotted in (C). *p<0.05; **p<0.001 by Student's t-test; all other comparisons not significantly different.

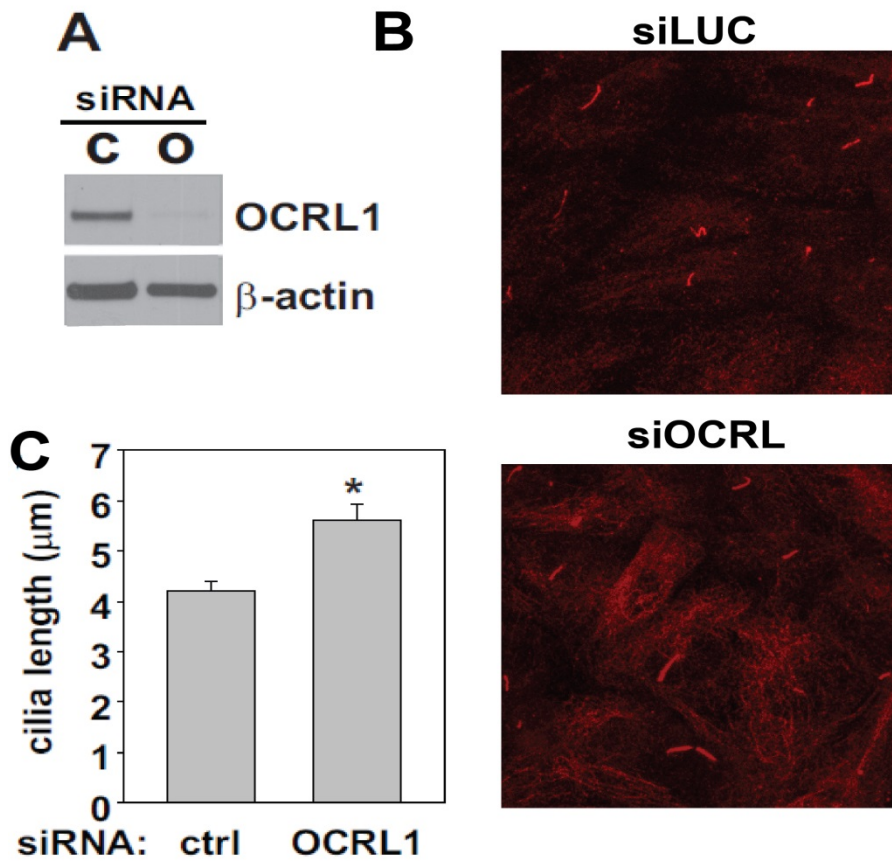
3.3 RESULTS

3.3.1 FSS stimulated apical endocytosis in OCRL1 depleted pt cells is defective

OCRL1 is known to bind to clathrin and to other endocytic adaptors through its C and N terminal clathrin binding boxes and its PH domain (136). Our lab tested to see if loss of OCRL1 caused reduction in apical endocytosis in renal epithelial cells using an MDCK cell system expressing rat mini-megalin, and repeatedly failed to observe any defects in the endocytic uptake of the megalin ligand lactoferrin (142). I therefore asked whether only flow stimulated responses rather than constitutive endocytosis in the proximal tubule epithelia are defective in cells lacking OCRL1. To test this hypothesis, I used HK-2 cells, a human immortalized proximal tubule cell line that expresses endogenous megalin and cubilin and which elaborates a primary cilium.

I depleted OCRL using small interfering siRNA against exon 2 of the OCRL gene, and as shown in Fig. 16A I routinely observe a ~60 to 70% KD of the endogenous protein. Strikingly, I also found that in three consecutive independent experiments, the FSS stimulated increase in endocytosis in OCRL depleted was completely ablated. In subsequent experiments I did not observe a complete loss of the endocytic response, and more recently I have started to observe an increase in non-specific basolateral signal in both control and OCRL depleted cells. On an average across how many experiments I found that the FSS stimulated endocytic response was decreased by nearly 60% in cells treated with OCRL1 siRNA. In addition to the first siRNA, I used a second siRNA against OCRL1 and noticed about 50% efficacy of knockdown which deteriorated to ~20% within a period of a month. This siRNA was ordered from Sigma, and I predict that the oligo was not stable for long-term usage.

Figure 17. OCRL1 depletion leads to increased cilia length in human proximal tubule cells



(A) HK-2 cells transfected with control or OCRL1 siRNA were solubilized and blotted with anti-OCRL1 antibodies or β -actin antibody as a loading control. Duplicate samples of cells were fixed, stained with anti-acetylated tubulin, and cilia length quantified from confocal images using ImageJ software. Representative images are shown in (B) and quantitation of mean cilia length \pm SEM in three experiments is shown in (C). $n=216$ cilia (control), 240 (OCRL1). $*p<0.01$ two tailed t-test.

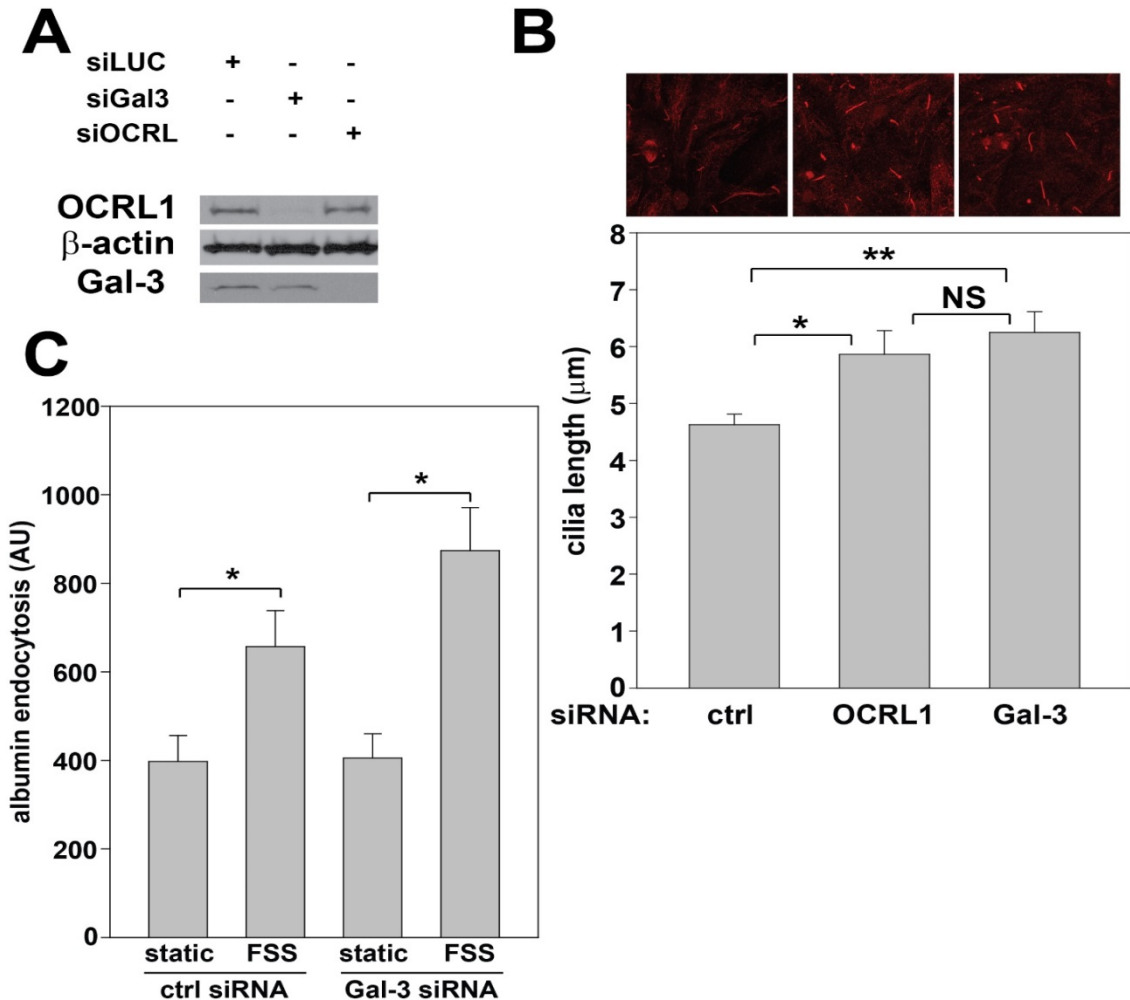
3.3.2 OCRL1 knockdown causes increase in cilia length in human proximal tubule cells

Knockdown of OCRL1 has no effect on the basal (constitutive) level of endocytosis, and studies to date have failed to explain how loss of this enzyme results in proteinuria in Lowe syndrome patients. Several labs, including our own, have found that knockdown of OCRL1 alters cilia length in canine kidney cells, in fibroblasts, and in zebrafish pronephric kidney. Morpholino-mediated depletion of OCRL1 also disrupts pronephric kidney function (133, 164, 195). Surprisingly, while our lab uniformly observed an increase in ciliary length upon depletion of OCRL1, other labs report shortened cilia (129, 134, 164). The reason for this discrepancy is unknown. Having determined that the flow-stimulated endocytic response is affected in these proximal tubule epithelia, I asked whether the loss in mechanosensation is caused by the defective ciliogenesis associated with OCRL1 depletion.

As shown in Fig. 17A, I knocked down OCRL1 in HK2 cells and measured cilia length using anti-acetylated tubulin as a marker. Across three experiments, I noticed that the length of cilia was approximately 50% greater in the OCRL1 depleted cells compared to the control cells. This result agrees with the previous findings from our lab in other cell types and underscores the importance of OCRL1 in ciliogenesis.

Having determined that cilia are longer in the OCRL1 depleted cells, malformed or longer cilia may be the cause underlying the loss of mechanosensitive response. Therefore to test this hypothesis, I used an alternative method to elongate cilia, and determined whether longer cilia are sufficient to trigger the FSS stimulated endocytic response.

Figure 18. Increase in cilia length does not cause defective FSS stimulated apical endocytosis



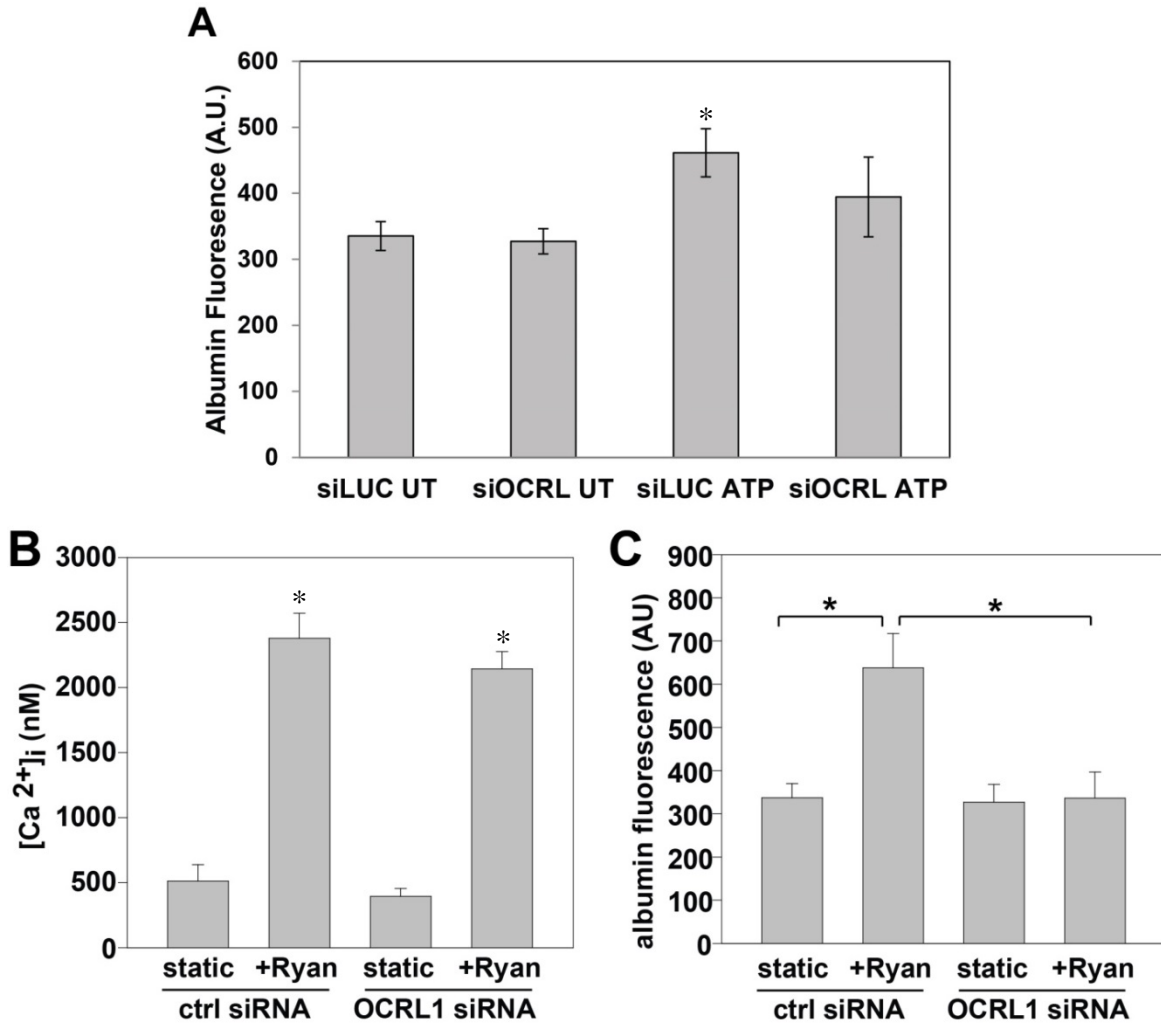
(A) HK-2 cells were solubilized three days after transfection with control siRNA, OCRL1, or Galectin-3 (Gal-3) siRNA and blotted with anti-OCRL1 and anti-Gal-3 antibodies or with β -actin antibody as a loading control. Duplicate samples of cells were fixed, stained with anti-acetylated tubulin, and cilia length quantified from confocal images using ImageJ software. Representative images are shown in (B) and quantitation of mean cilia length \pm SEM in three experiments is shown in (C). $n=589$ cilia (control), 557 (OCRL1), and 467 (Gal-3); * $p=0.024$; ** $p=0.017$ by ANOVA. NS: not significantly different. (D) Uptake of AlexaFluor 647-albumin was quantified in cells transfected with control or Gal-3 siRNA and incubated under static conditions or at 1 dyne/cm^2 FSS for 1 h. The mean \pm SEM of six independent experiments is plotted. * $p<0.01$ by student's t-test.

3.3.3 Increase in cilia length is not responsible for defective FSS stimulated apical endocytosis

To test whether the effect of OCRL1 depletion on the endocytic response to FSS is due to changes in ciliary length, I elongated cilia length using a different approach. Our lab and others have previously found that knockdown of galectin-3 increases cilia length, and we asked whether this maneuver also impairs the endocytic response to FSS (59, 61). Knockdown of galectin-3 was about ~80% efficient (Fig. 18A) and resulted in elongation of primary cilia in HK-2 cells to the same extent as OCRL1 depletion (Fig. 18B). The increase in cilia length of ~45% across three experiments was very comparable to the cilia elongation with the OCRL1 knockdown. However, despite having longer cilia, endocytosis in galectin-3-depleted cells was stimulated to the same extent as control upon exposure to FSS (Fig. 18C). Based on this evidence, I conclude that the effect of OCRL1 depletion on cilia length does not explain the impaired response to FSS.

A recent study conducted in a OCRL^{-/-} zebrafish model identified that the impairment in endocytosis cannot be attributed to the mild ciliogenesis effect they noticed in these fish. This once again echoes our conclusion that the defects in ciliary length is not responsible for the loss of mechanosensation.

Figure 19. ATP and ryanodine stimulated endocytosis is ablated in OCRL1 depleted cells



(A) Endocytosis of AlexaFluor 647-albumin was quantified in cells transfected with control or OCRL1 siRNA and incubated under static conditions with or without 100 μ M ATP for 1 h. SEM of seven independent experiments is plotted. * $p < 0.04$ by two-tailed t-test. (B) Intracellular Ca^{2+} was measured in Fura-2 loaded HK-2 cells transfected with control or OCRL1 siRNA. Cells were preincubated with ryanodine (Ryan, 10 μ M) for 30 min where indicated. The mean \pm SEM of 17 cells for each condition is plotted. * $p < 0.05$ by two-tailed t-test (C) Endocytosis of AlexaFluor 647-albumin was quantified in cells transfected with control or OCRL1 siRNA and incubated under static conditions with or without 10 μ M ryanodine for 1 h. The mean \pm SEM of four independent experiments is plotted. * $p < 0.05$ by student's t-test.

3.3.4 ATP and ryanodine stimulated endocytosis is ablated in OCRL1 depleted cells

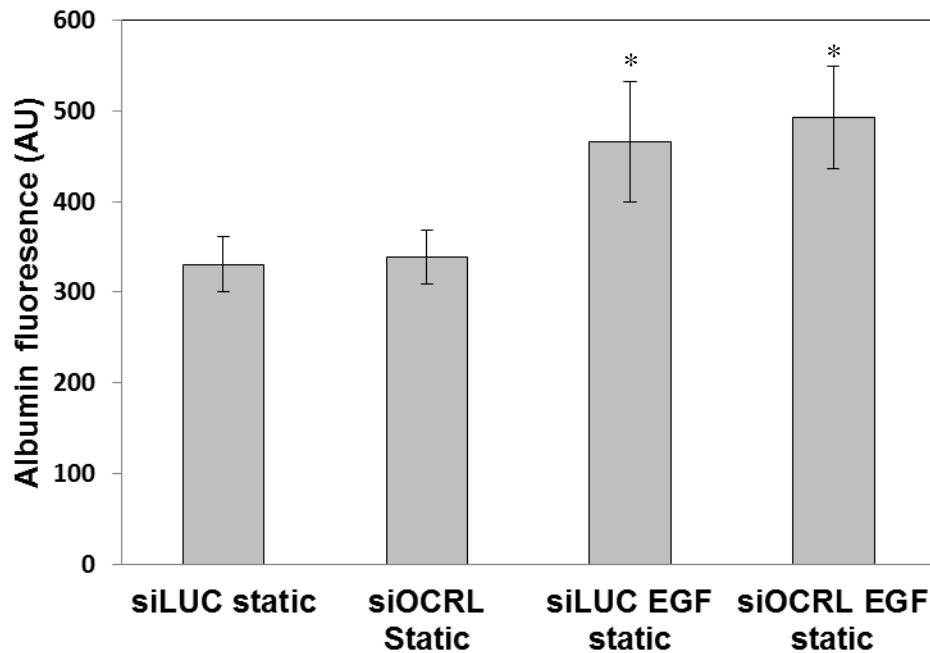
As discussed earlier in chapter 2, purinergic signaling, and the calcium stimulated calcium release from the ER are critically important for sustaining the FSS stimulated endocytic response in OK cells. I therefore tested whether I could rescue the effects of OCRL1 depletion in HK-2 cells by triggering downstream levers to stimulate apical endocytosis.

As shown in Fig. 14, OK cells, when incubated with 100 μ M ATP, increased their apical endocytic capacity by ~50%. Here I wanted to see if we could bypass the requirement for the presence of FSS, and increase the apical endocytic capacity of OCRL1-depleted HK-2 cells by incubating the cells with ATP. If both control and ATP stimulated cells responded equally, it would mean that OCRL1 played a critically important role in stimulating ATP release post-ciliary bending which is absent. However, the ATP stimulated response in OCRL1 depleted cells was partially defective as shown in Fig. 19A. ATP increased endocytosis in control cells by ~30% in control cells but this increase was not observed in OCRL1 depleted cells across 7 experiments. This result suggests that OCRL1 perhaps plays a role in regulating the endocytic response further downstream from the purinergic signaling response in the FSS stimulated endocytic cascade.

As shown in Fig. 12, Ca^{2+} stimulated Ca^{2+} release from the ER is mediated by the ryanodine receptor, and incubating OK cells with 10 μ M ryanodine, stimulates endocytosis of albumin in the absence of FSS. I incubated control or OCRL1-depleted cells with 10 μ M ryanodine and across four experiments, OCRL1-depleted cells failed to increase their endocytic capacity. I incubated control or OCRL1-depleted cells with the calcium biosensor Fura-2AM and

the ryanodine mediated increase $[Ca^{2+}]_i$ between the two conditions was not different across 17 cells. Thus I conclude that OCRL1 acts downstream of the FSS stimulated calcium response and regulate the FSS dependent endocytic cascade.

Figure 20. EGF stimulates endocytosis in control and OCRL depleted cells



Endocytosis of AlexaFluor 647-albumin was measured in HK-2 cells incubated for 1 h under static conditions with 1U/mL of the cdc42 activator EGF. The mean +/- SEM of four independent experiments is plotted. * $p < 0.04$ by two-tailed t-test in comparison to control, all other comparisons are not significant.

3.3.5 EGF stimulates endocytosis in control and OCRL1 depleted cells

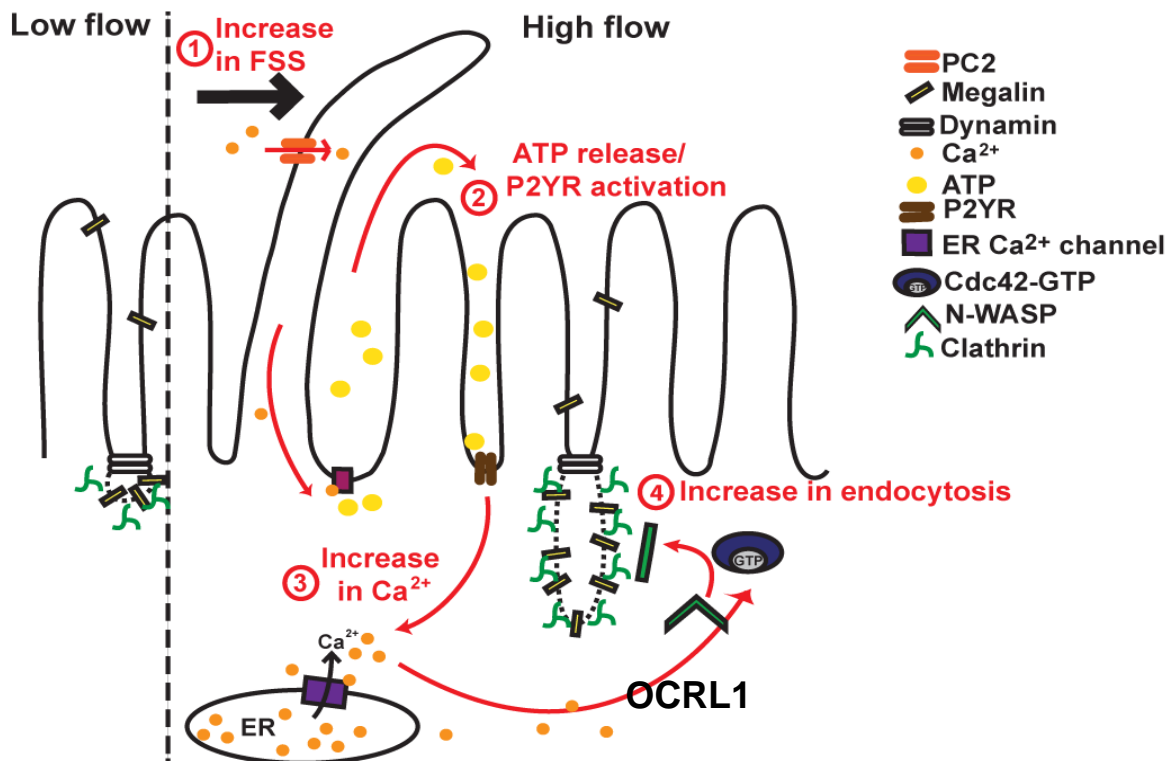
I next wanted to determine if I can rescue the effect of OCRL1 on the FSS stimulated endocytic response by triggering a target further downstream in the signaling cascade. I investigated the role of cdc42, a small GTPase in the FSS stimulated endocytic cascade, to test if activating the GTPase would rescue the loss of mechanosensation caused by OCRL1 depletion. (further information about the downstream players involved in this cascade is documented in Appendix A.)

EGF is known to modulate several signaling pathways in the cell, and one of the effects of incubating cells with EGF is that it causes an increase in the activity of cdc42 a small GTPase that is involved in regulating cytoskeletal remodeling. As the initial response to changes in FSS is an increase in $[Ca^{2+}]_i$, I focused on evaluating possible downstream effectors that could be involved in translating the changes in FSS to an increase in endocytosis. One such $[Ca^{2+}]_i$ modulated protein involved in regulating apical endocytosis was cdc42. Cdc42 is known to be recruited to CCPs and is in-turn known to recruit N-WASP, an actin nucleation promoting factor and ARP 2/3 an actin branching promoter. This allows for active actin cytoskeletal re-modelling and these proteins are important players in the regulation of apical endocytic traffic in epithelial cells.

EGF is known to activate cdc42 (shown in Fig. 25, Appendix A). I wanted to test if activating this small GTPase could rescue the effect of reduction in apical endocytosis in OCRL1 depleted cells. As Shown in Fig. 20, when OCRL1-depleted cells were incubated with 1U/mL of the cdc42 activator EGF, we noticed an increase of ~40% in both control and OCRL1-depleted

cells across five experiments. This implies that the apical endocytic capacity is not completely lost in the OCRL1-depleted PT epithelia, and that OCRL1 plays a critical role in the process of translating changes in $[Ca^{2+}]_i$ to elevation in cdc42 activity.

Figure 21. Proposed model



(1) Exposure of PT epithelia to FSS, triggers influx of calcium, possibly through ciliary localized mechanosensitive calcium channels, and (2) causes an initial influx of Ca^{2+} and ciliary bending also causes release of purines. We do not conclusively know if OCRL1 plays a role in this process at this point. (3) The release of ATP activates purinergic receptors located apically, and this causes a further increase in $[Ca^{2+}]_i$. the increase in $[Ca^{2+}]_i$ causes calcium stimulated calcium release from the ryanodine stores of calcium, and OCRL1 does not play a role in regulating this FSS stimulated effect. (4) However, depletion of OCRL1 reduces the flow stimulated endocytic response in PT epithelia, and this probably occurs because OCRL1 plays an important role in regulating the downstream signaling cascade, which translates the changes in $[Ca^{2+}]_i$ to changes in cdc42 activity. Cdc42 in turn recruits N-WASP and ARP2/3 to the apical clathrin coated pits to mediate actin nucleation and enables formation of more and larger pits. The downstream cascade discussed here has been tested in Appendix A of my thesis.

3.4 DISCUSSION:

Human PT cells depleted of OCRL1 possessed elongated primary cilia, suggesting a possible role for OCRL1 in FSS-stimulated endocytosis. Indeed, apical endocytosis in PT cells depleted of OCRL1 using siRNA did not respond to FSS. This effect was not due to changes in cilia length, as elongation of primary cilia by another maneuver did not impair the endocytic response to FSS. ER Ca^{2+} stores released by ryanodine were not different from control. Strikingly, addition of ATP or ryanodine in the absence of FSS stimulated apical endocytosis in control cells but not in OCRL1 knockdown cells, suggesting a defect in the ability to sense changes in $[\text{Ca}^{2+}]_i$. Apical endocytosis in both OCRL1 knockdown and control cells could be stimulated by downstream incubating cells with EGF. Loss of OCRL1-dependent FSS sensing in PT cells may explain the underlying cause of tubular proteinuria in Lowe syndrome patients.

As we observed previously in MDCK cells (133), OCRL1 knockdown was efficient and resulted in elongated cilia (Fig. 17A and B). Similar to the other PT cell lines I tested previously, apical endocytosis in HK-2 cells was significantly enhanced when cells were exposed to 1 dyne/cm² FSS. Strikingly, depletion of OCRL1 in these cells inhibited FSS-stimulated endocytosis but did not alter basal endocytic uptake of albumin (Fig. 16B). This ablation of the FSS stimulated endocytic response in OCRL1 depleted cells is not caused by the elongation of cilia, as I found that, even when the cilia were alternatively lengthened by knocking down Gal-3, the cells responded normally to FSS, and increased their apical endocytic capacity for albumin (Fig. 18). As previously mentioned in 3.5, a recent independent study conducted in Martin Lowe's lab found that OCRL^{-/-} zebrafish pronephros had a defect in endocytosis (131). The pronephros of the OCRL^{-/-} zebrafish had low accumulation of megalin in endocytic vesicles and low expression of megalin in comparison to control zebrafish. This study concluded that the

reason underlying tubular dysfunction in Lowe syndrome is caused because of defects in endocytosis and this effect cannot be attributed to defects in ciliogenesis (131). This study bolsters my findings, and my hypothesis that the defects in ciliogenesis do not contribute to the pathology of Lowe syndrome.

The response to ATP in control cells was moderate, and there was an increase of about 30% on an average, however, I noticed a lot of heterogeneity in the response of HK-2 cells to ATP in comparison to the OK cells. This is because of the intrinsic heterogeneity in the HK-2 cells coupled to the differences in knockdown efficacy I observed across the different experiments may be the reason for the variability in the endocytic responses I observed (Fig. 19A).

Further the release of $[Ca^{2+}]_i$ from the ER stores through the ryanodine channels is not disrupted on OCRL depletion in HK-2 cells, as the baseline levels of Ca^{2+} in both control and OCRL depleted cells were equally elevated in comparison to untreated controls. Incubating cells with 10 μ M ryanodine, increased apical endocytosis of albumin in control cells, but the OCRL1 depleted cells failed to respond, indicating that there was a clear defect in translating the increase in $[Ca^{2+}]_i$ to an increase in endocytosis (Fig. 19B,C).

Calmodulin is a widely studied calcium biosensor across several tissue types and is known for translating changes in the $[Ca^{2+}]_i$ to physiologically relevant responses. I hypothesize that CALM1, a calmodulin isoform expressed in renal epithelial cells acts as the calcium biosensor. This biosensor is in turn known to bind directly and regulate the activity IQGAP1, a GTPase Activating Protein which in turn regulates cdc42 cycling and activity. Also, Calmodulin kinases are capable of activating Cdc42. Cdc42 is a small GTPase associated with actin cytoskeleton remodeling, and it accomplishes this task by recruiting N-WASP and Arp2/3 to its

site of activation. In epithelial cells with very dense apical cortical actin networks, active actin remodeling is requisite for efficient clathrin mediated endocytosis.

I believe that OCRL1 acts downstream of ER calcium release which causes a tonic increase in $[Ca^{2+}]_i$. I believe that OCRL1 controls a key step or a switch along the downstream cascade, which is why depletion of endogenous levels of OCRL1 renders the cells insensitive to changes in $[Ca^{2+}]_i$. As OCRL1 is known to associate with several proteins, it is hard to predict the exact role of OCRL1 at this point.

Further investigation of the downstream signaling cascade is requisite for ascertaining the precise role of OCRL1 in regulating the FSS stimulated endocytic response.

3.5 FUTURE DIRECTIONS

Further investigation is required to determine the role of OCRL1 in regulating the FSS stimulated endocytic response.

We observed an increase in cilia length in OCRL1 depleted HK-2 cells, and it is possible that the FSS dependent increase in $[Ca^{2+}]_i$ caused by the opening of PC2 channels localized on the cilia may be defective. Also, addition of ATP to the OCRL1 depleted HK-2 cells failed to mobilize cytosolic levels of calcium to the same extent as in control cells (data not shown). Further study is required to understand the role of OCRL1 in regulating the FSS dependent regulation of $[Ca^{2+}]_i$.

As there was a lot of variability from cell to cell across my experiments using in HK-2 cells. Therefore, moving to a more responsive cell line like the OK cells would be a good

strategy, moving forward to investigate the molecular players involved in the signaling cascade. As the opossum transcriptome sequence is not completely available, it becomes hard to knockdown, or knockout genes of interest such as OCRL1 to study the outcomes of genetic manipulation. Also, there are limited resources such as antibodies, and other reagents that work on opossum samples and this imposes a technical limit on our ability to conduct and validate cell based assays. In addition, given that OCRL^{-/-} mice have no proteinuric phenotype due to compensation by INPP5B (130), it is very much possible that the Lowe syndrome model of OK cells might not exhibit any Lowe syndrome associated phenotypes.

Another complication in my studies was the incomplete knockdown of OCRL1 using siRNA. Studies in another lab have shown that a knockdown efficacy of >95% was required to observe changes in actin dynamics and recycling of megalin associated with OCRL1 depletion (135), and my knockdown efficiency was typically between 60% and 80%. It would certainly be very useful to have a OCRL1^{-/-} PT cell line in order to ascertain its role in endocytosis. A new graduate student in the lab has recently targeted OCRL1 in HK-2 cell lines using CRISPR technology, and I eagerly look forward to a better understanding of the role of OCRL1 in FSS in endocytosis in these cells. Polyploidy of the HK-2 cells and cell-to cell variability may complicate interpretation of these studies as CRISPR cells when generated using limited dilution cloning.

Another option is to utilize the kidneys from the Lowe syndrome model mice generated in Bob Nussbaum's lab to conduct single tubule microperfusion studies (130). A recent single tubule perfusion study conducted by Dr. Baty in collaboration with Dr. Satlin in Mount-Sinai has shown very promising results. Rabbit kidney derived single proximal tubules when perfused at a higher flow rate of 20 nL/min (which corresponds to 1 dyne/cm²) retrieved more albumin in

comparison to the PT subjected to a perfusion rate of 5 nL/min. These single tubule perfusion studies support our findings using immortalized cell cultures, and such complementary models would be useful as we iterate towards an experimental setup that would enable us to answer questions at different scales of detail.

Very clearly, the downstream signaling cascade stimulated in the presence of FSS has to be determined and I present a more in-depth review of this cascade in Appendix A.

4.0 MATERIALS AND METHODS

4.1 CELL CULTURE

OK cells were cultured in DMEM/F12 Ham with 10% FBS. For experiments measuring effects of fluid shear stress (FSS) on endocytosis, cells were plated at 200,000/chamber in Ibidi μ -slide VI 0.4 six-well ibi-treated chambers (<http://ibidi.com/xtproducts/en/ibidi-Labware/Channel-Slides/m-Slide-VI-0.4>) and the medium was changed twice per day until the cells reached superconfluence (typically 3–4 d). Human kidney proximal tubule HK-2 cells were obtained from ATCC and grown in DMEM-F12 medium (Sigma) supplemented with 5 μ g/mL insulin, 0.02 μ g/mL dexamethasone, 0.01 μ g/mL selenium, 0.05 μ g/mL transferrin, 2mM L-glutamine, and 10% FBS. HK-2 cells were passaged when 80-90% confluent. Cells were plated at 250,000/chamber in Ibidi μ -slide VI 0.4 six-well collagen IV coated chambers, and the medium was changed twice per day until the cells reached superconfluence (typically 3–4 d). Cells were deciliated where indicated by treatment for 3 h with 30 mM ammonium sulfate.

4.2 SIRNA SEQUENCES

The table below lists the siRNA sequences that were used to selectively deplete OCRL, or galectin-3 in HK-2 cells. siRNA against firefly luciferase was used as a negative control in all my experiments.

Table 2 siRNA Sequences

| Name of protein targeted (acronym used) | Sequence |
|---|-----------------------------|
| OCRL (siOCRL) | 5'-GGGUGAAGGUUGUGGAUGUUU-3' |
| Galectin-3 (siGAL-3) | 5'-GAAUGAUGUUGCCUCCACUU-3' |
| Firefly luciferase (siLUC) | 5'-GAAUAUUGUUGCACGAUUUUU-3' |

4.3 TRANSFECTION OF PROXIMAL TUBULE EPITHELIA

ARH-tomato transfection of OK cells in chapter 2 was conducted using lipofectamine 3000 (Invitrogen). On the day of transfection, semi-confluent OK cells grown on plastic were trypsinized and resuspended in the growth medium at the concentration of 2.4 million cells/mL. Meanwhile, DNA, lipofectamine 3000A+B were incubated separately in OPTI-MeM (Gibco) for 5 min at room temperature before they were combined and incubated for 20 min. 1 μ g ARH-Tomato, 1.5 μ L lipofectamine 3000A, 1.5 μ L lipofectamine 3000B, and 100 μ L OPTI-MeM were used for one single well of a 12 well plate. After the incubation, 100 μ L transfection

mixture and 100 μ L cells (approximately 240,000 cells) were added to the single well of a collagen IV coated coverslip in a 12 well plate. The medium was replaced the next day and cells were cultured for 3-4 days before being processed for TIRF microscopy.

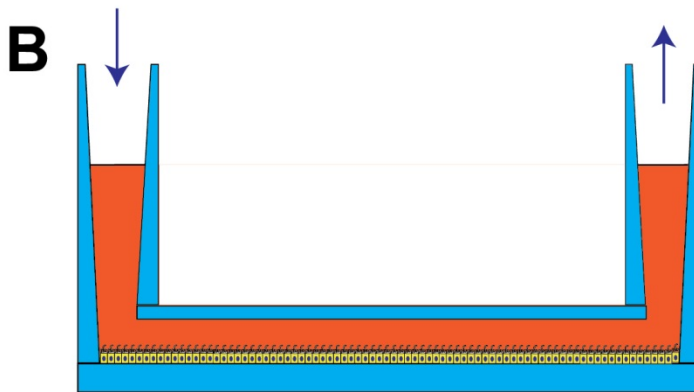
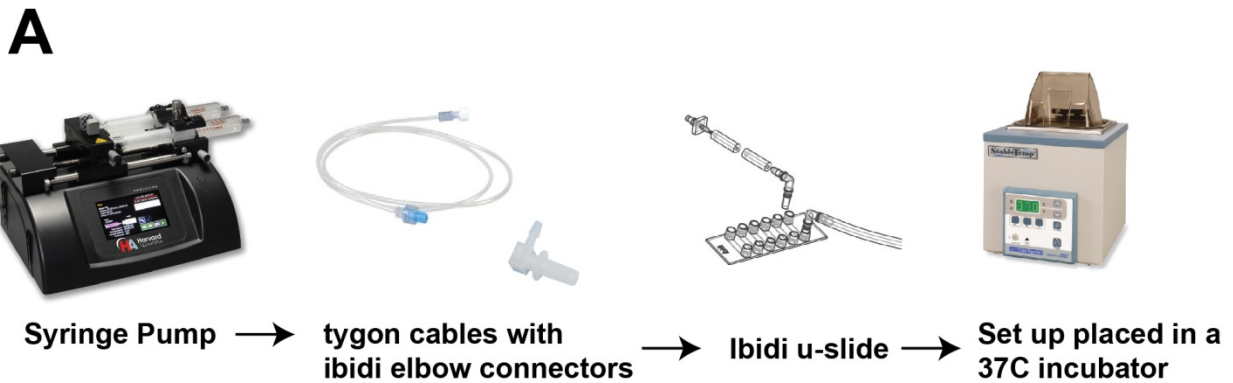
SiRNA transfection of HK2 cells in chapter 3 was performed using lipofectamine 3000 (Invitrogen). On the day of transfection, semi-confluent HK-2 cells grown on plastic were trypsinized and resuspended in the growth medium at the concentration of 5 million cells/mL. Meanwhile, siRNA, lipofectamine 3000A+B were incubated separately in OPTI-MeM (Gibco) for 5 min at room temperature before they were combined and incubated for 20 min. 1 μ g siRNA, 1 μ L lipofectamine 3000A, 1 μ L lipofectamine 3000B, and 50 μ L OPTI-MeM were used for one single well of a collagen IV coated ibidi uslide VI chamber. After the incubation, 50 μ L transfection mixture and 50 μ L cells (approximately 250,000 cells) were added to the single well of a collagen IV coated ibidi uslide VI chamber. The medium was replaced the next day and cells were cultured for 3-4 days before being processed for subsequent experiments (flow experiments and immunofluorescence). Cells from a duplicate pair of control and OCRL1 knockdown samples were collected in every experiment for Western blotting to determine the knockdown efficiency.

4.4 CALCULATION OF FSS

FSS was calculated using the Navier–Stokes and the continuity equations, i.e., $\tau = 6\mu Q/bh^2$, where τ is FSS, Q is flow rate, μ is medium viscosity, and b and h are channel width and height, respectively (2). Modeling studies have shown that median single-nephron glomerular filtration rates (GFRs) in humans are 65 nl/min (3). A shear stress of 1 dyne/cm² in

the human proximal tubule corresponds to a flow rate of 63 nl/min, which is ~ 115 mL/min/ 1.73m^2 (very close to the median GFR in humans). Similarly, calculations used in previous micropuncture studies of rat proximal tubules have concluded that the median single-nephron flow rate of 30 nl/min corresponds to 1 dyne/cm^2 (3–6). This has been the rationale behind the use of 1 dyne/cm^2 in mouse proximal tubule (PT) cells (2) and in OK cells (7) in previous studies.

Figure 22. Set-up of Flow-dependent endocytosis assay



(A) Schematic of the set up of the flow dependent endocytosis assay. (B) Schematic of a cross section of an ibidi well, depicting the simulation of apical fluid shear stress in PT epithelia.

4.5 SET-UP OF FLOW-DEPENDENT ENDOCYTOSIS ASSAY

OK cells were cultured on Ibidi six-well chambers as described above. μ -Slide Luer 0.1 elbows were used to connect the chambers to a syringe pump (Harvard Apparatus). Twenty-milliliter or ten-milliliter syringes were used to perfuse individual wells with 40 μ g/mL Alexa Fluor 647-BSA and/or 1 mg/mL lysine-fixable rhodamine-dextran at the indicated FSS. Cells were perfused or maintained under static conditions for 1 h at 37 °C unless otherwise indicated. Cells were fixed with 4% paraformaldehyde or periodate-lysine-paraformaldehyde (for experiments using dextran) for 20 min at ambient temperature, the fixative was removed, and 50 μ L of ProlongGold (Invitrogen) was added to each well.

4.6 QUANTIFICATION OF FLOW-DEPENDENT ENDOCYTOSIS

The chambers were imaged the next day using a Leica TCS SP5 confocal microscope. Five to ten confocal stacks of randomly selected fields were acquired per well. Images were exported as 8-bit tagged image file formats or Leica image files and analyzed using Fiji or Image J. Maximum intensity projections of stacks were obtained for each field and total intensity was calculated using the Measure function. Measurements for background were digitally subtracted from the total intensity of each field. No normalization was used, as raw values were generally reproducible across independent experiments.

4.7 MEASUREMENT OF $[Ca^{2+}]_i$ SIGNALING

OK cells were plated at 450,000 cells/mL on collagen-coated Ibidi μ -slide I chambers (0.4-mm clearance) and cultured for 3 d. Cells were loaded with Fura-2 AM (5 μ M) in HEPES buffered saline (135 mM NaCl, 4.5 mM KCl, 2.5 mM CaCl₂, 1 mM MgCl₂, 10 mM HEPES, 10 mM glucose, pH 7.4), rinsed, and incubated for 15 min for deesterification of the dye. Cells were imaged using a Nikon Eclipse Ti upright live cell microscope equipped with an ORCA-Flash 2.8 camera (Hamamatsu). A gravity flow apparatus controlled by an automated mechanical valve (Valvelink 8.2; AutoMate Scientific) was connected to the μ -slides using Luer elbow connectors. Temperature was maintained at 37 °C throughout the experiment using an inline heater (SH27B, Warner Instruments) controlled by a dual channel bipolar temperature controller (TC-344B, Warner Instruments). The minimum FSS that could be generated in the chamber using this setup was 2 dyne/cm².

Ca²⁺ responses measured using this setup were identical to those measured for OK cells cultured on parallel plate flow chambers compatible with glass coverslips (www.glycotech.com/apparatus/parallel.html) upon exposure to 1 dyne/cm² (data not shown). FSS-stimulated endocytic responses were similar in OK cells cultured in Ibidi collagen-coated or ibi-treated chambers. Cells were excited with a PhotoFluor II metal halide light source (89 North) connected to a Lambda 10–3 filter wheel system (Sutter Instruments) with 340- and 380-nm filters (Chroma Technology). Baseline measurements were acquired every 5 s for 1 min before initiation of FSS and for 5 min afterward. In situ calibration with ionomycin (Alomone) was conducted to define the Ca²⁺ calibration parameters under zero and saturating $[Ca^{2+}]_i$ concentrations. Cells were perfused with HEPES buffered saline with 5 μ M ionomycin and images were acquired every 10 s for 10 min to estimate Fura-2 ratios at saturating levels of

$[Ca^{2+}]_i$. Subsequently, cells were perfused with Ca^{2+} -free buffer (135 mM NaCl, 4.5 mM KCl, 2 mM EGTA, 1 mM $MgCl_2$, 10 mM HEPES, 10 mM glucose, pH 7.4) with ionomycin to estimate ratios at zero concentration of $[Ca^{2+}]_i$. NIS Elements (Nikon) was used to select individual cells (6–10 per experiment) and the ratio of 340:380-nm emission intensity was calculated at each time point. The $[Ca^{2+}]_i$ values of cells at each time point was normalized to the initial $[Ca^{2+}]_i$ value (at $t = 0$ s) to estimate the fold changes in $[Ca^{2+}]_i$ over time. $[Ca^{2+}]_i$ changes across experimental and control conditions were averaged across 3–5 experiments (17–48 total cells) and the statistical significance between average peak fold change values was determined using the rank-sum test.

4.8 INDIRECT IMMUNOFLUORESCENCE

HK-2 cells were fixed with Periodate Lysine Paraformaldehyde pH 7.4 at RT for 15 min, quenched in PBS with 20 mM glycine and 75 mM NH_4Cl for 5 min, permeabilized using 0.1% Triton X-100 in the quench solution for 10 min with gentle shaking, and blocked in PBS with 1% BSA and 0.1% saponin for 1h at ambient temperature. Anti-acetylated tubulin monoclonal antibody (Sigma) was used at a dilution of 1:400, and the goat anti-mouse Alexa Fluor 568 secondary antibody was used to immunostain the cells, and visualize the cilia. Samples were mounted in ProLong Gold Antifade with DAPI (Invitrogen). Confocal images were acquired on a Leica SP5 confocal microscope (40x/1.4 NA objective) and processed using FIJI.

4.9 MEASUREMENT OF CILIA LENGTH

siRNA transfected HK-2 cells grown on collagen coated coverslips were fixed and processed for indirect immunofluorescence as described above. Anti-acetylated tubulin monoclonal antibody (Sigma) was used at a dilution of 1:400 to visualize cilia, with secondary antibody and mounting media as described above. Multiple fields of cells were acquired using a Leica DM16000B epifluorescence microscope with a 40x/1.4 NA objective, 1.7X zoom. Images were opened in FIJI and individual cilia were traced using the freehand drawing tool to measure length.

4.10 TOTAL INTERNAL REFLECTION FLUORESCENCE IMAGING

OK cells were grown on coverslips and transfected with ARH-Tomato and processed for immunofluorescence described above. Cells were imaged using a Nikon Eclipse Ti automated inverted microscope with a motorized stage, repurposed for total internal reflection fluorescence (TIRF) imaging. A 100x 1.49 NA TIRF objective and solid-state laser of 561 nm was used as light source to acquire the images. Images were acquired with an iXon+ 897 EM-CCD camera driven by NIS Elements. The depth of field of illumination was about 150 nm. Imaris (Bitplane Scientific Software) was used to quantitate the number of ARH spots per cell. The expected spot size was set to 0.3 μm and the threshold was set automatically to determine the number of spots in each frame. The area of each cell was determined using ImageJ software (NIH) to calculate the number of spots per square micron.

4.11 WESTERN BLOTTING

The Western blotting to detect OCRL1 knockdown was performed using primary antibodies including an affinity-purified monoclonal antibody directed against OCRL1 (1:5; hybridoma bank, made by Dr. Nussbaum and Dr. Suchy), anti-Galectin-3 antibody (1:1000, R&D systems) and a mouse monoclonal anti β -actin antibody (1:5000; Sigma; used as the loading control).

APPENDIX A

A.1 INTRODUCTION

In this section, I will be presenting a potential signaling cascade that connects the FSS stimulated Ca^{2+} and endocytic responses. From my conclusions in chapter 2, we know that the increase in Ca^{2+} on exposure to FSS is instantaneous, but it takes between 15 to 30 min for the FSS stimulated increase in endocytosis to start (174). This suggests that a potential multi-step downstream signaling cascade connects the FSS stimulated responses. I predict that a calmodulin and Cdc42 dependent signaling cascade is responsible for the increase in apical endocytosis in renal proximal tubules. Calmodulin is a calcium biosensor that directly binds to calcium and activates downstream CaMKII and CaMKK (202), and also interacts with IQGAP1, a GTPase Activating Protein (GAP) (203). Both calmodulin activated kinases and IQGAP1 are capable of regulating the activity of a downstream small GTPase called Cdc42 (203, 204). Cdc42 in turn is capable of recruiting and activating N-WASP, an actin nucleation promoting factor which recruits the ARP2/3 complex to the site of activity to modulate actin dynamics (205, 206). Active actin remodeling is required for endocytosis in cell types with dense apical cortical actin networks (207). I hypothesize that active remodeling around the clathrin coated pits on the apical surface is responsible for the increase the size of endocytic pits documented in chapter 2.6. I also

hypothesize that this cascade is highly upregulated in PT cells exposed to FSS and hence causes an increase in both the number of clathrin coated pits and in the size of these pits. This appendix systematically explores the possible roles of Calmodulin, CaMKs, IQGAP1, Cdc42, N-WASP, and apical actin dynamics in connecting the FSS stimulated changes in $[Ca^{2+}]_i$ to the endocytic response. As these experiments were conducted as a part of a fishing expedition, experiments were not repeated sufficient number of times to gain statistically significant evidence to bolster my hypothesis. However, I present here the leads that the lab would like to pursue in the future.

A.1.1 Cellular functions of Calmodulin

Calmodulins (CaM) are ubiquitously expressed calcium sensors that translate changes in cellular levels of the Ca^{2+} to cause physiological responses in the cell. CaM is expressed in many cell types and can have different subcellular locations, including the cytoplasm, within organelles, or associated with the plasma or organelle membranes (208). Many of the proteins that CaM binds are unable to bind calcium themselves, and as such use CaM as a calcium sensor and signal transducer (209). CaM can also make use of the calcium stores in the endoplasmic reticulum, and the sarcoplasmic reticulum. CaM undergoes a conformational change upon binding to calcium, which enables it to bind to specific proteins for a specific response (210). CaM can bind up to four calcium ions, and can undergo post-translational modifications, such as phosphorylation, acetylation, methylation and proteolytic cleavage, each of which can potentially modulate its actions.

CaM is known to activate downstream kinases which trigger various downstream signaling cascades by phosphorylating or activating their corresponding substrates (211). Most Calmodulin-activated kinases (CaMKs) have auto-inhibitory domain and CaM binding domains,

and the kinases tend to exist in an auto-inhibited state (211). When $[Ca^{2+}]_i$ increases, CaM binds to the free cytosolic Ca^{2+} and associates with the CaMKs. This association of CaMKs with Ca^{2+} /CaM displaces the auto-inhibitory domain, and the CaMKs become activated. Two such multi-functional kinases are CaMKK and CaMKII. CaMKII is a very unique CaMK and exists as a holoenzyme made of a twelve subunit complex (212, 213). CaMKII is capable of auto-phosphorylation and activates several other downstream effector kinases such as CaMKK, and Guanine exchange factors (GEFs) which activate the Rho family of small GTPases (212). This function of CaMKII is extensively studied in the context of neural spine formations and synaptic plasticity.

CaMKK has been extensively studied over the past two decades and is one of the most upstream triggers in the CaM signaling pathway. Like most CaMKs, CaMKK is held in an auto-inhibitory and activates on association with Ca^{2+} /CaM. CaMKK once activated phosphorylates and activates Rac guanine exchange factor (β PIX) which is a Cdc42 GEF highly expressed in kidney tissue (204, 214). I hypothesize that activated CaMKII and CaMKK activate Cdc42 in PT epithelia.

Ca^{2+} /CaM- CaMKII complex formation causes the disassociation of IQGAP1(a GAP for Cdc42) from CaM (203). I hypothesize that activation of both the GEF and the GAP for Cdc42 causes continuous cycling of the GTPase and is responsible for the sustained activation of the FSS stimulated signaling pathway.

A.1.2 Cdc42

Cdc42 is a small GTPase belonging to the Rho family of GTPases, and works as a molecular switch to regulate a wide range of signaling pathways. Cell polarity and vesicle

trafficking are two principal processes that Cdc42 is known to regulate. Cdc42 is known to modulate cell polarity by regulating the directionality of cell movement. It is known to control the organization of the microtubule organizing center and is also known to regulate the formation of lamellipodia and filopodia in migrating cells.

Cdc42 and vesicle trafficking: Cdc42 coordinates a number of vesicle trafficking events in mammalian cells. In most cases, Cdc42 directs membrane trafficking by regulating actin dynamics through its association with nucleation promoting factors like N-WASP. Cdc42 is known to activate N-WASP by directly binding to the protein and by releasing its auto-inhibitory VCA domain (215, 216). Activated N-WASP can now recruit and bind to ARP2/3 complex which in turn regulates actin branching and polymerization (216, 217). Actin polymerization is thought to contribute to membrane trafficking by (a) inducing membrane deformations; (b) driving vesicle formation; (c) scission and (d) fusion. Cdc42 is known to localize and regulate tubulation and vesicle scission from the Golgi by associating with coatamer which is a COPI coat protein (218). However, Cdc42 does not seem to play a role beyond vesicle formation from the Golgi in non-polarized mammalian cell lines.

In polarized MDCK cells, Cdc42 localizes to the Golgi and has been shown to regulate polarized biosynthetic traffic. Basolaterally sorted proteins are mistargeted to the apical surface when the Dominant Negative mutant of Cdc42 is over-expressed in MDCK cells (219-221). The over expression of the dominant negative mutant or the constitutively active mutant caused similar effects concluding that the cycling of the Cdc42 GTPase is critically important for its cellular functions. Cdc42 is also known to associate with the cortical actin network in MDCK cells. Dominant negative Cdc42 has been shown to inhibit apical endocytosis in MDCK cells as well (222).

A.1.2 N-WASP

Nucleation promoting factors (NPFs) bind to the ARP2/3 complex and initiate actin nucleation by inducing a conformational change in the ARP2/3 complex. NPFs can be segregated into 2 distinct categories, Type I and Type II NPFs. Type I NPFs possess a characteristic verprolin-homology domain (VCA), the cofilin homology domain and an acidic domain that interacts with g-actin and ARP2/3. These include WASP (wiskott aldrich syndrome protein), neuronal-WASP (N-WASP), WASP family verprolin-homologous protein (WAVE or Scar) and WASP and Scar homolog (WASH). Type II NPFs lack complete VCA domains but have amino-termini that bind ARP2/3 and tandem repeat domains that bind F-actin. Cortactin is an example of a type II NPF. WASP and N-WASP exist in an auto-inhibited state by an intramolecular association of its GTPase binding domain with the VCA domain (215). Binding with Cdc-42 induces a conformational change and activates WASP proteins (215). Activated N-WASP recruits ARP2/3 and triggers F-actin branching and polymerization at the site of activation (217). This is known to drive clathrin mediated endocytosis when the endocytic capacity is limited by the density of the apical cortical actin network (223).

A.1.3 Cellular functions of ARP2/3

The ARP2/3 complex was first identified as an interacting factor of profilin (an actin binding protein which assists in assembly of F-actin) (217). The name of the complex is derived from Actin related protein 2 & 3 which are two critical subunits of the complex. This complex is the key regulator of branched actin filament nucleation and is conserved in all higher eukaryotes. Extensive studies have shown that ARP2/3 complex binds to Actin mother filaments and initiates

formation of daughter filaments at a characteristic 70° angle (224). Majority of the studies done to characterize the ARP 2/3 complex stems from rigorous in vitro studies(225-227). After initial isolation and characterization studies, it was evident that ARP2/3 complex had relatively poor in vitro actin nucleating ability and this led to the identification of other important co-factors (Like NPFs listed above and branching inhibitors). All data currently support a model in which in which the filament nucleation and branching events are tightly interrelated with the ARP2 and ARP3 subunits, as they contribute the first two subunits of the new filament upon a conformational change and rearrangement of multiple subunits of the complex (227).

Formation of the leading edge, lamellipodia, filopodia, invadopodia, podosomes, modulating endocytosis and phagocytosis, endosomal fission, formation of adherens junctions, and cytoplasmic streaming are the major cellular functions of the ARP2/3 complex.

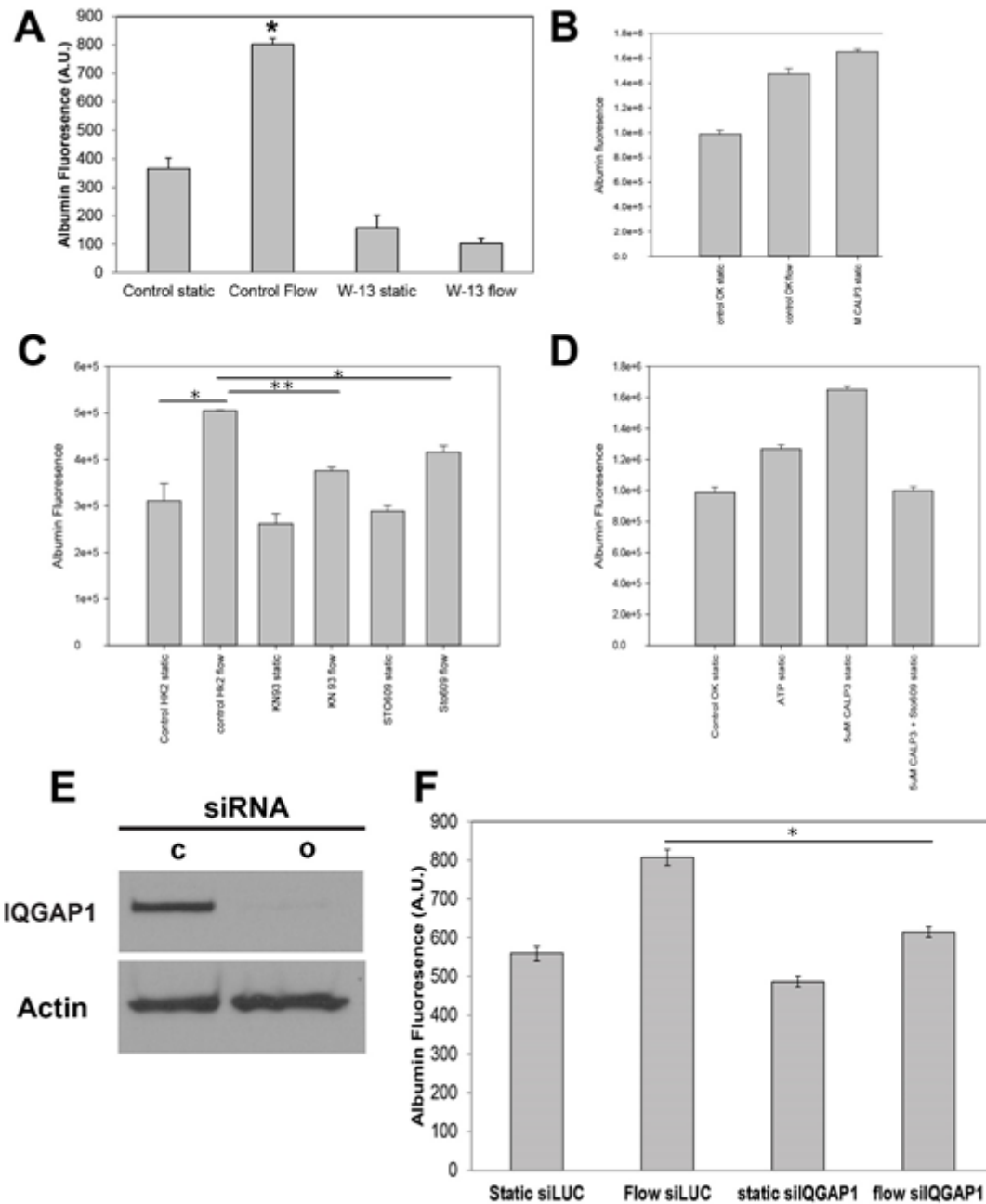
A.1.4 CDC42, N-WASP and ARP2/3 together orchestrate apical endocytosis in epithelial cells by modulating the cortical actin network

Live-cell total internal reflection fluorescence microscopy (TIRFM) has been a strong technique used in the field to identify the dynamics of Clathrin coated pit formation, and to study in detail the sequential recruitment of critical components required for this process. Live-cell TIRFM studies were the first to document the association of N-WASP and the ARP2/3 complex to clathrin coated pits in cultured mammalian fibroblasts (228-231).

In one study, the recruitment of N-WASP and ARP2/3 was very important for the endocytosis of EGF in fibroblasts, as the endocytosis of the clathrin coated vesicles was limited by the density of the apical cortical actin network. Deletion of N-WASP in these fibroblasts significantly reduced the rates of EGF endocytosis (232). In another study in HEK-293 cells,

Intersectin-I, a modular scaffolding protein that is recruited to the clathrin coated pits was found to possess GEF activity for Cdc42, and was found to recruit the small GTPase to the coated pits. Cdc42 in turn was found to recruit and activate N-WASP, and modulate actin re-modeling at the pits through ARP2/3 complex (233). I hypothesize that in the FSS stimulated cascade, Cdc42 cycles much faster, and is recruited to clathrin coated pits by GEFs, thus promoting formation of many more, bigger vesicles (seen in Fig. 9).

Figure 23. Role of calmodulin and immediate downstream effectors in FSS stimulated endocytosis



(
A) Calmodulin activation may be requisite for FSS stimulated endocytosis in PT epithelia. HK-2 cells incubated with 10 μ M W-13, a cell permeable CaM inhibitor and were incubated with Alexa 647 albumin either under static conditions or subjected to FSS for 1h. N=1. (B) Activating CaM may be necessary and sufficient for triggering an increase in apical endocytosis of albumin. OK cells were incubated either with 5 μ M Calcium-Like Peptide 3 (CALP3, a cell permeable CaM agonist) under static condition, subjected to FSS or were left untreated under

static condition and were incubated with Alexa 647 albumin and incubated for 1h. N=1. (C) CaM activated CaMKII and CaMKK are important regulators of the signal transduction cascade. HK-2 Cells were treated with 10 μ M KN-93 (CaMKII inhibitor) or 1 μ g/mL STO609 (CaMKK inhibitor) for 30 min prior to incubation with Alexa 647 albumin and incubated either under static conditions or subjected to FSS for 1h. Cells were treated with TPCK trypsin for 15 min to reduce non-specific haze. N=2, * p <0.05; ** p <0.03 by Student's t-test. (D) CaMKK activation is necessary for connecting the increased activation of CaM to increased endocytosis. OK cells were either untreated, treated with 100 μ M ATP, treated with 5 μ M CALP3, or treated with 5 μ M CALP3+1 μ g/mL STO609 and then incubated with Alexa 647 tagged albumin under static conditions. N=1. (E) Western blot of HK-2 cells transfected with either siRNA against firefly luciferase (control) or with siRNA against IQGAP1. (F) The release of free IQGAP1(Cdc42 GAP) on CaM activation is necessary for sustaining the FSS stimulated endocytic response. Control or IQGAP1 depleted cells were incubated with Alexa 647 albumin either under static conditions or subjected to FSS for 1h. * p <0.01 using Student's t-test.

A.2 ROLE OF CAM AND CAM ACTIVATED PROTEINS IN REGULATING FSS STIMULATED ENDOCYTOSIS

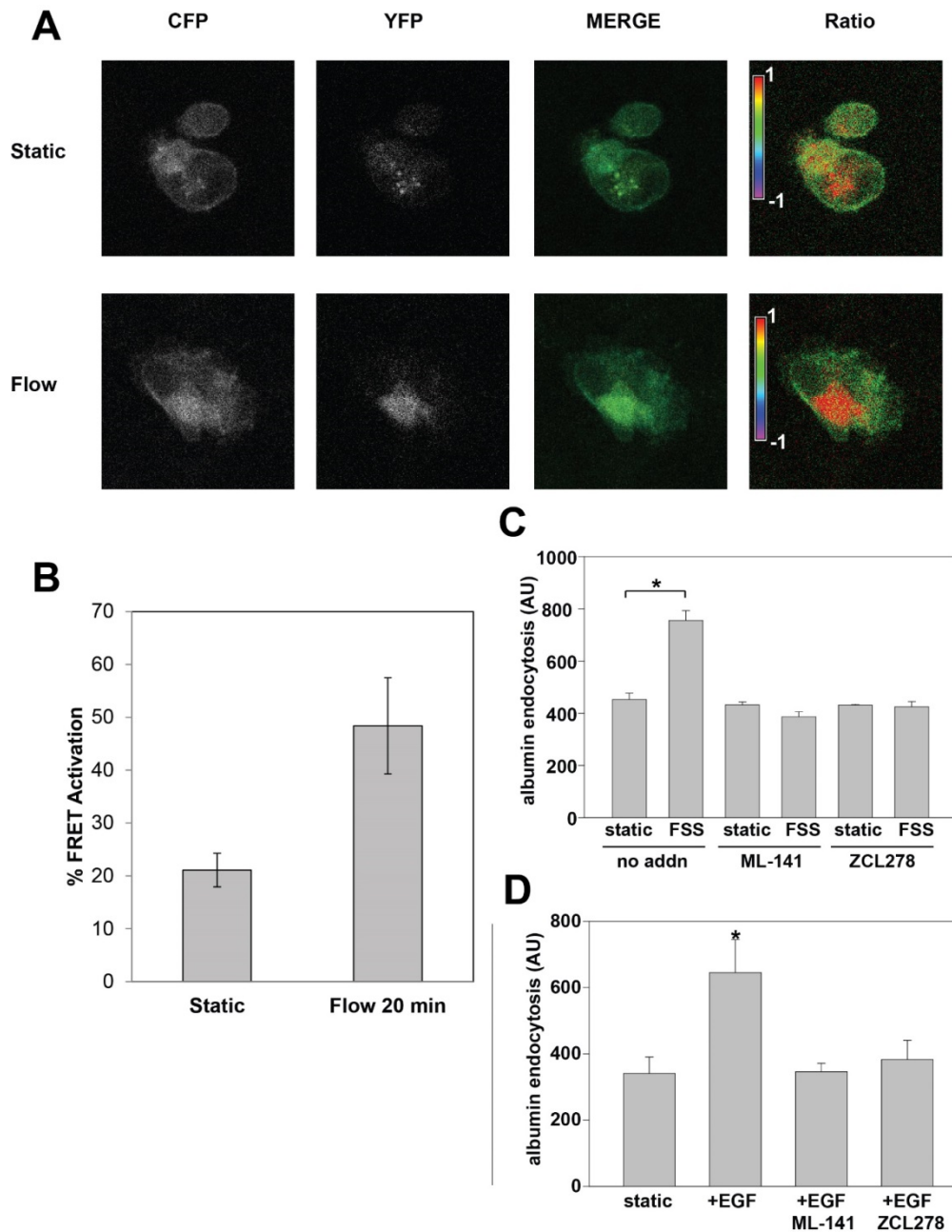
As mentioned in A.1, I observed an instantaneous stimulation of $[Ca^{2+}]_i$ in PT cells exposed to FSS. I first wanted to ask: what is the immediate effector that could translate changes at the ion level to the protein level in PT epithelia? To answer that question, I hypothesized that a calcium binding protein was most probably involved in triggering and regulating the responses. Calmodulins were an obvious first choice to test as they are very evolutionarily conserved, ubiquitously expressed group of proteins capable of regulating multiple signaling cascades in response to changes in $[Ca^{2+}]_i$ (208, 210). As shown in Fig. 23A treating HK-2 cells with 10 μ M W-13 a cell permeable inhibitor of CaM ablated both static as well as FSS stimulated increase in endocytosis, suggesting a possible role for CaMs in regulating endocytosis in PT cells. Conversely, I asked the question: Is CaM activation sufficient for stimulating apical endocytosis?

From two experiments in OK cells (Fig 23 B,D), incubating cells with a cell permeable CaM agonist CALP 3 was sufficient in increasing apical endocytosis of PT epithelia.

Given that CaM is suggested to play a critically important role, I wanted to ask: What signaling cascade downstream of CaM is activated in the presence of flow? I used small molecule inhibitors of CaM dependent Kinases namely CaMKII and CaMKK. As seen in Fig. 23 C, inhibition of both CaMKs in HK-2 cells led to a reduction in amount of albumin endocytosed in the presence of FSS. I also observed that the CaMKK inhibitor STO609 ablated the CALP3 stimulated increase in the apical endocytosis of albumin in OK cells. Together these results suggest that CaM activation, and dependent CaMKK activation is necessary and sufficient for increasing the apical endocytic capacity in PT model cell lines. Rigorous testing of the hypothesis using complementary methods has to be conducted before we make these conclusions.

Before binding to Ca^{2+} and being activated, CaM is known to be bound to IQGAP1 in its inactive state (234-237). This sequestration of IQGAP1 prevents it from conducting its physiologic function as a GTPase Activator Protein (237). I wanted to ask the question: Does IQGAP1 play a role in regulating the FSS stimulated endocytic response? To answer this question, I utilized siRNA mediated Knockdown as a strategy to deplete endogenous levels of IQGAP1 in HK-2 cells. In two experiments, I noticed that the knockdown of this GAP protein ablated the FSS stimulated endocytic response.

Figure 24. Role of Cdc42 in FSS stimulated endocytosis



(A) & (B) Exposure of OK cells to FSS increases Cdc42 activity. OK cells were transfected with the Cdc42-Raichu construct and the experiment was conducted as described in the materials and methods. (A) Depicts a pseudocolored FRET image, with the scale demarcating the ratio between YFP and CFP in fixed OK cells, either kept under static conditions for 20 min, or subjected to FSS for 20 min. (B) Depicts YFP/CFP ratio denoting

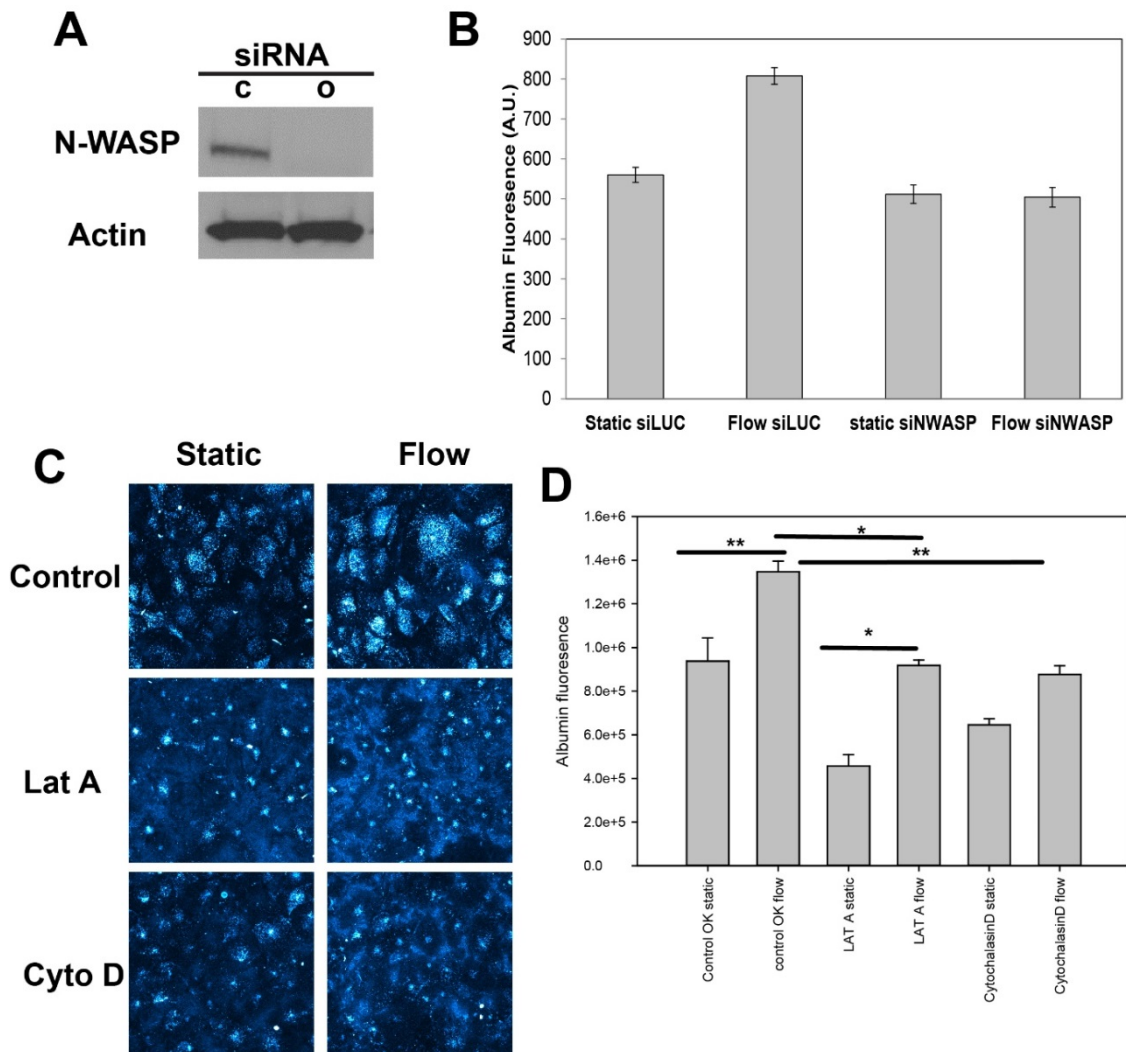
%FRET signal post-normalization to inactive negative control. Static number of cells = 5; Flow number of cells = 7. (C) Activation of Cdc42 is requisite for the FSS stimulated endocytic cascade. Endocytosis of AlexaFluor 647-albumin was measured in HK-2 cells incubated under static conditions or exposed to FSS. The Cdc42 inhibitors ML141 and ZCL278 were included where indicated. Mean +/- range of two independent experiments is plotted. (D) Endocytosis of AlexaFluor 647-albumin was measured in HK-2 cells incubated for 1 h under static conditions with the Cdc42 activator EGF. Where indicated, ML141 or ZCL278 were included to confirm that the effect of EGF on endocytosis was via Cdc42. The mean +/- SEM of 3-4 independent experiments is plotted for each condition. * $p < 0.02$ vs control (static) by ANOVA.

A.3 ROLE OF CDC42 IN FSS STIMULATED ENDOCYTOSIS

I employed a FRET assay, previously described in (238) to visualize the activation of Cdc42, a small GTPase in OK cells subjected to FSS. To conduct this assay, I employed a fluorescent, FRET based Cdc42 biosensor. When Cdc42 is inactive or GDP bound, the CFP and YFP molecules of the FRET sensor are spatially separated, and there is very poor energy transfer from the CFP molecule to the YFP molecule, and the FRET signal is low. In contrast, when Cdc42 is GTP bound and active, a conformational change occurs in the molecule which brings the CFP and YFP molecules close to each other, causing an increase in the FRET signal. My goal was to assess differences in FRET between cells subjected to FSS, to cells kept under static conditions. I normalized my FRET signal to a Dominant negative Cdc42 biosensor, as described in the methods below. In a small sample-set of about 5-7 cells, I noticed a 2.5 fold increase in the FRET signal between the static cells and the cells subjected to FSS.

To test if this activation of Cdc42 was important for the FSS stimulated endocytic cascade, I pre-incubated cells with small molecule inhibitors of Cdc42 activity, ML-141 and ZCL-278 before conducting the endocytosis assay, and the small molecule inhibitors were added to the perfusate while conducting the experiment. Across two experiments, ML-141 and ZCL-278 completely ablated the FSS stimulated increase in endocytosis in PT epithelia, suggesting an important role for Cdc42 in this cascade. Conversely, I wanted to ask: does activating Cdc42 was sufficient to trigger the cascade? As identified previously (in Fig. 20) incubating cells with EGF was sufficient to stimulate the FSS stimulated endocytic cascade. In addition, I show here that the small molecule inhibitors of Cdc42 activity are capable of ablating the increase in endocytic capacity achieved by incubating cells with EGF.

Figure 25. Critical role of actin dynamics in the FSS stimulated endocytic response



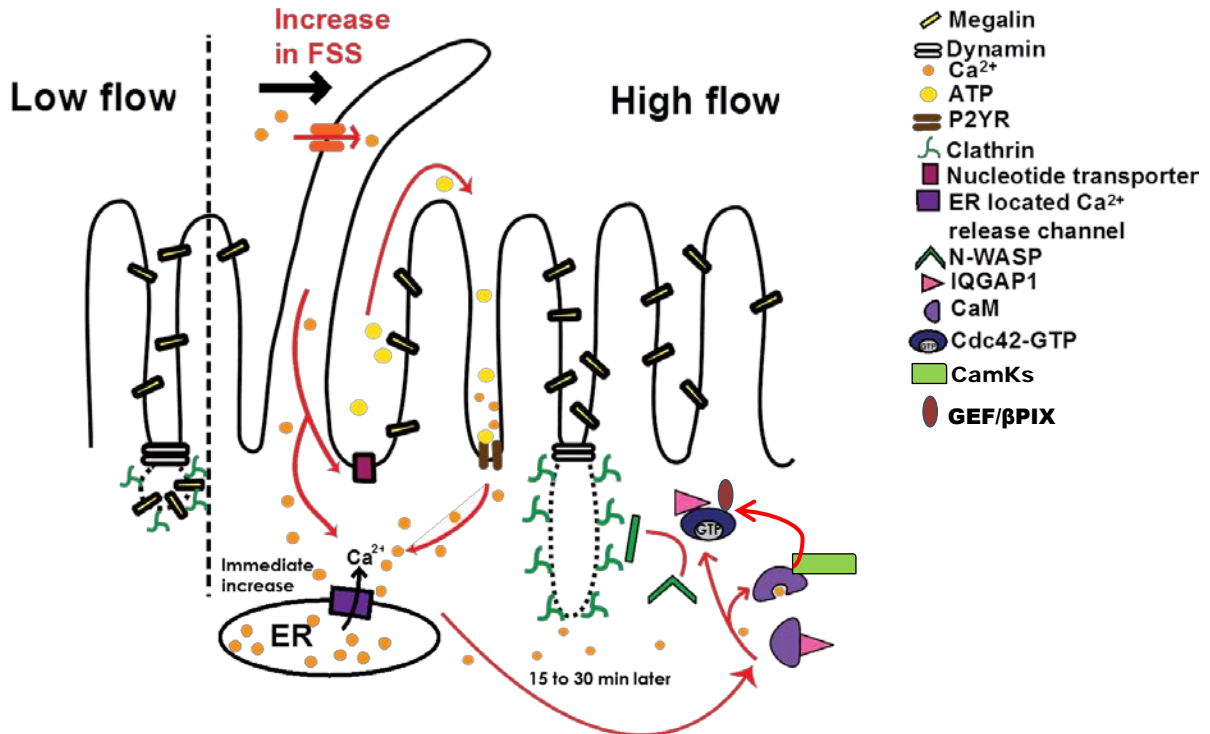
(A) Western blot of HK-2 cells transfected with either siRNA against firefly luciferase (control) or with siRNA against N-WASP. (B) N-WASP might play a role in the FSS stimulated endocytic cascade. Control or N-WASP depleted cells were incubated with Alexa 647 albumin either under static conditions or subjected to FSS for 1h. N=1 (C) & (D) Actin dynamics are important for the FSS stimulated endocytic responses. OK cells were either left untreated, or treated with 5 μ M Latrunculin A (Lat A, actin polymerization inhibitor), or 5 μ M Cytochalasin-D (Cyto D, an actin polymerization inhibitor) and subsequently incubated with AlexaFluor-647 Albumin either under static conditions or under FSS of 1 dyne/cm². N=3, *p<0.05, **p<0.01 using pairwise Student's t-test.

A.4 ROLE OF ACTIN DYNAMICS IN REGULATING FSS STIMULATED ENDOCYTOSIS

As Cdc42 was found to be activated, and to be critical for the FSS stimulated endocytosis, I wanted to assess the importance of N-WASP in this cascade. As previously discussed, Cdc42 is known to recruit N-WASP to clathrin coated pits, and modulate actin polymerization at these sites (206). To assess the contribution of N-WASP in this cascade, I used a siRNA geared approach to knockdown endogenous amounts of N-WASP in HK-2 cells. In one experiment, I observed that the FSS stimulated increase in N-WASP depleted cells was completely ablated. Suggesting a possible role for N-WASP in the FSS stimulated endocytosis cascade.

Next, I wanted to assess the necessity of actin dynamics in regulating FSS stimulated endocytosis. When OK cells were incubated with Latrunculin A (Lat A; a G-actin sequestering toxin) or Cytochalasin D (Cyto D, an F-Actin depolymerizing toxin), both the static and the FSS stimulated responses were significantly diminished, hinting that actin dynamics are important for both the cascades. Although the fold-change increase in the LatA treated cells across three experiments were very comparable to control, the increase in signal came from non-specific haze like stain in cells treated with Lat A.

Figure 26. Proposed model for the downstream signaling cascade



As described previously in Chapter 2, I observed an instantaneous increase in $[Ca^{2+}]_i$ when PT cells were exposed to physiologically relevant FSS. I propose the above model based on my findings from this appendix. The changes in $[Ca^{2+}]_i$ are sensed by cytosolic Calmodulin, which is bound to IQGAP1 in its initial inactive state. After binding to calcium, the Ca^{2+}/CaM complex associates with CaMKII, and CaMKK and in turn activates Cdc42 GEFs such as β PIX. The presence of free GAP, and GEF make Cdc42 cycle faster in the presence of physiologically relevant FSS, in comparison to static conditions. This increased activity of Cdc42 leads to increased activation of N-WASP at the apical surface, and therefore increased association of N-WASP to the clathrin coated pits. This in turn causes an increase in both the size and the number of clathrin coated pits. Findings from this appendix support this model, however, rigorous testing of my hypotheses has to be done before we can conclusively move forward with this model.

A.5 DISCUSSION

These results are preliminary, and further investigation is required to bolster our hypothesis. However, I believe that there is merit to this work, because it gives our lab perspective on avenues to explore moving forward.

To synthesize my findings in this section, I propose a novel mechanism that may be involved in regulating the FSS stimulated responses in PT epithelia (Fig. 26). My data suggest that CaM may have an important role in translating changes in $[Ca^{2+}]_i$ to trigger downstream signaling cascades, specifically, by triggering CaMKII, and CaMKK which may in turn trigger GEFs like β PIX to stimulate Cdc42 recruitment and activity. My data also suggests that IQGAP1, a GAP for Cdc42 may be released from its inactive conformation to stimulate Cdc42 activity. I employed FRET to visualize Cdc42 activity in OK cells and used small molecule interventions to block Cdc42 activity. Cdc42 is activated in cells exposed to FSS; and blocking cdc42 activity causes ablation of the FSS stimulated endocytic response. My data also suggests a role for N-WASP and actin dynamics in regulating the FSS stimulated endocytic pathway.

These results can certainly be augmented by repeating experiments, as well as by conducting complementary studies. (i) Apart from small molecule approaches to activating and blocking CaM, We can assess the activity of CaM using commercially available CaM biosensors. (ii) The role of CaMKK and β PIX in regulating Cdc42 activity can be tested rigorously by conducting live-cell experiments looking at Cdc42 activity as an endpoint. We can follow up this study by looking at the importance of a GEF like β PIX in regulating the endocytic

response. (iii) The role for IQGAP1 can be tested similarly to that of β PIX as both would have opposing roles in regulating Cdc42 activity. (iv) The role of Cdc42 can be more rigorously tested by using alternative activation assays complementary to the FRET assay used above (eg. G-LISA assays). Also, FRET-assays if done with live-cell microscopy, would help us better understand the kinetics of Cdc42 activation (v) N-WASP biosensors can be used similarly to ascertain the kinetics of N-WASP activation under FSS. (vi) My initial experiments with CK-666 (an ARP2/3 inhibitor) showed ablation of FSS stimulated endocytosis, but this effect was not reproducible. I would investigate the role of ARP2/3 in regulating apical actin dynamics further. (vii) Lastly, there is no easy way to assess the role of actin in a process without disrupting the cytoskeletal architecture of the cell. And it is not possible to conduct live-cell TIRFM, if we have to subject the cells to FSS. Therefore, I would try to assess the role of actin in FSS stimulated endocytosis by conducting live-cell microscopy on Life-Act transfected cells, perfused with pH sensitive Albumin, to observe if any significant changes in apical actin dynamics are seen.

A.6 MATERIALS AND METHODS:

Reagents and cell lines:

HK-2 cells were cultured as explained in Chapter 4.1. W-13 and CALP-3 were purchased from Sigma, and stock solutions were made in sterile DDH₂O. KN-93 and STO609 were purchased from TOCRIS bioscience. 1000X stock solutions were made in DMSO. Comparable amounts of DMSO were used in control conditions. ML141 was purchased from Calbiochem and ZCL 278 from TOCRIS bioscience. The cdc42 activator II (EGF) from cytoskeleton was used to activate cdc42 at the working concentration of 1U/mL. Cdc-42 Raichu, and the DN-Cdc42 Raichu were gifts from the Matsuda Lab (238). Latrunculin A and Cytochalasin D were purchased from EMD-Millipore.

siRNA:

siRNA transfections in ibidi chambers were conducted as described previously in section 4.3. The siRNA sequence against IQGAP1 used in this appendix is 5'-GGATGAGTCAGCTGTGTTATGGTTG-3' and the sequence against N-WASP is 5'-CCAAUGAAGAAGAAGCAAA-3'. The control siRNA used is siRNA against firefly luciferase, and the sequence can be found in table 4.1.

FRET assay:

FRET studies were conducted in conjunction with the Friedman lab at the University of Pittsburgh with the help of Dr. McGarvey. OK cells were transfected with either the WT-Cdc42-Raichu construct or the DN-Cdc42-Raichu construct (Negative control). Cells were either kept

under static condition or were exposed to FSS of 1dyne/cm^2 and were fixed for imaging. Cells were imaged using a Nikon A1R multi-spectral detector microscope using a 100X oil objective. Cells were illuminated with the CFP laser and signal from the YFP channel and the CFP channel were collected. Images were processed using Fiji to subtract the background and quantify the FRET signal. Intramolecular FRET signal from the Dominant negative was taken as a negative control, and the (YFP/CFP) ratios were normalized to the negative control.

APPENDIX B

B.1 INTRODUCTION

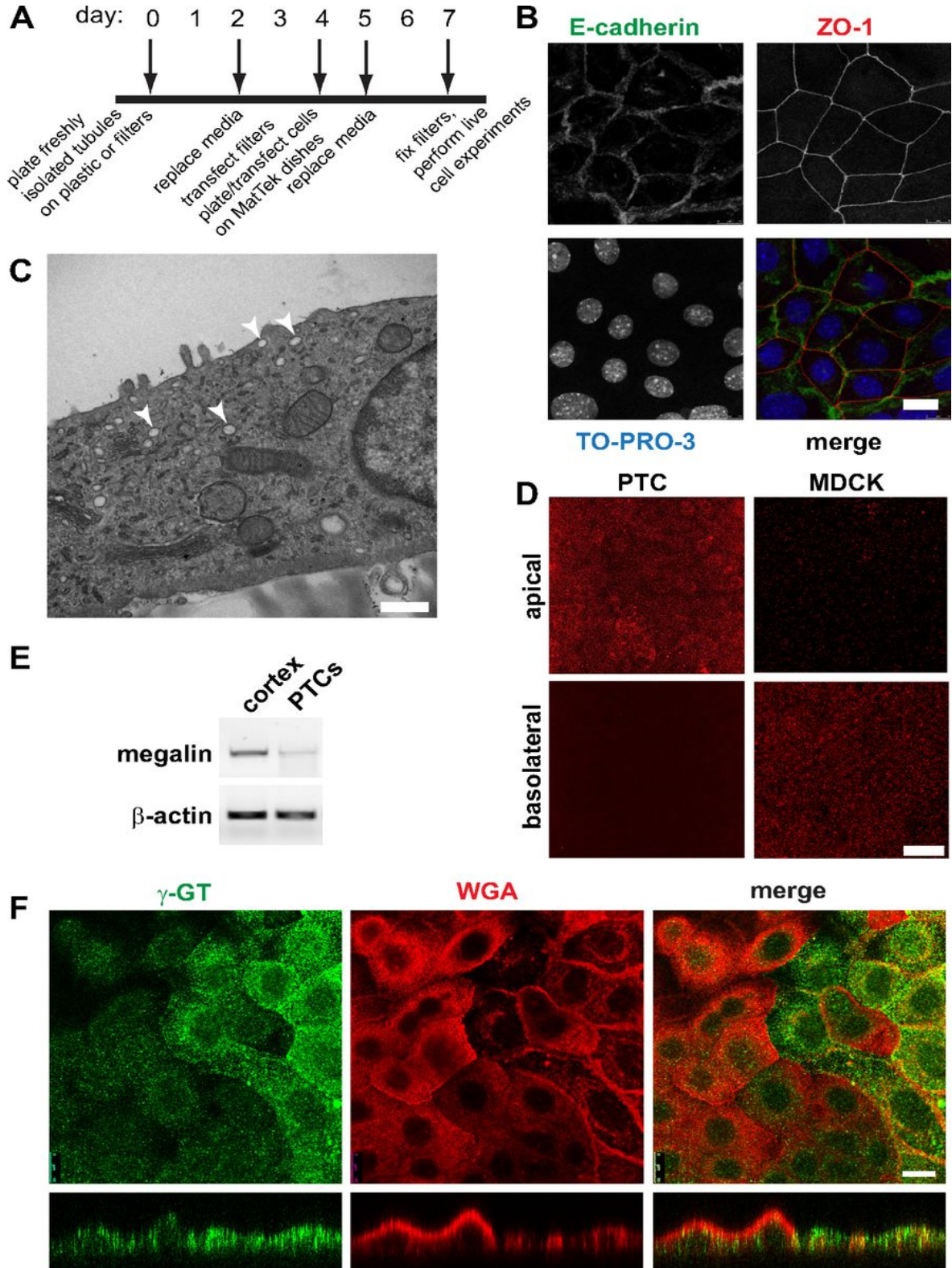
The kidney is the principal organ involved in the regulation of acid-base balance, blood pressure, electrolyte balance, and blood plasma composition in higher mammals. The nephron is the fundamental functional unit of the kidney and is divided into five functional segments: glomerulus, proximal tubule (PT), loop of Henle, distal tubule, and collecting duct. The PT is responsible for reabsorption of ~70% of sodium, bicarbonate, and chloride ions, phosphate, glucose, and water from the glomerular filtrate (reviewed in Refs. (239, 240)). The PT is further divided into S1, S2, and S3 segments on the basis of physiological, ultrastructural, and functional differences (241). The S1 segment is characterized by high expression of megalin, whereas the PT marker γ -glutamyltranspeptidase (γ -GT) is expressed at highest concentration in S2 and S3 cells (4, 242, 243).

Although endocytosis is critical for normal PT function, little is known about the endocytic pathway in these cells. Much of our understanding of the apical endocytic pathway in these cells comes from electron microscopy studies examining the internalization pathway of fluid-phase and membrane tracers (49, 65, 67-69). These tracers are internalized into clathrin-coated vesicles that bud from the base of the brush border microvilli and are thought to fuse with a subapical network of tubules (65). Fast recycling to the apical surface may occur from these sites. These fluid-phase and membrane tracers have access to large apical compartments, termed apical vacuoles (AVs), within 1–15 min after internalization (49, 65, 69). Tubule-like structures that are believed to carry recycling proteins back to the apical surface can be observed emanating

from these AVs (49, 69, 244). Nonrecycling proteins are thought to be transported to lysosomes for degradation and/or transcytosed to the basolateral membrane (48, 245). Although the endocytic structures accessed by markers have been described, the identity of these structures remains unknown. Notably, the organization of this pathway in PT cells (PTCs) differs considerably from that of the apical recycling pathway described in cells derived from different kidney segments (87, 246). Therefore, we sought to examine the itinerary of apically internalized albumin in a PTC model that retains essential features of this endocytic pathway.

We have developed a primary cell culture model of mouse PTCs to study the organization and molecular identity of compartments along the apical endocytic pathway. Cultured primary cells form a differentiated polarized monolayer that maintains characteristics of the PT segments from which they were derived. We have investigated the structure and distribution of known endocytic compartment markers in our primary culture system and determined the pathway for internalization and sorting of a fluid-phase marker and the megalin/cubilin ligand albumin. Our studies suggest that the Rab11a-positive compartments represent the AVs reported in ultrastructural studies of PTs and that these structures receive and sort fluid and membrane cargoes. The unique organization of the apical endocytic pathway in PTCs likely reflects the specific functional demands of this kidney segment.

Figure 27. Characterization of primary proximal tubule cell (PTC) cultures.



A) timeline of cell-plating schedule after isolation of PTCs from mouse kidney cortex. B) PTCs grown on permeable supports were fixed and processed for indirect immunofluorescence

to detect the lateral adherens junction marker E-cadherin (green), the tight junction marker zonula occludens 1 (ZO-1; red), and nuclei using TO-PRO-3 (blue). Scale bar, 10 μm . C) PTCs grown on permeable supports were processed for transmission electron microscopy. Arrowheads denote subapical structures that may correspond to apical vacuoles observed in vivo. Scale bar, 500 nm. D) filter-grown PTCs or Madin-Darby canine kidney (MDCK) cells were incubated with apically or basolaterally added rhodamine-dextran (1 mg/ml) for 20 min and processed for immunofluorescence. PTCs internalized dextran primarily from the apical surface, whereas the opposite was observed for MDCK cells. Scale bar, 15 μm . E) RT-PCR was performed to detect megalin expression from reverse-transcribed mRNA isolated from mouse cortex or from PTCs after 7 days in culture. β -Actin is included as a loading control. F) filter-grown PTCs were incubated with rhodamine-conjugated wheat germ agglutinin (WGA) for 30 min (red), fixed, and then processed to detect γ -glutamyltranspeptidase (γ -GT; green). Cells were analyzed by confocal microscopy, and individual optical sections and xz reconstructions are shown. Note that cells expressing higher levels of γ -GT bind to and internalize less WGA and are markedly flatter in cross section. Scale bar, 10 μm .

B.2 PRIMARY CULTURES OF MOUSE PT ARE POLARIZED AND EXPRESS PT

MARKERS:

To generate primary PTC cultures, renal tubules isolated from mouse kidney cortex were plated on collagen I-coated plastic or directly onto collagen IV-coated permeable supports. A timeline of the isolation and plating schedule is shown in Fig. 27A. Cells plated on plastic migrated from these tubules over several days and formed proliferating islands of cells that eventually coalesced to form a confluent monolayer. Similarly, tubules plated directly onto collagen IV-coated permeable supports formed confluent monolayers within several days, as assessed using 4',6-diamidino-2-phenylindole staining (not shown). Cells in these monolayers were polarized as assessed by indirect immunofluorescence to visualize the tight junction marker ZO-1 (Fig. 27B). Moreover, the adherens junction marker E-cadherin localized exclusively to the lateral domains of these cells (Fig. 27B).

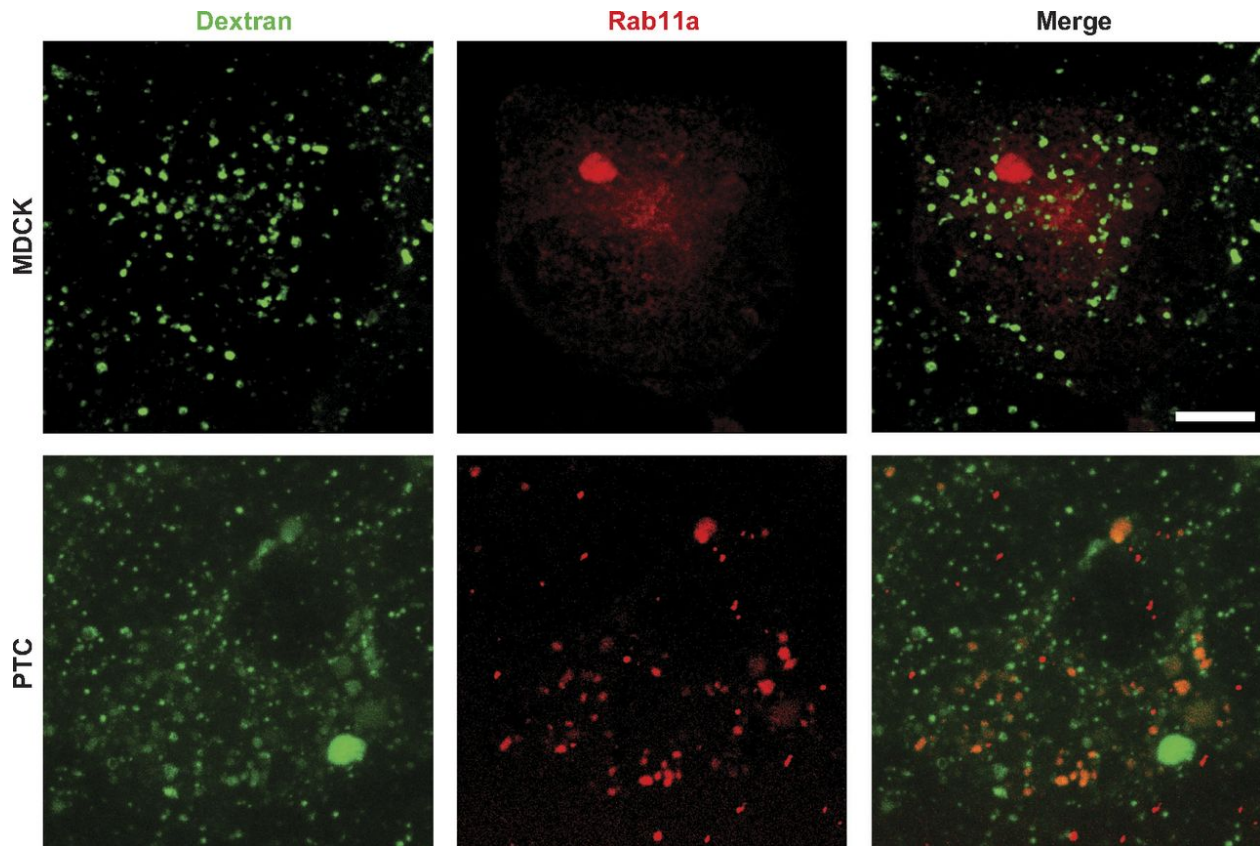
PTCs *in vivo* are characterized by the presence of highly regular and tall apical microvilli, as well as numerous AVs that receive internalized fluid and membrane markers (65, 67). To test whether these structures are retained in our primary cultures, freshly isolated PTCs cultured on permeable supports for 7 days were fixed and processed for transmission electron microscopy (see MATERIALS AND METHODS). In contrast to PTCs *in vivo*, our cultured cells were fairly flat and had only a few scattered microvilli (Fig. 27C). Tight junctions were readily detected between adjacent cells, as predicted by our ZO-1 staining in Fig. 1C (not shown). This morphology is similar to that reported in numerous other studies of primary cultures isolated using similar approaches (247-249). Notably, however, we did observe large

vacuolar structures near the apical surface of many cells (arrowheads in Fig. 27C). We speculate that these structures may represent the AVs described *in vivo* from which internalized apical cargo is recycled (49, 65, 67-69).

A unique characteristic of PTCs is high capacity for apical endocytosis. To test this, we added the fluid-phase marker rhodamine-dextran to the apical or basolateral chamber of filter-grown PTCs and compared the extent of uptake after 20 min. As shown in Fig. 27D, rhodamine-dextran was internalized to a much greater extent from the apical than basolateral surface in PTCs (Fig. 27D). In contrast, this marker was endocytosed primarily from the basolateral surface of Madin-Darby canine kidney (MDCK) cells, consistent with prior observations that basolateral internalization of membrane and fluid is more robust than apical endocytosis in these cells (150, 151).

We next examined the expression of PT-specific markers in our primary cell cultures. PCR amplification of reverse-transcribed mRNA confirmed that primary cultures continued to express the PT marker megalin, albeit at lower levels than in freshly isolated kidney cortex (Fig. 27E). Indirect immunofluorescence using antibodies directed against γ -GT revealed strong staining in a subset of cells, consistent with the presence of cells derived from S2 and S3 segments of the PT (Fig. 27F). Interestingly, when cells were incubated at 37°C with rhodamine-WGA prior to fixation and staining with anti- γ -GT antibody, we observed considerably more robust surface binding and internalization of WGA in the population of cells expressing low levels of γ -GT (Fig. 27F). As revealed by xz reconstructions of confocal stacks, the population of cells binding to WGA was typically taller than the fraction expressing higher levels of γ -GT. These studies also confirmed γ -GT staining primarily at the apical surface of PTCs, consistent with its known distribution *in vivo*.

Figure 28. Fluid-phase markers are not enriched in Rab11a-positive compartments in MDCK cells.



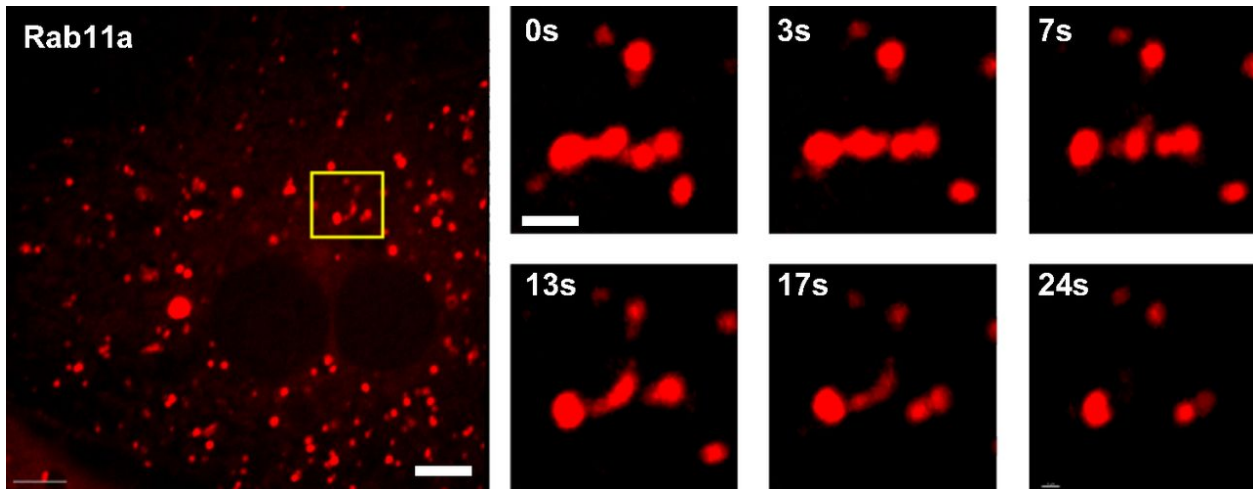
Filter-grown MDCK cells (top) or PTCs (bottom) expressing S-nitroso-N-acetylpenicillamine (SNAP)-Rab11a were labeled with tetramethylrhodamine (TMR)-Star and incubated with apically added FITC-dextran (1 mg/ml) for 20 min, fixed, and then examined by confocal microscopy. In contrast to the readily observed accumulation of dextran in Rab11a-positive compartments in PTCs, dextran has little access to this compartment in MDCK cells. Scale bar, 7.5 μ m.

B.3 RAB11A POSITIVE COMPARTMENTS IN PT CELLS RECEIVE FLUID PHASE

CARGO

In MDCK cells, Rab11a localizes to a condensed network of subapical recycling endosomes (250). Moreover, internalized fluid-phase markers have been reported to be excluded from Rab11a-positive compartments in these cells (251, 252). To confirm this, we incubated polarized MDCK cells or PTCs expressing SNAP-Rab11a with apically added FITC-dextran for 20 min and then fixed and imaged the cells. As shown in Fig. 28, Rab11a in MDCK cells was present in a subapical cluster, as previously observed, and as expected, the majority of internalized dextran localized to small punctate compartments, consistent with early endosomes. In contrast, a much larger fraction of internalized dextran was present in Rab11a-positive compartments in PTCs [$23.0 \pm 3.9\%$ in PTCs ($n = 8$) vs. $6.6 \pm 1.6\%$ in MDCK cells ($n = 17$), $P < 0.001$ by rank-sum test; Fig. 28] These results are consistent with the interpretation that apically internalized fluid-phase markers are largely segregated from membrane proteins in earlier compartments along the endocytic pathway in MDCK cells compared with PTCs.

Figure 29. Rab11a-positive compartments in PTCs are highly dynamic

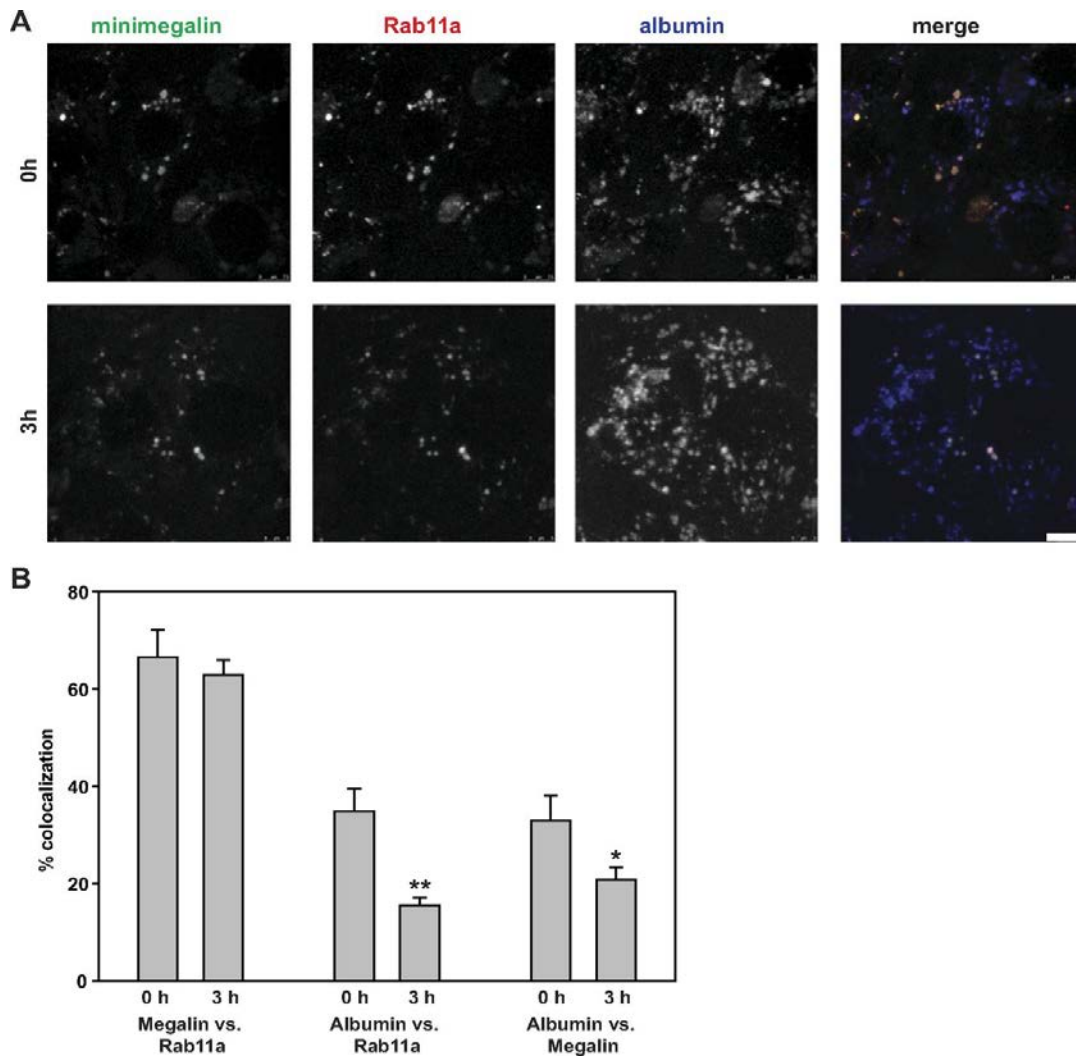


PTCs cultured on MatTek dishes were transfected with cDNA encoding SNAP-tagged Rab11a. After 2 days, cells were incubated with Cell-SNAP TMR-Star to label the SNAP tag, washed, and then imaged by live-cell microscopy to visualize Rab11a dynamics. Rab11a localizes to multiple variously sized spherical compartments that are highly dynamic. Left: a representative cell. Scale bar, 7.5 μm . Right: time-lapse (0–24 s) images of a tubule emanating from the Rab11a-positive structure enclosed in the box in the image at left. Scale bar, 1 μm .

B.4 RAB11A POSITIVE COMPARTMENTS IN PTS RESEMBLE APICAL VACUOLES FOUND IN PROXIMAL TUBULES INVIVO.

Ultrastructural analysis of AVs in rat kidney has revealed tubules emanating from these structures, suggesting that AVs may mediate sorting of membrane and fluid cargo (49, 69). To test whether Rab11a-positive structures in PTCs also undergo tubulation, we expressed SNAP-tagged Rab11a in PTCs by transient transfection, incubated cells with tetramethylrhodamine-SNAP to label Rab11a-positive compartments, and imaged living cells. Rab11a-positive structures were highly dynamic and were observed to undergo fusion and fission. Fig. 29 shows a tubule forming and dissociating from a Rab11a-positive structure. These data are consistent with the interpretation that Rab11a is a marker of the AV structures observed in vivo.

Figure 30. Segregation of megalin and albumin in PTC Rab11a-positive compartments.



A: PTCs grown on MatTek dishes were transfected with plasmids encoding mCherry-Rab11a and GFP-minimegalin. Cells were incubated with 40 $\mu\text{g/ml}$ Alexa Fluor 647-albumin for 20 min, and confocal images of random fields were acquired immediately (0 h) or after a 3-h chase. Maximum projections of albumin, GFP-minimegalin, and Rab11a distribution, as well as merged images, are shown. Scale bar, 5 μm . B: amount of total cellular GFP-minimegalin in Rab11a-positive compartments and amount of albumin in Rab11a- or GFP-minimegalin-positive compartments in 6 images for each time point. Values are means \pm SE. * $P = 0.014$; ** $P = 0.025$ by Student's t-test. Whereas distribution of GFP-minimegalin does not change, albumin segregates from both markers during the chase period.

B.5 APICAL VACUOLE LIKE COMPARTMENTS IN MOUSE PTS ARE HIGHLY DYNAMIC AND SORT MEMBRANE AND FLUID-PHASE CARGO:

Albumin is thought to dissociate from megalin/cubilin in early endosomal compartments. We therefore asked whether albumin exits Rab11a-positive compartments in concert with a known fluid-phase marker (rhodamine-dextran). PTCs expressing SNAP-Rab11a were labeled with SNAP-Cell 505, incubated for 30 min with 40 μ g/ml Alexa Fluor 647-albumin and 1 mg/ml rhodamine-dextran, and chased for 30 min. Cells were imaged in real time to visualize membrane dynamics. Albumin and dextran were largely colocalized and readily detected in rapidly moving Rab11a-positive structures, as well as in tubular carriers containing both cargoes. While we speculate that these tubular carriers emanate from Rab11a-positive compartments, we were unable to unambiguously identify individual fission events.

Next, we assessed whether membrane and fluid-phase cargoes are sorted in Rab11a-positive compartments. We transfected PTCs with plasmids encoding Rab11a-SNAP and GFP-tagged truncated megalin (GFP-minimegalin), which retains the capacity to bind albumin (12, 142). Cells were incubated for 20 min at 37°C with Alexa Fluor 647-albumin and then imaged immediately (0 h) or after a 3-h chase (Fig. 30). GFP-minimegalin was detected at low levels on the cell surface and concentrated intracellularly in Rab11a-positive compartments. The distribution of this protein was qualitatively similar at 0 and 3 h, as expected for a protein at steady state (Fig. 30A). Quantitation of maximally projected confocal stacks confirmed this result: $67 \pm 5.5\%$ of the total GFP-minimegalin was present in Rab11a-positive compartments at 0 h vs. $63 \pm 2.9\%$ at 3 h (Fig. 30B). In contrast, more albumin was present in compartments containing Rab11a and GFP-minimegalin at 0 h than 3 h (Fig. 30B). Quantitation revealed a statistically significant drop in the total amount of albumin in Rab11a-positive compartments

over this time period (from $35 \pm 4.6\%$ to $16 \pm 1.6\%$, $P < 0.02$). Similarly, the amount of albumin colocalizing with GFP-minimegalin decreased from $33 \pm 5.1\%$ to $21 \pm 2.6\%$ ($P = 0.025$). Illustrate the rapid dynamics of these cargoes in PTCs and confirm that heterologous expression of Rab11a in PTCs does not qualitatively alter the distribution or dynamics of GFP-minimegalin or albumin

B.6 DISCUSSION

Despite the essential role of apical endocytosis in PT function, little is known about how the endocytic pathway is organized and regulated in PTCs. I found that Rab11a-positive compartments are dynamic structures that receive membrane and fluid-phase cargo internalized from the apical surface of PTCs. In contrast, apical endocytosis is far less robust in immortalized cells derived from other kidney segments. The unique morphology and function of Rab11a-positive compartments may reflect the high endocytic demands of PTCs compared with cells in more distal segments of the kidney tubule.

We used standard protocols to isolate primary cultures of PTCs. The resulting cell populations formed polarized monolayers with intact tight junctions and laterally localized E-cadherin. Moreover, ultrastructural analysis revealed the presence of subapical vacuolar structures consistent with those described previously in the PT. However, while our cells elaborated a few microvilli, they lacked the regular and highly differentiated brush border observed *in vivo*. Isolated PTCs expressed endogenous megalin, and subpopulations of cells could be distinguished on the basis of their expression of high levels of γ -GT (consistent with S2/S3-derived cells) or robust internalization of albumin (consistent with S1-derived cells).

Rab11a-positive structures in PTCs were highly dynamic and were observed to undergo cycles of fusion and fission. Moreover, fluid-phase markers (rhodamine-dextran) and fluorescent albumin (which dissociates from megalin in acidic endosomal compartments) readily accessed these compartments. This is in contrast to observations in MDCK cells, where fluid markers are efficiently segregated from membrane proteins in early endosomes and are largely excluded from recycling endosomes (251, 252).

In vivo perfusion studies in rat kidney have determined that fluid-phase markers are internalized into tubular structures that may represent early endosomes and later appear in AVs (22, 65, 67). We attempted to determine whether internalized albumin and dextran appear in EEA1-positive early endosomes prior to reaching Rab11a-positive compartments, but our results were inconclusive. Thus it remains unclear whether there is a linear progression of cargo from early endosomes to Rab11a-positive compartments in our PTC cultures.

The differences we observed between cells from the PT and cells derived from other kidney segments have important consequences for our understanding of how this pathway is regulated in response to physiological need. In contrast to most other polarized epithelial cells [with the exception of intercalated cells of the kidney (253)], the PT is highly specialized for apical endocytosis. High apical endocytic capacity in the PT is required for the efficient internalization of filtered proteins, vitamins, and other solutes. Although the mechanism is unclear, we speculate that the unique size and geometry of Rab11a-positive compartments that we observed in PTCs enhance the segregation efficiency of internalized fluid and membrane cargoes to maintain robust PT apical endocytic capacity.

Importantly, many of the features essential for maintaining PT function are preserved in commonly used immortalized PTC lines. For example, apical endocytosis in OK and LLC-PK1

cells, derived from opossum and porcine kidney, respectively, is robust relative to basolateral internalization, similar to that observed in our primary cell culture model (unpublished data). Rab11a has been localized to the subapical region of OK cells (254), where recent higher-resolution images suggest that it is present in variously sized spherical compartments (255). Interestingly, these compartments become enlarged upon inhibition of class III phosphoinositide 3-kinase, and release of this block triggers rapid formation of tubular structures containing albumin (255).

The conclusions of our studies are limited by several technical shortcomings. 1) Our cell cultures are relatively flat and lack a prominent brush border, suggesting that they have dedifferentiated to some extent. While our PTCs maintain a robust apical endocytic capacity, the regulation of this pathway likely does not exactly replicate that *in vivo*. For example, ultrastructural analysis of our cells did not reveal the prominent network of subapical tubules described *in vivo* (65, 67, 69). This network is also absent in immortalized PT-derived cell lines. 2) While we confirmed by Western blotting that PTCs express endogenous Rab11a (not shown), we were unable, using multiple approaches, to confirm that the Rab11a-positive compartments we visualized correspond to the AVs described *in vivo*. 3) Although we focused on “low-expressing” cells in our imaging studies (in high-expressing cells, Rab11a was distributed throughout the cytoplasm), it is possible that overexpression of Rab11a alters the normal sorting recycling pathway in our PTC cultures. Despite these caveats, our results provide important new information about the unique organization and function of the apical endocytic pathway in PTCs. Future studies are required to determine how the unique morphology of AVs facilitates efficient sorting and recycling to maintain PT function.

B.7 APPENDIX B MATERIALS AND METHODS:

Reagents: Reagents for cell culture and analysis were obtained as follows: collagen I from EMD-Millipore (Billerica, MA), bovine collagen IV from Rockland Immunochemicals (Gilbertsville, PA), DMEM/Ham's F-12 medium (DMEM/F-12) and media additives (insulin, transferrin, selenium, and dexamethasone) from Sigma-Aldrich (St. Louis, MO), permeable supports (0.4- μ m-pore Transwell inserts) from Corning (Corning, NY), collagenase type II from Worthington (Lakewood, NJ), paraformaldehyde from Electron Microscopy Sciences (Hatfield, PA), and trypsin (catalog no. 12563-029) from GIBCO Life Technologies (Carlsbad, CA).

Isolation, culture, and transfection of PTCs. The protocol for isolating PTCs from 6- to 8-wk-old male mice was adapted from a previously published method (249). Mice were euthanized in accordance with procedures approved by the University of Pittsburgh Institutional Animal Care and Use Committee, and the kidneys were removed and placed in ice-cold renal PTC (RPTC) buffer (in mM: 115 NaCl, 24 NaHCO₃, 5 KCl, 1.5 CaCl₂, 10 MgSO₄, 2 KH₂PO₄, 5 glucose, and 50 mannitol, pH 7.4). The kidney capsule was removed, the kidney was cut sagittally, and the medulla was removed. The cortex was minced under sterile conditions into 1-mm pieces and gently washed to remove debris, and collagenase type II and BSA were added to achieve a final concentration of 0.1% and 0.5%, respectively. The tissue was digested for 45 min at 37°C, and digestion was stopped by addition of ice-cold RPTC buffer with 5% BSA for 5 min on ice. The tissue was centrifuged for 30 s and resuspended in 20 ml of RPTC buffer. The suspension was sequentially passed through a series of stackable metal sieves with 180-, 90-, and 45- μ m pores, respectively (Alfa Aesar USA standard sieve, Ward Hill, MA). The final isolate was collected, resuspended in DMEM/F-12 + L-glutamine-10% FBS, and plated on collagen I-coated plates or collagen IV-coated permeable supports. The medium was replaced with RPTC

medium with 1% FBS (DMEM/F-12 supplemented with 5 $\mu\text{g/ml}$ insulin, 0.02 $\mu\text{g/ml}$ dexamethasone, 0.01 $\mu\text{g/ml}$ selenium, 5 $\mu\text{g/ml}$ transferrin, 2 mM L-glutamine, 10^{-9} M triiodothyronine, and 1% FBS) after 24 h, and the cells were used for experiments as described in the timeline in Fig. 1A. Cells were transfected as follows for live-cell-imaging experiments: plasmids encoding S-nitroso-N-acetyl-penicillamine (SNAP)-Rab11a (0.25–0.5 μg) and minimegalin-green fluorescent protein (GFP, 0.5 μg) were suspended in 63 μl of OptiMEM (GIBCO) and incubated at ambient temperature for 5 min. One microliter of Lipofectamine 2000 was resuspended in 63 μl of OptiMEM and incubated at ambient temperature for 5 min. Lipofectamine and DNA suspensions were mixed and incubated at ambient temperature for 20 min. RPTCs were trypsinized, and 2×10^5 cells were resuspended with transfection mix and plated onto collagen IV-coated dishes (MatTek, Ashland, MA). The medium was changed 6 h postplating to avoid lipid toxicity.

Indirect immunofluorescence. Anionic lysine-fixable rhodamine-dextran (10,000 mol wt) and Alexa Fluor 555- and Alexa Fluor 647-conjugated BSA were obtained from Life Technologies. Rhodamine-conjugated wheat germ agglutinin (WGA) was from Vector Laboratories (Burlingame, CA). Rabbit anti- γ -GT antibody (1:100 dilution) and rat anti-zonula occludens 1 (ZO)-1 monoclonal antibody were gifts from Dr. Rebecca Hughey and Dr. Gerard Apodaca, respectively. Monoclonal anti-E-cadherin antibody (1:200 dilution) from BD Transduction Laboratories (San Jose, CA). Cells plated on permeable supports were transfected on day 4 and fixed on day 7 in 4% paraformaldehyde-100 mM sodium cacodylate, pH 7.4. Filters were incubated in 0.1% Triton X-100 in 75 mM NH_4Cl_2 -20 mM glycine-PBS for 10 min, washed, and blocked in 1% BSA-0.1% saponin for 1 h. Primary antibodies were added in 0.5% BSA-0.025% saponin in PBS for 1 h at ambient temperature, and filters were washed three times

with 0.5% BSA-0.025% saponin in PBS. Secondary Alexa Fluor-conjugated antibodies (Invitrogen) were used at a dilution of 1:500 for 30 min, and TO-PRO-3 (1:1,000 dilution; Molecular Probes, Eugene, OR) was included where indicated. The filters were washed and then mounted onto glass slides with ProLong Gold (Life Technologies). Imaging was performed on a Leica SP5 confocal microscope ($\times 100/1.5$ numerical aperture objective) and processed using Adobe Photoshop CS4.

PCR detection of murine megalin mRNA. mRNA was extracted using the Ambion RNAqueous phenol-free total RNA isolation kit (Life Technologies). One microgram of RNA was used for synthesis of cDNA using Moloney's murine leukemia virus reverse transcriptase (Life Technologies) according to the manufacturer's recommendations. PCR was performed in 50- μ l reactions using the Bio-Rad iCycler and Phusion High-Fidelity PCR system (New England Biolabs, Ipswich, MA). Primer sets against megalin were designed using PrimerQuest on the Integrated DNA Technologies website: 5'-CTAACCAAGGCAGGACGTTTC-3' (forward) and 5'-TCCACCGTGGACACAAGTAAA-3' (reverse) for megalin and 5'-ACCTTCAACTCCATCATGAAG-3' (forward) and 5'-CTGCTGGAAGGTGGACAG-3' (reverse) for actin. Denaturing temperature was 95°C, annealing temperature was 54.5°C, and extension temperature was 72°C for 25 amplification cycles.

Live-cell imaging of PTCs. Isolated PTCs grown on collagen I-coated dishes were transfected with the indicated combination of plasmids [mCherry-Rab11a, SNAP-tagged Rab11a, and GFP-tagged minimegalin (142, 256)] and plated on collagen I-coated dishes (MatTek). At 3 days posttransfection, PTCs were incubated as indicated with SNAP-Cell TMR-Star or SNAP-Cell 505 (New England Biolabs; 3 μ M final concentration) for 30 min at 37°C to label Rab11a-SNAP. Cells were then incubated with serum-free RPTC buffer containing

rhodamine-dextran (1 mg/ml) and/or Alexa Fluor 647-albumin at 37°C, and live-cell time-lapse microscopy was performed. Live-cell imaging to visualize SNAP-tagged Rab11a dynamics in RPTCs was performed using the Andor revolution XD platform. A live-cell chamber compatible with the inverted spinning-disk microscope was used to maintain a temperature of 37°C and PCO₂ of 5%. Images were captured using a 12-bit electron-multiplying charge-coupled device iXON camera controlled by the Andor iQ interface. Images were continuously acquired over a 10-min period. Live-cell imaging to visualize cargo sorting from the Rab11a-positive compartments was performed using the Leica TCS SP5 platform. A live-cell chamber compatible with the inverted laser-scanning microscope was used to maintain a temperature of 37°C. Images were captured using a 16-bit dynamic hybrid detector in 5-s intervals over 5 min. Images were exported in a 16-bit TIFF format for qualitative analyses. Time-lapse images were reconstructed using Imaris (Bitplane), and a 3 × 3 median filter was applied to the images. Fission and fusion events were recorded as audio-video interleave. Signal overlap of dextran, albumin, and megalin with the Rab11a-positive compartments was computed using MetaMorph (Molecular Devices, Sunnyvale, CA). Integrated morphometry analysis was used to construct a mask based on area thresholding. The integrated density overlap of megalin and albumin over the Rab11a-positive compartments was computed using the colocalization package where in the percentage overlap between the two channels was determined.

BIBLIOGRAPHY

1. Ovalle WK, Nahirney, P.C. (2008) Netter's Essential Histology. *Elsevier Inc.* .
2. Douglas Eaton JP (2012) Vanders Renal Physiology, Eighth Edition *Lange Medical Books*.
3. Mattila PE, Raghavan V, Rbaibi Y, Baty CJ, & Weisz OA (2013) Rab11a-positive compartments in proximal tubule cells sort fluid phase and membrane cargo. *American journal of physiology. Cell physiology*.
4. Moestrup SK & Verroust PJ (2001) Megalin- and cubilin-mediated endocytosis of protein-bound vitamins, lipids, and hormones in polarized epithelia. *Annu Rev Nutr* 21:407-428.
5. Kerjaschki D & Farquhar MG (1982) The pathogenic antigen of Heymann nephritis is a membrane glycoprotein of the renal proximal tubule brush border. *Proc Natl Acad Sci U S A* 79(18):5557-5561.
6. Ozawa M, Yonezawa S, Sato E, & Muramatsu T (1982) A new glycoprotein antigen common to teratocarcinoma, visceral endoderm, and renal tubular brush border. *Developmental biology* 91(2):351-359.
7. Farquhar MG, Saito A, Kerjaschki D, & Orlando RA (1995) The Heymann nephritis antigenic complex: megalin (gp330) and RAP. *Journal of the American Society of Nephrology : JASN* 6(1):35-47.
8. Saito A, Pietromonaco S, Loo AK, & Farquhar MG (1994) Complete cloning and sequencing of rat gp330/"megalin," a distinctive member of the low density lipoprotein receptor gene family. *Proc Natl Acad Sci U S A* 91(21):9725-9729.
9. Hjalm G, *et al.* (1996) Cloning and sequencing of human gp330, a Ca(2+)-binding receptor with potential intracellular signaling properties. *European journal of biochemistry / FEBS* 239(1):132-137.

10. Jeon H & Blacklow SC (2005) Structure and physiologic function of the low-density lipoprotein receptor. *Annual review of biochemistry* 74:535-562.
11. Yuseff MI, Farfan P, Bu G, & Marzolo MP (2007) A cytoplasmic PPPSP motif determines megalin's phosphorylation and regulates receptor's recycling and surface expression. *Traffic* 8(9):1215-1230.
12. Takeda T, Yamazaki H, & Farquhar MG (2003) Identification of an apical sorting determinant in the cytoplasmic tail of megalin. *American journal of physiology. Cell physiology* 284(5):C1105-1113.
13. Bachinsky DR, *et al.* (1993) Detection of two forms of GP330. Their role in Heymann nephritis. *The American journal of pathology* 143(2):598-611.
14. Zou Z, *et al.* (2004) Linking receptor-mediated endocytosis and cell signaling: evidence for regulated intramembrane proteolysis of megalin in proximal tubule. *J Biol Chem* 279(33):34302-34310.
15. Christ A, *et al.* (2010) The soluble intracellular domain of megalin does not affect renal proximal tubular function in vivo. *Kidney international* 78(5):473-477.
16. Li Y, Cong R, & Biemesderfer D (2008) The COOH terminus of megalin regulates gene expression in opossum kidney proximal tubule cells. *Am J Physiol Cell Physiol* 295(2):C529-537.
17. Birn H, Vorum H, Verroust PJ, Moestrup SK, & Christensen EI (2000) Receptor-associated protein is important for normal processing of megalin in kidney proximal tubules. *Journal of the American Society of Nephrology : JASN* 11(2):191-202.
18. Willnow TE, *et al.* (1996) RAP, a specialized chaperone, prevents ligand-induced ER retention and degradation of LDL receptor-related endocytic receptors. *EMBO J* 15(11):2632-2639.
19. Czekay RP, Orlando RA, Woodward L, Lundstrom M, & Farquhar MG (1997) Endocytic trafficking of megalin/RAP complexes: dissociation of the complexes in late endosomes. *Mol Biol Cell* 8(3):517-532.
20. Juhlin C, *et al.* (1987) Monoclonal antibodies with exclusive reactivity against parathyroid cells and tubule cells of the kidney. *Proc Natl Acad Sci U S A* 84(9):2990-2994.

21. Christensen EI, Gliemann J, & Moestrup SK (1992) Renal tubule gp330 is a calcium binding receptor for endocytic uptake of protein. *The journal of histochemistry and cytochemistry : official journal of the Histochemistry Society* 40(10):1481-1490.
22. Christensen EI, Birn H, Storm T, Weyer K, & Nielsen R (2012) Endocytic receptors in the renal proximal tubule. *Physiology* 27(4):223-236.
23. Leheste JR, *et al.* (1999) Megalin knockout mice as an animal model of low molecular weight proteinuria. *The American journal of pathology* 155(4):1361-1370.
24. Cui S, Verroust PJ, Moestrup SK, & Christensen EI (1996) Megalin/gp330 mediates uptake of albumin in renal proximal tubule. *The American journal of physiology* 271(4 Pt 2):F900-907.
25. Seetharam B, Alpers DH, & Allen RH (1981) Isolation and characterization of the ileal receptor for intrinsic factor-cobalamin. *J Biol Chem* 256(8):3785-3790.
26. Seetharam B, Christensen EI, Moestrup SK, Hammond TG, & Verroust PJ (1997) Identification of rat yolk sac target protein of teratogenic antibodies, gp280, as intrinsic factor-cobalamin receptor. *The Journal of clinical investigation* 99(10):2317-2322.
27. Sahali D, *et al.* (1988) Characterization of a 280-kD protein restricted to the coated pits of the renal brush border and the epithelial cells of the yolk sac. Teratogenic effect of the specific monoclonal antibodies. *The Journal of experimental medicine* 167(1):213-218.
28. Moestrup SK, *et al.* (1998) The intrinsic factor-vitamin B12 receptor and target of teratogenic antibodies is a megalin-binding peripheral membrane protein with homology to developmental proteins. *J Biol Chem* 273(9):5235-5242.
29. Amsellem S, *et al.* (2010) Cubilin is essential for albumin reabsorption in the renal proximal tubule. *Journal of the American Society of Nephrology : JASN* 21(11):1859-1867.
30. Kozyraki R, *et al.* (2001) Megalin-dependent cubilin-mediated endocytosis is a major pathway for the apical uptake of transferrin in polarized epithelia. *Proc Natl Acad Sci U S A* 98(22):12491-12496.
31. Strobe S, Rivi R, Metzger T, Manova K, & Lacy E (2004) Mouse amnionless, which is required for primitive streak assembly, mediates cell-surface localization and endocytic function of cubilin on visceral endoderm and kidney proximal tubules. *Development* 131(19):4787-4795.

32. He Q, *et al.* (2005) Amnionless function is required for cubilin brush-border expression and intrinsic factor-cobalamin (vitamin B12) absorption in vivo. *Blood* 106(4):1447-1453.
33. Ahuja R, *et al.* (2008) Interactions of cubilin with megalin and the product of the amnionless gene (AMN): effect on its stability. *The Biochemical journal* 410(2):301-308.
34. Anderson CL, *et al.* (2006) Perspective-- FcRn transports albumin: relevance to immunology and medicine. *Trends in immunology* 27(7):343-348.
35. Chaudhury C, *et al.* (2003) The major histocompatibility complex-related Fc receptor for IgG (FcRn) binds albumin and prolongs its lifespan. *The Journal of experimental medicine* 197(3):315-322.
36. Akilesh S, *et al.* (2008) Podocytes use FcRn to clear IgG from the glomerular basement membrane. *Proc Natl Acad Sci U S A* 105(3):967-972.
37. Tenten V, *et al.* (2013) Albumin is recycled from the primary urine by tubular transcytosis. *Journal of the American Society of Nephrology : JASN* 24(12):1966-1980.
38. Tojo A & Endou H (1992) Intrarenal handling of proteins in rats using fractional micropuncture technique. *Am J Physiol* 263(4 Pt 2):F601-606.
39. Gekle M (2007) Renal albumin handling: a look at the dark side of the filter. *Kidney international* 71(6):479-481.
40. Russo LM, *et al.* (2007) The normal kidney filters nephrotic levels of albumin retrieved by proximal tubule cells: retrieval is disrupted in nephrotic states. *Kidney international* 71(6):504-513.
41. Tanner GA (2009) Glomerular sieving coefficient of serum albumin in the rat: a two-photon microscopy study. *Am J Physiol Renal Physiol* 296(6):F1258-1265.
42. Peti-Peterdi J & Sipos A (2010) A high-powered view of the filtration barrier. *Journal of the American Society of Nephrology : JASN* 21(11):1835-1841.
43. Marino M, Andrews D, Brown D, & McCluskey RT (2001) Transcytosis of retinol-binding protein across renal proximal tubule cells after megalin (gp 330)-mediated endocytosis. *Journal of the American Society of Nephrology : JASN* 12(4):637-648.
44. Cui S, Nielsen S, Bjerke T, & Christensen EI (1993) Transcellular transport of ferritin in rabbit renal proximal tubules. *Experimental nephrology* 1(5):309-318.

45. Sandoval RM, *et al.* (2012) Multiple factors influence glomerular albumin permeability in rats. *Journal of the American Society of Nephrology : JASN* 23(3):447-457.
46. Sandoval RM, Kennedy MD, Low PS, & Molitoris BA (2004) Uptake and trafficking of fluorescent conjugates of folic acid in intact kidney determined using intravital two-photon microscopy. *Am J Physiol Cell Physiol* 287(2):C517-526.
47. Park CH & Maack T (1984) Albumin absorption and catabolism by isolated perfused proximal convoluted tubules of the rabbit. *The Journal of clinical investigation* 73(3):767-777.
48. Gudehithlu KP, Pegoraro AA, Dunea G, Arruda JA, & Singh AK (2004) Degradation of albumin by the renal proximal tubule cells and the subsequent fate of its fragments. *Kidney international* 65(6):2113-2122.
49. Hatae T, Fujita M, Sagara H, & Okuyama K (1986) Formation of apical tubules from large endocytic vacuoles in kidney proximal tubule cells during absorption of horseradish peroxidase. *Cell Tissue Res* 246(2):271-278.
50. Rabito CA (1983) Phosphate uptake by a kidney cell line (LLC-PK1). *Am J Physiol* 245(1):F22-31.
51. Ryan MJ, *et al.* (1994) HK-2: an immortalized proximal tubule epithelial cell line from normal adult human kidney. *Kidney Int* 45(1):48-57.
52. da Costa SR, Okamoto CT, & Hamm-Alvarez SF (2003) Actin microfilaments et al.--the many components, effectors and regulators of epithelial cell endocytosis. *Adv Drug Deliv Rev* 55(11):1359-1383.
53. Grant BD & Donaldson JG (2009) Pathways and mechanisms of endocytic recycling. *Nature reviews. Molecular cell biology* 10(9):597-608.
54. Huotari J & Helenius A (2011) Endosome maturation. *The EMBO journal* 30(17):3481-3500.
55. Sheff DR, Daro EA, Hull M, & Mellman I (1999) The receptor recycling pathway contains two distinct populations of early endosomes with different sorting functions. *The Journal of cell biology* 145(1):123-139.
56. Cramm-Behrens CI, Dienst M, & Jacob R (2008) Apical cargo traverses endosomal compartments on the passage to the cell surface. *Traffic* 9(12):2206-2220.

57. Ang AL, Folsch H, Koivisto UM, Pypaert M, & Mellman I (2003) The Rab8 GTPase selectively regulates AP-1B-dependent basolateral transport in polarized Madin-Darby canine kidney cells. *The Journal of cell biology* 163(2):339-350.
58. Ang AL, *et al.* (2004) Recycling endosomes can serve as intermediates during transport from the Golgi to the plasma membrane of MDCK cells. *The Journal of cell biology* 167(3):531-543.
59. Sato T, *et al.* (2007) The Rab8 GTPase regulates apical protein localization in intestinal cells. *Nature* 448(7151):366-369.
60. Huber LA, *et al.* (1993) Rab8, a small GTPase involved in vesicular traffic between the TGN and the basolateral plasma membrane. *The Journal of cell biology* 123(1):35-45.
61. Knodler A, *et al.* (2010) Coordination of Rab8 and Rab11 in primary ciliogenesis. *Proceedings of the National Academy of Sciences of the United States of America* 107(14):6346-6351.
62. Kelly EE, *et al.* (2010) Class I Rab11-family interacting proteins are binding targets for the Rab14 GTPase. *Biology of the cell / under the auspices of the European Cell Biology Organization* 102(1):51-62.
63. Kitt KN, *et al.* (2008) Rab14 regulates apical targeting in polarized epithelial cells. *Traffic* 9(7):1218-1231.
64. Seaman MN (2012) The retromer complex - endosomal protein recycling and beyond. *Journal of cell science* 125(Pt 20):4693-4702.
65. Rodman JS, Seidman L, & Farquhar MG (1986) The membrane composition of coated pits, microvilli, endosomes, and lysosomes is distinctive in the rat kidney proximal tubule cell. *The Journal of cell biology* 102(1):77-87.
66. Rodman JS, Kerjaschki D, Merisko E, & Farquhar MG (1984) Presence of an extensive clathrin coat on the apical plasmalemma of the rat kidney proximal tubule cell. *The Journal of cell biology* 98(5):1630-1636.
67. Birn H, Christensen EI, & Nielsen S (1993) Kinetics of endocytosis in renal proximal tubule studied with ruthenium red as membrane marker. *Am J Physiol* 264(2 Pt 2):F239-250.
68. Nielsen S (1993) Endocytosis in proximal tubule cells involves a two-phase membrane-recycling pathway. *Am J Physiol* 264(4 Pt 1):C823-835.

69. Hatae T, Ichimura T, Ishida T, & Sakurai T (1997) Apical tubular network in the rat kidney proximal tubule cells studied by thick-section and scanning electron microscopy. *Cell Tissue Res* 288(2):317-325.
70. Shmuel M, Nodel-Berner E, Hyman T, Rouvinski A, & Altschuler Y (2007) Caveolin 2 regulates endocytosis and trafficking of the M1 muscarinic receptor in MDCK epithelial cells. *Molecular biology of the cell* 18(5):1570-1585.
71. Zhuang Z, Marshansky V, Breton S, & Brown D (2011) Is caveolin involved in normal proximal tubule function? Presence in model PT systems but absence in situ. *American journal of physiology. Renal physiology* 300(1):F199-206.
72. Gekle M, Mildenerger S, Freudinger R, Schwerdt G, & Silbernagl S (1997) Albumin endocytosis in OK cells: dependence on actin and microtubules and regulation by protein kinases. *Am J Physiol* 272(5 Pt 2):F668-677.
73. Zhai XY, *et al.* (2000) Cubilin- and megalin-mediated uptake of albumin in cultured proximal tubule cells of opossum kidney. *Kidney Int* 58(4):1523-1533.
74. Decorti G, Malusa N, Furlan G, Candussio L, & Klugmann FB (1999) Endocytosis of gentamicin in a proximal tubular renal cell line. *Life sciences* 65(11):1115-1124.
75. Lui EC & Bendayan R (1998) Gentamicin uptake by LLCPK1 cells: effect of intracellular and extracellular pH changes. *Canadian journal of physiology and pharmacology* 76(2):155-160.
76. Nagai M, Meerloo T, Takeda T, & Farquhar MG (2003) The adaptor protein ARH escorts megalin to and through endosomes. *Molecular biology of the cell* 14(12):4984-4996.
77. Marzolo MP, *et al.* (2003) Differential distribution of low-density lipoprotein-receptor-related protein (LRP) and megalin in polarized epithelial cells is determined by their cytoplasmic domains. *Traffic* 4(4):273-288.
78. Anzenberger U, *et al.* (2006) Elucidation of megalin/LRP2-dependent endocytic transport processes in the larval zebrafish pronephros. *Journal of cell science* 119(Pt 10):2127-2137.
79. Schnatwinkel C, *et al.* (2004) The Rab5 effector Rabankyrin-5 regulates and coordinates different endocytic mechanisms. *PLoS biology* 2(9):E261.

80. Rangel-Filho A, Lazar J, Moreno C, Geurts A, & Jacob HJ (2013) Rab38 modulates proteinuria in model of hypertension-associated renal disease. *Journal of the American Society of Nephrology : JASN* 24(2):283-292.
81. Saito A, Sato H, Iino N, & Takeda T (2010) Molecular mechanisms of receptor-mediated endocytosis in the renal proximal tubular epithelium. *J Biomed Biotechnol* 2010:403272.
82. Gotoh N, *et al.* (2010) Altered renal proximal tubular endocytosis and histology in mice lacking myosin-VI. *Cytoskeleton (Hoboken)* 67(3):178-192.
83. Brown D & Wagner CA (2012) Molecular mechanisms of acid-base sensing by the kidney. *Journal of the American Society of Nephrology : JASN* 23(5):774-780.
84. Schmidt MM, *et al.* (2013) Crystal structure of an HSA/FcRn complex reveals recycling by competitive mimicry of HSA ligands at a pH-dependent hydrophobic interface. *Structure* 21(11):1966-1978.
85. Nagai J, *et al.* (2005) Mutually dependent localization of megalin and Dab2 in the renal proximal tubule. *American journal of physiology. Renal physiology* 289(3):F569-576.
86. Marzolo MP & Farfan P (2011) New insights into the roles of megalin/LRP2 and the regulation of its functional expression. *Biological research* 44(1):89-105.
87. Kolb RJ, Woost PG, & Hopfer U (2004) Membrane trafficking of angiotensin receptor type-1 and mechanochemical signal transduction in proximal tubule cells. *Hypertension* 44(3):352-359.
88. Kur E, *et al.* (2011) Loss of Lrp2 in zebrafish disrupts pronephric tubular clearance but not forebrain development. *Developmental dynamics : an official publication of the American Association of Anatomists* 240(6):1567-1577.
89. Caruso-Neves C, Pinheiro AA, Cai H, Souza-Menezes J, & Guggino WB (2006) PKB and megalin determine the survival or death of renal proximal tubule cells. *Proceedings of the National Academy of Sciences of the United States of America* 103(49):18810-18815.
90. Frick A, Rumrich G, Ullrich KJ, & Lassiter WE (1965) Microperfusion study of calcium transport in the proximal tubule of the rat kidney. *Pflugers Archiv fur die gesamte Physiologie des Menschen und der Tiere* 286(2):109-117.

91. Bank N, Yarger WE, & Aynedjian HS (1971) A microperfusion study of sucrose movement across the rat proximal tubule during renal vein constriction. *The Journal of clinical investigation* 50(2):294-302.
92. Bank N, Aynedjian HS, & Weinstein SW (1974) A microperfusion study of phosphate reabsorption by the rat proximal renal tubule. Effect of parathyroid hormone. *The Journal of clinical investigation* 54(5):1040-1048.
93. Corman B, Roinel N, & De Rouffignac C (1981) Water reabsorption capacity of the proximal convoluted tubule: a microperfusion study on rat kidney. *The Journal of physiology* 316:379-392.
94. Burg MB & Knepper MA (1986) Single tubule perfusion techniques. *Kidney international* 30(2):166-170.
95. Essig M, Terzi F, Burtin M, & Friedlander G (2001) Mechanical strains induced by tubular flow affect the phenotype of proximal tubular cells. *American journal of physiology. Renal physiology* 281(4):F751-762.
96. Weinbaum S, Duan Y, Satlin LM, Wang T, & Weinstein AM (2010) Mechanotransduction in the renal tubule. *American journal of physiology. Renal physiology* 299(6):F1220-1236.
97. Quinlan MR, Docherty NG, Watson RW, & Fitzpatrick JM (2008) Exploring mechanisms involved in renal tubular sensing of mechanical stretch following ureteric obstruction. *American journal of physiology. Renal physiology* 295(1):F1-F11.
98. Rice WL, *et al.* (2013) High resolution helium ion scanning microscopy of the rat kidney. *PloS one* 8(3):e57051.
99. Duan Y, *et al.* (2008) Shear-induced reorganization of renal proximal tubule cell actin cytoskeleton and apical junctional complexes. *Proceedings of the National Academy of Sciences of the United States of America* 105(32):11418-11423.
100. Young B & Wheater PR (2006) *Wheater's functional histology : a text and colour atlas* (Churchill Livingstone, Oxford) 5th Ed pp x, 437 p.
101. Tarbell JM & Ebong EE (2008) The endothelial glycocalyx: a mechano-sensor and -transducer. *Science signaling* 1(40):pt8.
102. Latta H, Maunsbach AB, & Madden SC (1961) Cilia in different segments of the rat nephron. *The Journal of biophysical and biochemical cytology* 11:248-252.

103. Sackin H (1995) Stretch-activated ion channels. *Kidney international* 48(4):1134-1147.
104. Alexander LD, Alagarsamy S, & Douglas JG (2004) Cyclic stretch-induced cPLA2 mediates ERK 1/2 signaling in rabbit proximal tubule cells. *Kidney international* 65(2):551-563.
105. Peyronnet R, *et al.* (2013) Piezo1-dependent stretch-activated channels are inhibited by Polycystin-2 in renal tubular epithelial cells. *EMBO reports* 14(12):1143-1148.
106. Bocanegra V, *et al.* (2014) RhoA and MAPK signal transduction pathways regulate NHE1-dependent proximal tubule cell apoptosis after mechanical stretch. *American journal of physiology. Renal physiology* 307(7):F881-889.
107. Orton DJ, Doucette AA, Maksym GN, & MacLellan DL (2014) Proteomic analysis of rat proximal tubule cells following stretch-induced apoptosis in an in vitro model of kidney obstruction. *Journal of proteomics* 100:125-135.
108. Hamzeh MT, Sridhara R, & Alexander LD (2015) Cyclic stretch-induced TGF-beta1 and fibronectin expression is mediated by beta1-integrin through c-Src- and STAT3-dependent pathways in renal epithelial cells. *American journal of physiology. Renal physiology* 308(5):F425-436.
109. Riveline D, *et al.* (2001) Focal contacts as mechanosensors: externally applied local mechanical force induces growth of focal contacts by an mDia1-dependent and ROCK-independent mechanism. *The Journal of cell biology* 153(6):1175-1186.
110. Filipovic D & Sackin H (1991) A calcium-permeable stretch-activated cation channel in renal proximal tubule. *The American journal of physiology* 260(1 Pt 2):F119-129.
111. Lowe CU, Terrey M, & Mac LE (1952) Organic-aciduria, decreased renal ammonia production, hydrophthalmos, and mental retardation; a clinical entity. *A.M.A. American journal of diseases of children* 83(2):164-184.
112. Lowe CU (1960) Oculo-cerebral-renal syndrome. *Maandschrift voor kindergeneeskunde* 28:77-80.
113. Silver DN, Lewis RA, & Nussbaum RL (1987) Mapping the Lowe oculocerebrorenal syndrome to Xq24-q26 by use of restriction fragment length polymorphisms. *The Journal of clinical investigation* 79(1):282-285.
114. Schurman SJ & Scheinman SJ (2009) Inherited cerebrorenal syndromes. *Nature reviews. Nephrology* 5(9):529-538.

115. Franceschetti A (1962) [Aminoaciduria in cataract and glaucoma of congenital origin. Analogies with the Lowe-Terrey-Mac-Lachlan oculo-cerebro-renal syndrome (hyperaminoaciduria, psychomotor retardation and muscular hypotonia with cataract and glaucoma)]. *Bulletin der Schweizerischen Akademie der Medizinischen Wissenschaften* 17:414-422.
116. Gaary EA, Rawnsley E, Marin-Padilla JM, Morse CL, & Crow HC (1993) In utero detection of fetal cataracts. *Journal of ultrasound in medicine : official journal of the American Institute of Ultrasound in Medicine* 12(4):234-236.
117. Charnas LR & Gahl WA (1991) The oculocerebrorenal syndrome of Lowe. *Adv Pediatr* 38:75-107.
118. Mao Y, *et al.* (2009) A PH domain within OCRL bridges clathrin-mediated membrane trafficking to phosphoinositide metabolism. *The EMBO journal* 28(13):1831-1842.
119. Ungewickell A, Ward ME, Ungewickell E, & Majerus PW (2004) The inositol polyphosphate 5-phosphatase Ocr1 associates with endosomes that are partially coated with clathrin. *Proceedings of the National Academy of Sciences of the United States of America* 101(37):13501-13506.
120. Zhang X, Jefferson AB, Auethavekiat V, & Majerus PW (1995) The protein deficient in Lowe syndrome is a phosphatidylinositol-4,5-bisphosphate 5-phosphatase. *Proceedings of the National Academy of Sciences of the United States of America* 92(11):4853-4856.
121. Schmid AC, Wise HM, Mitchell CA, Nussbaum R, & Woscholski R (2004) Type II phosphoinositide 5-phosphatases have unique sensitivities towards fatty acid composition and head group phosphorylation. *FEBS letters* 576(1-2):9-13.
122. Ponting CP (2006) A novel domain suggests a ciliary function for ASPM, a brain size determining gene. *Bioinformatics* 22(9):1031-1035.
123. McCrea HJ, *et al.* (2008) All known patient mutations in the ASH-RhoGAP domains of OCRL affect targeting and APPL1 binding. *Biochemical and biophysical research communications* 369(2):493-499.
124. Faucherre A, *et al.* (2003) Lowe syndrome protein OCRL1 interacts with Rac GTPase in the trans-Golgi network. *Human molecular genetics* 12(19):2449-2456.

125. Noakes CJ, Lee G, & Lowe M (2011) The PH domain proteins IPIP27A and B link OCRL1 to receptor recycling in the endocytic pathway. *Molecular biology of the cell* 22(5):606-623.
126. Dressman MA, Olivos-Glander IM, Nussbaum RL, & Suchy SF (2000) Ocr11, a PtdIns(4,5)P(2) 5-phosphatase, is localized to the trans-Golgi network of fibroblasts and epithelial cells. *The journal of histochemistry and cytochemistry : official journal of the Histochemistry Society* 48(2):179-190.
127. Grieve AG, *et al.* (2011) Lowe Syndrome protein OCRL1 supports maturation of polarized epithelial cells. *PloS one* 6(8):e24044.
128. Nandez R, *et al.* (2014) A role of OCRL in clathrin-coated pit dynamics and uncoating revealed by studies of Lowe syndrome cells. *eLife* 3:e02975.
129. Luo N, *et al.* (2012) OCRL localizes to the primary cilium: a new role for cilia in Lowe syndrome. *Human molecular genetics* 21(15):3333-3344.
130. Bothwell SP, *et al.* (2011) Mouse model for Lowe syndrome/Dent Disease 2 renal tubulopathy. *Journal of the American Society of Nephrology : JASN* 22(3):443-448.
131. Oltrabella F, *et al.* (2015) The Lowe syndrome protein OCRL1 is required for endocytosis in the zebrafish pronephric tubule. *PLoS genetics* 11(4):e1005058.
132. Devuyt O & Thakker RV (2010) Dent's disease. *Orphanet J Rare Dis* 5:28.
133. Rbaibi Y, *et al.* (2012) OCRL1 Modulates Cilia Length in Renal Epithelial Cells. *Traffic* 13(9):1295-1305.
134. Luo N, *et al.* (2014) Primary cilia signaling mediates intraocular pressure sensation. *Proceedings of the National Academy of Sciences of the United States of America* 111(35):12871-12876.
135. Vicinanza M, *et al.* (2011) OCRL controls trafficking through early endosomes via PtdIns4,5P(2)-dependent regulation of endosomal actin. *The EMBO journal* 30(24):4970-4985.
136. Erdmann KS, *et al.* (2007) A role of the Lowe syndrome protein OCRL in early steps of the endocytic pathway. *Developmental cell* 13(3):377-390.
137. Nakatsu F, *et al.* (2010) The inositol 5-phosphatase SHIP2 regulates endocytic clathrin-coated pit dynamics. *The Journal of cell biology* 190(3):307-315.

138. van Rahden VA, *et al.* (2012) The 5-phosphatase OCRL mediates retrograde transport of the mannose 6-phosphate receptor by regulating a Rac1-cofilin signalling module. *Human molecular genetics* 21(23):5019-5038.
139. Hagemann N, Hou X, Goody RS, Itzen A, & Erdmann KS (2012) Crystal structure of the Rab binding domain of OCRL1 in complex with Rab8 and functional implications of the OCRL1/Rab8 module for Lowe syndrome. *Small GTPases* 3(2):107-110.
140. Rodriguez-Gabin AG, *et al.* (2010) Interaction of Rab31 and OCRL-1 in oligodendrocytes: its role in transport of mannose 6-phosphate receptors. *Journal of neuroscience research* 88(3):589-604.
141. Dambournet D, *et al.* (2011) Rab35 GTPase and OCRL phosphatase remodel lipids and F-actin for successful cytokinesis. *Nature cell biology* 13(8):981-988.
142. Cui S, *et al.* (2010) OCRL1 function in renal epithelial membrane traffic. *American journal of physiology. Renal physiology* 298(2):F335-345.
143. Golub T & Pico C (2005) Spatial control of actin-based motility through plasmalemmal PtdIns(4,5)P2-rich raft assemblies. *Biochemical Society symposium* (72):119-127.
144. Wu G, *et al.* (2012) Suppression of intestinal calcium entry channel TRPV6 by OCRL, a lipid phosphatase associated with Lowe syndrome and Dent disease. *American journal of physiology. Cell physiology* 302(10):C1479-1491.
145. Thomson SC & Blantz RC (2008) Glomerulotubular balance, tubuloglomerular feedback, and salt homeostasis. *Journal of the American Society of Nephrology : JASN* 19(12):2272-2275.
146. Nielsen R & Christensen EI (2010) Proteinuria and events beyond the slit. *Pediatric nephrology* 25(5):813-822.
147. McDonough AA (2010) Mechanisms of proximal tubule sodium transport regulation that link extracellular fluid volume and blood pressure. *Am J Physiol Regul Integr Comp Physiol* 298(4):R851-861.
148. Du Z, *et al.* (2004) Mechanosensory function of microvilli of the kidney proximal tubule. *Proceedings of the National Academy of Sciences of the United States of America* 101(35):13068-13073.

149. Du Z, *et al.* (2006) Axial flow modulates proximal tubule NHE3 and H-ATPase activities by changing microvillus bending moments. *American journal of physiology. Renal physiology* 290(2):F289-296.
150. Bomsel M, Prydz K, Parton RG, Gruenberg J, & Simons K (1989) Endocytosis in filter-grown Madin-Darby canine kidney cells. *The Journal of cell biology* 109(6 Pt 2):3243-3258.
151. Szalinski CM, *et al.* (2013) PIP5KIbeta Selectively Modulates Apical Endocytosis in Polarized Renal Epithelial Cells. *PLoS one* 8(1):e53790.
152. Chou CL & Marsh DJ (1987) Measurement of flow rate in rat proximal tubules with a nonobstructing optical method. *Am J Physiol* 253(2 Pt 2):F366-371.
153. Maunsbach AB, Giebisch GH, & Stanton BA (1987) Effects of flow rate on proximal tubule ultrastructure. *Am J Physiol* 253(3 Pt 2):F582-587.
154. Gekle M (2005) Renal tubule albumin transport. *Annu Rev Physiol* 67:573-594.
155. Ferrell N, Ricci KB, Groszek J, Marmorstein JT, & Fissell WH (2012) Albumin handling by renal tubular epithelial cells in a microfluidic bioreactor. *Biotechnol Bioeng* 109(3):797-803.
156. Nauli SM, *et al.* (2003) Polycystins 1 and 2 mediate mechanosensation in the primary cilium of kidney cells. *Nat Genet* 33(2):129-137.
157. Yoder BK (2007) Role of primary cilia in the pathogenesis of polycystic kidney disease. *Journal of the American Society of Nephrology : JASN* 18(5):1381-1388.
158. Liu W, *et al.* (2003) Effect of flow and stretch on the [Ca²⁺]_i response of principal and intercalated cells in cortical collecting duct. *American journal of physiology. Renal physiology* 285(5):F998-F1012.
159. Praetorius HA & Leipziger J (2013) Primary cilium-dependent sensing of urinary flow and paracrine purinergic signaling. *Semin Cell Dev Biol* 24(1):3-10.
160. Tojo A, *et al.* (2001) Reduced albumin reabsorption in the proximal tubule of early-stage diabetic rats. *Histochem Cell Biol* 116(3):269-276.
161. Cureton DK, Massol RH, Saffarian S, Kirchhausen TL, & Whelan SP (2009) Vesicular stomatitis virus enters cells through vesicles incompletely coated with clathrin that depend upon actin for internalization. *PLoS pathogens* 5(4):e1000394.

162. Liu W, *et al.* (2005) Mechanoregulation of intracellular Ca²⁺ concentration is attenuated in collecting duct of monocilia-impaired orpk mice. *American journal of physiology. Renal physiology* 289(5):F978-988.
163. Verghese E, *et al.* (2009) Renal primary cilia lengthen after acute tubular necrosis. *Journal of the American Society of Nephrology : JASN* 20(10):2147-2153.
164. Coon BG, *et al.* (2012) The Lowe syndrome protein OCRL1 is involved in primary cilia assembly. *Human molecular genetics* 21(8):1835-1847.
165. Berrout J, *et al.* (2012) Function of transient receptor potential cation channel subfamily V member 4 (TRPV4) as a mechanical transducer in flow-sensitive segments of renal collecting duct system. *The Journal of biological chemistry* 287(12):8782-8791.
166. Kottgen M, *et al.* (2008) TRPP2 and TRPV4 form a polymodal sensory channel complex. *The Journal of cell biology* 182(3):437-447.
167. Pochynyuk O, Zaika O, O'Neil RG, & Mamenko M (2013) Novel insights into TRPV4 function in the kidney. *Pflugers Arch* 465(2):177-186.
168. Zaika O, *et al.* (2013) TRPV4 Dysfunction Promotes Renal Cystogenesis in Autosomal Recessive Polycystic Kidney Disease. *Journal of the American Society of Nephrology : JASN* 24(4):604-616.
169. Tian W, *et al.* (2004) Renal expression of osmotically responsive cation channel TRPV4 is restricted to water-impermeant nephron segments. *American journal of physiology. Renal physiology* 287(1):F17-24.
170. Delling M, DeCaen PG, Doerner JF, Febvay S, & Clapham DE (2013) Primary cilia are specialized calcium signalling organelles. *Nature* 504(7479):311-314.
171. Jin X, *et al.* (2014) Cilioplasm is a cellular compartment for calcium signaling in response to mechanical and chemical stimuli. *Cellular and molecular life sciences : CMLS* 71(11):2165-2178.
172. Rydholm S, *et al.* (2010) Mechanical properties of primary cilia regulate the response to fluid flow. *American journal of physiology. Renal physiology* 298(5):F1096-1102.
173. Besschetnova TY, *et al.* (2010) Identification of signaling pathways regulating primary cilium length and flow-mediated adaptation. *Current biology : CB* 20(2):182-187.
174. Raghavan V, Rbaibi Y, Pastor-Soler NM, Carattino MD, & Weisz OA (2014) Shear stress-dependent regulation of apical endocytosis in renal proximal tubule cells mediated

- by primary cilia. *Proceedings of the National Academy of Sciences of the United States of America* 111(23):8506-8511.
175. Lazarowski ER, Sesma JI, Seminario-Vidal L, & Kreda SM (2011) Molecular mechanisms of purine and pyrimidine nucleotide release. *Advances in pharmacology* 61:221-261.
176. Svenningsen P, Burford JL, & Peti-Peterdi J (2013) ATP releasing connexin 30 hemichannels mediate flow-induced calcium signaling in the collecting duct. *Front Physiol* 4:292.
177. Haefliger JA, *et al.* (2006) Connexin43-dependent mechanism modulates renin secretion and hypertension. *J Clin Invest* 116(2):405-413.
178. Hills CE, Kerr MI, Wall MJ, & Squires PE (2013) Visfatin reduces gap junction mediated cell-to-cell communication in proximal tubule-derived epithelial cells. *Cell Physiol Biochem* 32(5):1200-1212.
179. Sainio K, *et al.* (1992) Differential expression of gap junction mRNAs and proteins in the developing murine kidney and in experimentally induced nephric mesenchymes. *Development* 115(3):827-837.
180. Stoessel A, Himmerkus N, Bleich M, Bachmann S, & Theilig F (2010) Connexin 37 is localized in renal epithelia and responds to changes in dietary salt intake. *American journal of physiology. Renal physiology* 298(1):F216-223.
181. Zhang JT & Nicholson BJ (1989) Sequence and tissue distribution of a second protein of hepatic gap junctions, Cx26, as deduced from its cDNA. *The Journal of cell biology* 109(6 Pt 2):3391-3401.
182. Hanner F, Lam L, Nguyen MT, Yu A, & Peti-Peterdi J (2012) Intrarenal localization of the plasma membrane ATP channel pannexin1. *American journal of physiology. Renal physiology* 303(10):F1454-1459.
183. Bjaelde RG, Arnadottir SS, Overgaard MT, Leipziger J, & Praetorius HA (2013) Renal epithelial cells can release ATP by vesicular fusion. *Front Physiol* 4:238.
184. Bailey MA, *et al.* (2000) Axial distribution and characterization of basolateral P2Y receptors along the rat renal tubule. *Kidney Int* 58(5):1893-1901.

185. Bailey MA, *et al.* (2001) Evidence for basolateral P2Y(6) receptors along the rat proximal tubule: functional and molecular characterization. *Journal of the American Society of Nephrology : JASN* 12(8):1640-1647.
186. Ralevic V & Burnstock G (1998) Receptors for purines and pyrimidines. *Pharmacol Rev* 50(3):413-492.
187. Filipovic DM, Adebajo OA, Zaidi M, & Reeves WB (1998) Functional and molecular evidence for P2X receptors in LLC-PK1 cells. *Am J Physiol* 274(6 Pt 2):F1070-1077.
188. Turner CM, Vonend O, Chan C, Burnstock G, & Unwin RJ (2003) The pattern of distribution of selected ATP-sensitive P2 receptor subtypes in normal rat kidney: an immunohistological study. *Cells Tissues Organs* 175(2):105-117.
189. Goncalves RG, *et al.* (2006) The role of purinergic P2X7 receptors in the inflammation and fibrosis of unilateral ureteral obstruction in mice. *Kidney Int* 70(9):1599-1606.
190. Cureton DK, Massol RH, Whelan SP, & Kirchhausen T (2010) The length of vesicular stomatitis virus particles dictates a need for actin assembly during clathrin-dependent endocytosis. *PLoS Pathog* 6(9):e1001127.
191. Choudhury R, *et al.* (2005) Lowe syndrome protein OCRL1 interacts with clathrin and regulates protein trafficking between endosomes and the trans-Golgi network. *Molecular biology of the cell* 16(8):3467-3479.
192. Choudhury R, Noakes CJ, McKenzie E, Kox C, & Lowe M (2009) Differential clathrin binding and subcellular localization of OCRL1 splice isoforms. *The Journal of biological chemistry* 284(15):9965-9973.
193. Lowe M (2005) Structure and function of the Lowe syndrome protein OCRL1. *Traffic* 6(9):711-719.
194. Fukuda M, Kanno E, Ishibashi K, & Itoh T (2008) Large scale screening for novel rab effectors reveals unexpected broad Rab binding specificity. *Molecular & cellular proteomics : MCP* 7(6):1031-1042.
195. Hyvola N, *et al.* (2006) Membrane targeting and activation of the Lowe syndrome protein OCRL1 by rab GTPases. *The EMBO journal* 25(16):3750-3761.
196. Ungewickell AJ & Majerus PW (1999) Increased levels of plasma lysosomal enzymes in patients with Lowe syndrome. *Proceedings of the National Academy of Sciences of the United States of America* 96(23):13342-13344.

197. Bockenhauer D, *et al.* (2008) Renal phenotype in Lowe Syndrome: a selective proximal tubular dysfunction. *Clin J Am Soc Nephrol* 3(5):1430-1436.
198. Norden AG, Gardner SC, Van't Hoff W, & Unwin RJ (2008) Lysosomal enzymuria is a feature of hereditary Fanconi syndrome and is related to elevated CI-mannose-6-P-receptor excretion. *Nephrol Dial Transplant* 23(9):2795-2803.
199. Conduit SE, Dyson JM, & Mitchell CA (2012) Inositol polyphosphate 5-phosphatases; new players in the regulation of cilia and ciliopathies. *FEBS letters* 586(18):2846-2857.
200. Drummond IA & Davidson AJ (2010) Zebrafish kidney development. *Methods Cell Biol* 100:233-260.
201. Hentschel DM, *et al.* (2005) Acute renal failure in zebrafish: a novel system to study a complex disease. *American journal of physiology. Renal physiology* 288(5):F923-929.
202. Lee JC & Edelman AM (1994) A protein activator of Ca(2+)-calmodulin-dependent protein kinase Ia. *The Journal of biological chemistry* 269(3):2158-2164.
203. Ho YD, Joyal JL, Li Z, & Sacks DB (1999) IQGAP1 integrates Ca²⁺/calmodulin and Cdc42 signaling. *The Journal of biological chemistry* 274(1):464-470.
204. Saneyoshi T, *et al.* (2008) Activity-dependent synaptogenesis: regulation by a CaM-kinase kinase/CaM-kinase I/betaPIX signaling complex. *Neuron* 57(1):94-107.
205. Prehoda KE, Scott JA, Mullins RD, & Lim WA (2000) Integration of multiple signals through cooperative regulation of the N-WASP-Arp2/3 complex. *Science* 290(5492):801-806.
206. Rohatgi R, Ho HY, & Kirschner MW (2000) Mechanism of N-WASP activation by CDC42 and phosphatidylinositol 4, 5-bisphosphate. *The Journal of cell biology* 150(6):1299-1310.
207. Da Costa SR, *et al.* (2003) Impairing actin filament or syndapin functions promotes accumulation of clathrin-coated vesicles at the apical plasma membrane of acinar epithelial cells. *Molecular biology of the cell* 14(11):4397-4413.
208. Klee CB, Crouch TH, & Richman PG (1980) Calmodulin. *Annual review of biochemistry* 49:489-515.
209. Wang JH, Pallen CJ, Sharma RK, Adachi AM, & Adachi K (1985) The calmodulin regulatory system. *Current topics in cellular regulation* 27:419-436.

210. Wang CL (1985) A note on Ca²⁺ binding to calmodulin. *Biochemical and biophysical research communications* 130(1):426-430.
211. Soderling TR (1999) The Ca-calmodulin-dependent protein kinase cascade. *Trends in biochemical sciences* 24(6):232-236.
212. Hudmon A & Schulman H (2002) Structure-function of the multifunctional Ca²⁺/calmodulin-dependent protein kinase II. *The Biochemical journal* 364(Pt 3):593-611.
213. Hoelz A, Nairn AC, & Kuriyan J (2003) Crystal structure of a tetradecameric assembly of the association domain of Ca²⁺/calmodulin-dependent kinase II. *Molecular cell* 11(5):1241-1251.
214. Staruschenko A & Sorokin A (2012) Role of betaPix in the Kidney. *Frontiers in physiology* 3:154.
215. Kim AS, Kakalis LT, Abdul-Manan N, Liu GA, & Rosen MK (2000) Autoinhibition and activation mechanisms of the Wiskott-Aldrich syndrome protein. *Nature* 404(6774):151-158.
216. Luna A, *et al.* (2002) Regulation of protein transport from the Golgi complex to the endoplasmic reticulum by CDC42 and N-WASP. *Molecular biology of the cell* 13(3):866-879.
217. Suetsugu S, Miki H, & Takenawa T (2001) Identification of another actin-related protein (Arp) 2/3 complex binding site in neural Wiskott-Aldrich syndrome protein (N-WASP) that complements actin polymerization induced by the Arp2/3 complex activating (VCA) domain of N-WASP. *The Journal of biological chemistry* 276(35):33175-33180.
218. Wu WJ, Erickson JW, Lin R, & Cerione RA (2000) The gamma-subunit of the coatamer complex binds Cdc42 to mediate transformation. *Nature* 405(6788):800-804.
219. Kroschewski R, Hall A, & Mellman I (1999) Cdc42 controls secretory and endocytic transport to the basolateral plasma membrane of MDCK cells. *Nature cell biology* 1(1):8-13.
220. Cohen D, Musch A, & Rodriguez-Boulan E (2001) Selective control of basolateral membrane protein polarity by cdc42. *Traffic* 2(8):556-564.

221. Musch A, Cohen D, Kreitzer G, & Rodriguez-Boulan E (2001) cdc42 regulates the exit of apical and basolateral proteins from the trans-Golgi network. *The EMBO journal* 20(9):2171-2179.
222. Rojas R, Ruiz WG, Leung SM, Jou TS, & Apodaca G (2001) Cdc42-dependent modulation of tight junctions and membrane protein traffic in polarized Madin-Darby canine kidney cells. *Molecular biology of the cell* 12(8):2257-2274.
223. Galovic M, Xu D, Areces LB, van der Kammen R, & Innocenti M (2011) Interplay between N-WASP and CK2 optimizes clathrin-mediated endocytosis of EGFR. *Journal of cell science* 124(Pt 12):2001-2012.
224. Mullins RD, Heuser JA, & Pollard TD (1998) The interaction of Arp2/3 complex with actin: nucleation, high affinity pointed end capping, and formation of branching networks of filaments. *Proceedings of the National Academy of Sciences of the United States of America* 95(11):6181-6186.
225. Ideses Y, Brill-Karniely Y, Haviv L, Ben-Shaul A, & Bernheim-Groswasser A (2008) Arp2/3 branched actin network mediates filopodia-like bundles formation in vitro. *PloS one* 3(9):e3297.
226. Singh S, *et al.* (2003) Identification of the p16-Arc subunit of the Arp 2/3 complex as a substrate of MAPK-activated protein kinase 2 by proteomic analysis. *The Journal of biological chemistry* 278(38):36410-36417.
227. Ho HY, Rohatgi R, Lebensohn AM, & Kirschner MW (2006) In vitro reconstitution of cdc42-mediated actin assembly using purified components. *Methods in enzymology* 406:174-190.
228. Merrifield CJ, Qualmann B, Kessels MM, & Almers W (2004) Neural Wiskott Aldrich Syndrome Protein (N-WASP) and the Arp2/3 complex are recruited to sites of clathrin-mediated endocytosis in cultured fibroblasts. *European journal of cell biology* 83(1):13-18.
229. Merrifield CJ, Perrais D, & Zenisek D (2005) Coupling between clathrin-coated-pit invagination, cortactin recruitment, and membrane scission observed in live cells. *Cell* 121(4):593-606.

230. Merrifield CJ, Feldman ME, Wan L, & Almers W (2002) Imaging actin and dynamin recruitment during invagination of single clathrin-coated pits. *Nature cell biology* 4(9):691-698.
231. Millard TH, Sharp SJ, & Machesky LM (2004) Signalling to actin assembly via the WASP (Wiskott-Aldrich syndrome protein)-family proteins and the Arp2/3 complex. *The Biochemical journal* 380(Pt 1):1-17.
232. Benesch S, *et al.* (2005) N-WASP deficiency impairs EGF internalization and actin assembly at clathrin-coated pits. *Journal of cell science* 118(Pt 14):3103-3115.
233. Hussain NK, *et al.* (2001) Endocytic protein intersectin-1 regulates actin assembly via Cdc42 and N-WASP. *Nature cell biology* 3(10):927-932.
234. Owen D, *et al.* (2008) The IQGAP1-Rac1 and IQGAP1-Cdc42 interactions: interfaces differ between the complexes. *The Journal of biological chemistry* 283(3):1692-1704.
235. Briggs MW & Sacks DB (2003) IQGAP1 as signal integrator: Ca²⁺, calmodulin, Cdc42 and the cytoskeleton. *FEBS letters* 542(1-3):7-11.
236. Bashour AM, Fullerton AT, Hart MJ, & Bloom GS (1997) IQGAP1, a Rac- and Cdc42-binding protein, directly binds and cross-links microfilaments. *The Journal of cell biology* 137(7):1555-1566.
237. Andrews WJ, *et al.* (2012) A calcium-dependent interaction between calmodulin and the calponin homology domain of human IQGAP1. *Molecular and cellular biochemistry* 371(1-2):217-223.
238. Itoh RE, *et al.* (2002) Activation of rac and cdc42 video imaged by fluorescent resonance energy transfer-based single-molecule probes in the membrane of living cells. *Molecular and cellular biology* 22(18):6582-6591.
239. Christensen EI & Gburek J (2004) Protein reabsorption in renal proximal tubule-function and dysfunction in kidney pathophysiology. *Pediatric nephrology* 19(7):714-721.
240. Verrey F, *et al.* (2009) Kidney amino acid transport. *Pflugers Arch* 458(1):53-60.
241. Jacobson HR & Kokko JP (1976) Intrinsic differences in various segments of the proximal convoluted tubule. *The Journal of clinical investigation* 57(4):818-825.
242. Helbert MJ, Dauwe SE, Van der Biest I, Nouwen EJ, & De Broe ME (1997) Immunodissection of the human proximal nephron: flow sorting of S1S2S3, S1S2 and S3 proximal tubular cells. *Kidney international* 52(2):414-428.

243. Briere N, Martel M, Plante G, & Petitclerc C (1984) Heterogeneous distribution of alkaline phosphatase and gamma-glutamyl transpeptidase in the mouse nephron. *Acta Histochem* 74(1):103-108.
244. Cui S & Christensen EI (1993) Three-dimensional organization of the vacuolar apparatus involved in endocytosis and membrane recycling of rat kidney proximal tubule cells. An electron-microscopic study of serial sections. *Experimental nephrology* 1(3):175-184.
245. Goligorsky MS & Hruska KA (1986) Transcytosis in cultured proximal tubular cells. *J Membr Biol* 93(3):237-247.
246. Wolff NA, Lee WK, Abouhamed M, & Thevenod F (2008) Role of ARF6 in internalization of metal-binding proteins, metallothionein and transferrin, and cadmium-metallothionein toxicity in kidney proximal tubule cells. *Toxicol Appl Pharmacol* 230(1):78-85.
247. Bell CL, Tenenhouse HS, & Scriver CR (1988) Initiation and characterization of primary mouse kidney epithelial cultures. *In Vitro Cell Dev Biol* 24(7):683-695.
248. Inoue CN, *et al.* (2003) Reconstruction of tubular structures in three-dimensional collagen gel culture using proximal tubular epithelial cells voided in human urine. *In Vitro Cell Dev Biol Anim* 39(8-9):364-367.
249. Terryn S, *et al.* (2007) A primary culture of mouse proximal tubular cells, established on collagen-coated membranes. *American journal of physiology. Renal physiology* 293(2):F476-485.
250. Casanova JE, *et al.* (1999) Association of Rab25 and Rab11a with the apical recycling system of polarized Madin-Darby canine kidney cells. *Molecular biology of the cell* 10(1):47-61.
251. Leung SM, Ruiz WG, & Apodaca G (2000) Sorting of membrane and fluid at the apical pole of polarized Madin-Darby canine kidney cells. *Molecular biology of the cell* 11(6):2131-2150.
252. Brown PS, *et al.* (2000) Definition of distinct compartments in polarized Madin-Darby canine kidney (MDCK) cells for membrane-volume sorting, polarized sorting and apical recycling. *Traffic* 1(2):124-140.

253. Lencer WI, Weyer P, Verkman AS, Ausiello DA, & Brown D (1990) FITC-dextran as a probe for endosome function and localization in kidney. *The American journal of physiology* 258(2 Pt 1):C309-317.
254. Akhter S, *et al.* (2002) Na(+)/H(+) exchanger 3 is in large complexes in the center of the apical surface of proximal tubule-derived OK cells. *American journal of physiology. Cell physiology* 283(3):C927-940.
255. Carpentier S, *et al.* (2013) Class III Phosphoinositide 3-Kinase/VPS34 and Dynamin are Critical for Apical Endocytic Recycling. *Traffic* 14(8):933-948.
256. Mattila PE, *et al.* (2012) Multiple biosynthetic trafficking routes for apically secreted proteins in MDCK cells. *Traffic* 13(3):433-442.